

Dissertation zur Erlangung des Doktorgrades  
der Fakultät für Chemie und Pharmazie  
der Ludwig-Maximilians-Universität München

# Local and Targeted Delivery of Proteins

Madeleine Yvonne Witting  
Aus Rosenheim, Deutschland

2016

## Erklärung

Diese Dissertation wurde im Sinne von § 7 der Promotionsordnung vom 28. November 2011 von Herrn Prof. Dr. Wolfgang Frieß betreut.

## Eidesstattliche Versicherung

Diese Dissertation wurde eigenständig und ohne unerlaubte Hilfe erarbeitet.

Ludwigshafen, den 06.08.2016

---

Madeleine Witting

Dissertation eingereicht am: 07.03.2016

1. Gutachter: Prof. Dr. Wolfgang Frieß
2. Gutachter: Prof. Dr. Sarah Hedtrich, geb. Küchler

Mündliche Prüfung am: 25.04.2016



*For my family*

With the stillness of the night  
There comes a time to understand  
To reach out and touch tomorrow  
Take the future in our hand.

We can see a new horizon  
Built on all that we have done  
And our dreams begin  
Another thousand circles 'round the sun.

We go on  
To the joy and through the tears  
We go on  
To discover new frontiers  
Moving on  
With the current of the years.

We go on  
Moving forward, now as one  
Moving on  
With a spirit born to run  
Ever on  
With each rising sun.

To a new day  
We go on.

("We Go On" Illuminations Lyrics by Don Dorsey (c) 1999 by Walt Disney Music Co.)

# Acknowledgements

My highest gratitude goes to Prof. Dr. Wolfgang Frieß, who not only offered me the opportunity to do my PhD thesis in his scientific group, but also guided me through highs and lows of my student life. His patience towards me during my writing time, his valuable advice and continuous encouragement during the PhD years are highly appreciated.

With the same magnitude, a heartily “Thank You” goes to Prof. Dr. Sarah Hedtrich (née KÜchler). Being my second supervisor, I had the honor to work with her as her first PhD student at the LMU Munich. With her persistence and encouragement, she made me the (hopefully successful) scientist I am today. Her support, especially through my tough time, is highly valued and will never be forgotten.

For her help with the skin models and the important experiments with the TGase1, Katja Obst is greatly acknowledged. As my project successor, I wish her all the best for her ongoing PhD thesis and tons of amazing results. My compliments go to Leonie Wallmeyer, Stefan Hönzke and Guy Yealland from the FU Berlin as well.

I want to thank the whole group of Prof. Frieß and Prof. Winter for the pleasant and supportive working atmosphere. Especially, I would like to thank my lab mates Kay and Verena for all the happy times in the “Gemischte Sauna”. Likewise, my times at the university wouldn’t have been the same without Marie-Paule, Kerstin, Laura and Elisa. The legendary coffee and Rotkäppchen breaks will always be cherished memories!

The students Francesca Rapolla, Nico Erlewein, Angelika Nistler, Josephine Pott, Michaela Wimmer, Rebekka Bernard, Nina Omeragic, Lucia Auctor and Larissa Bendiks are acknowledged for the good work they have done.

Cihad Anamur, Sabine Eichling, Christian and Janina Ried, Susanne Kremer, Klaus Diry, Sheetal Pai-Wechsung and Rainer Saedler cheered me up during my writing time in Ludwigshafen (AbbVie) and shared some memorable moments with me. Thanks a ton.

Prof. Dr. Stefan Zahler is thankfully acknowledged for his support with fluorescence scanning microscopy. A heartily “Thanks” goes also to Jana Peliskova.

Furthermore, I like to thank my project partners for enlightening scientific discussions and fruitful co-operations:

Prof. Dr. Marcelo Calderón and his group, especially Dr. Maria Molina

Prof. Dr. Rainer Haag and his group, especially Dr. Dirk Steinhilber

Prof. Dr. Ulrike Alexiev and her group, especially Dr. Alexander Boreham and Dr. Tai-Yang Kim

Dr. Hans Christian Hennies, Prof. Dr. Markus Pietzsch, Prof. Dr. Kateřina Vávrová

I’d like to thank Michael Wiggenhorn and the whole Coriolis Team for the good exchange of ideas and the opportunity for additional business during my PhD time.

And last but not least I want to thank my entire family on earth and in heaven.

Words cannot describe what a grateful heart feels.

# Abbreviations

ABU	arbitrary brightness units
AD	atopic dermatitis
APS	ammonium persulfate
AsnB / Asp	L-asparaginase II
ATR	attenuated total reflection
BCA	bicinchoninic acid
BSA	bovine serum albumin
CD	circular dichroism
Da	Dalton
DLS	dynamic light scattering
(d)PG	(dendritic) polyglycerols
FLG	filaggrin
FLIM	fluorescence lifetime microscopy
FT-IR	Fourier-transformed infrared spectrometer
FRET	(Förster) fluorescence resonance energy transfer
GC	glucocorticoids
GPC	gel permeation chromatography
HA	hyaluronic acid
HA-hGH	hyaluronic acid – human growth hormone conjugate
HA-MANT	n-methylantraniloyl-hyaluronic acid conjugate
HEC	hydroxyethyl cellulose
HPLC	high pressure liquid chromatography
i.v.	intravenous
IFN	interferon
IL	interleukin
IV	ichthyosis vulgaris
LCST	lower critical solution temperature
MANT	n-methylantraniloyl
MIA	n-methylisatoic anhydride
MN	microneedle/microneedles
MWCO	molecular weight cut-off
NMF	natural moisturizing factor
NMR	nuclear magnetic resonance
NSAID	non-steroidal anti-inflammatory drugs
PBS	phosphate buffered saline
PDI	polydispersity index
PEG	polyethylene glycol
PG	polyglycerol
pHBA	poly(p-hydroxybenzoic acid)
PLA	polylactide
PLGA	poly(lactic-co-glycolic acid)
PNIPAM	poly(N-isopropylacrylamide)
p-PBDMA	polybutadienmaleinic acid
PS	polystyrene
PV	psoriasis vulgaris
RhB ITC	rhodamine B isothiocyanate
RT	room temperature
s.c.	subcutaneous
SC	stratum corneum
SDS	sodium dodecyl sulfate
SEC	size exclusion chromatography
TEMED	tetramethylethylenediamine
TGase-1	transglutaminase-1
THPA	tetrahydrophthalic acid
THPTA	tris(3-hydroxypropyltriazolymethyl)amine
T <sub>p</sub>	thermal trigger point temperature

## Table of Contents

Acknowledgements .....	V
Abbreviations.....	VI
Table of Contents .....	VII

## **Chapter 1** ..... 1

Introduction .....	1
1. Human skin .....	1
1.1 Anatomy and physiology .....	1
1.2 Genetic skin disorders .....	2
1.2.1 Atopic dermatitis.....	3
1.2.2 Psoriasis.....	3
1.2.3 Ichthyosis vulgaris .....	4
1.2.4 Current pharmacotherapy for PV, AD and IV .....	4
2. Dermal drug delivery and skin penetration .....	7
2.1 Characteristics of skin penetration .....	7
2.2 Systems for dermal drug delivery testing .....	8
2.3 Expectations and challenges of dermal biomacromolecule delivery .....	9
3. Systems for dermal drug delivery .....	10
3.1 Nanoparticle-based release systems .....	12
3.1.1 Polyglycerol-based nanogels.....	13
3.1.2 Functionalization and targeted drug delivery .....	13
3.1.3 The potential of dPG-based nanogels in drug delivery .....	14
3.2 Hyaluronic acid for dermal drug delivery .....	15
3.2.1 Structure and physic-chemical characteristics of HA.....	15
3.2.2 HA in drug delivery .....	16
3.2.2.1 General drug delivery aspects of HA .....	16
3.2.2.2 Transdermal and dermal drug delivery of HA .....	16
3.3 Solid microneedles for dermal drug delivery .....	17
3.3.1 MN fabrication and characterization .....	17
3.3.2 Drug application techniques and formulation aspects .....	17
3.3.3 Dermal drug delivery mediated by MN .....	18
4. Objectives of the thesis .....	18
5. References .....	19

## **Chapter 2 ..... 25**

### **Biodegradable dendritic polyglycerol nanogels for encapsulation and release of pharmaceutical biomacromolecules**

Abstract.....	26
1. Introduction .....	27
2. Methods .....	29
2.1 Preparation of dPG <sub>7.7</sub> functionalized with 10 p-PBDMA units (dPG <sub>7.7</sub> -10-p-PBDMA) .....	29
2.2 Preparation of polyglycerol nanogels by nanoprecipitation.....	29
2.3 Encapsulation of asparaginase into the nanogels .....	30
2.4 Determination of nanogel degradation kinetics.....	30
2.5 Determination of proteins' secondary structure - Fourier-transformed-infrared spectroscopy (FT-IR).....	30
2.6 Determination of asparaginase activity.....	30
2.7 Drug release study .....	31
2.8 Size exclusion HPLC (SE-HPLC) analysis .....	31
3. Results and discussion .....	31
3.1 Nanogel preparation by inverse nanoprecipitation and in situ gelation.....	31
3.2 Enzyme encapsulation by co-precipitation .....	33
3.3 Degradation triggered release under acidic conditions.....	34
3.4 Structure-activity assay of encapsulated and released asparaginase .....	35
3.4.1 Determination of proteins' secondary structure by Fourier-transformed-infrared spectroscopy (FT-IR).....	35
3.4.2 Determination of asparaginase activity .....	37
4. Conclusion .....	38
5. Acknowledgements .....	38
6. References.....	38

## **Chapter 3** ..... 42

### **Thermosensitive dendritic polyglycerol-based nanogels for cutaneous delivery of biomacromolecules**

Abstract.....	43
1. Introduction .....	44
2. Methods .....	45
2.1 Synthesis, characterization, and protein encapsulation of PNIPAM-dPG nanogels.....	45
2.2 Fluorescence labeling of bovine serum albumin (BSA) .....	46
2.3 PNIPAM-dPG nanogel size, thermosensitive kinetics, and protein release .	46
2.4 Protein stability testing.....	47
2.5 Determination of protein secondary structure - Fourier transformed infrared spectroscopy (FT-IR).....	47
2.6 Asparaginase (Asp) activity .....	47
2.7 Skin penetration experiments .....	47
2.7.1 Cutaneous protein delivery efficiency - pig skin .....	47
2.7.2 Cutaneous protein delivery efficiency - normal and filaggrin-deficient reconstructed skin.....	48
2.7.3 Cutaneous delivery of therapeutic protein TGase-1 in TGase-1-deficient reconstructed skin .....	48
2.8 Skin permeability testing.....	49
2.9 Statistical analysis .....	49
3. Results .....	49
3.1 Particle synthesis and characterization .....	49
3.2 Protein Release, structural integrity, and maintenance of bioactivity.....	50
3.3 Cutaneous protein delivery efficiency of PNIPAM-dPG nanogels .....	52
4. Discussion.....	54
5. Acknowledgement.....	57
6. Referenzen.....	58

**Chapter 4** ..... 61

**Interactions of Hyaluronic Acid with the Skin and Implications for the Dermal Delivery of Biomacromolecules**

Abstract.....	62
1. Introduction .....	63
2. Materials and Methods.....	64
2.1 Materials.....	64
2.2 HEC and HA solution Preparation .....	64
2.2.1 Fluorescence Labeling of BSA and HA.....	64
2.2.2 Preparation of Protein-Containing HEC and HA Hydrogels .....	65
2.3 Attenuated Total Reflectance Fourier Transform Infrared (ATR-FTIR) Spectroscopy Measurements .....	66
2.4 Skin Penetration Experiments .....	66
2.5 Fluorescence Lifetime Imaging Microscopy (FLIM) .....	67
2.6 Statistical Analysis.....	68
3. Results .....	68
3.1 Penetration of HA into normal and tape-stripped skin .....	68
3.2 Penetration of BSA into normal and tape-stripped skin .....	68
3.3. Effects of HA on BSA penetration.....	70
3.4 Molecular interactions between HA and BSA in skin .....	71
3.5 Stratum corneum hydration, keratin conformation, and interactions with the skin lipids.....	74
4. Discussion.....	77
5. Conclusion .....	79
6. Acknowledgments .....	80
7. References.....	80

**Chapter 5** ..... 84

**Feasibility Study for Intra-Epidermal Delivery of Proteins Using A Solid Microneedle Array**

Abstract.....	85
1. Introduction .....	86
2. Materials and Methods.....	87
2.1 Materials.....	87
2.2 Assessment of Optimal Insertion Depth, Fracture and Insertion Force .....	87
2.3 Fluorescence Labeling of Bovine Serum Albumin (BSA).....	88
2.4 Formulation of the Coating Solution .....	88
2.5 Dip-Coating of the MN .....	88
2.6 Determination of Protein Activity.....	89
2.7 Storage Stability of the MN Coatings and Proteins.....	90
2.9 MN Insertion in Pig Skin and Reconstructed Human Skin.....	90
2.10 Cytokine Release Following MN Insertion .....	90
2.11 Statistical Analysis.....	91
3. Results and Discussion.....	91
3.1 Optimal Insertion Depth, Fracture and Insertion Force.....	91
3.2 Dip-Coating, Coating Efficiency and Protein Stability .....	92
3.3 Storage Stability of Protein-Coated MN Arrays .....	94
3.4 Application of Protein Coated MN into Pig Skin and Reconstructed Skin Models.....	96
4. Conclusion .....	97
5. Acknowledgements .....	98
6. References.....	98

**Chapter 6** ..... 100

**Final Conclusion**

1. Dendritic PG-based nanogels with trigger-mediated protein release ..... 100

    1.1 Acid-cleavable dPG-based nanogels for targeted protein delivery ..... 100

    1.2 Thermoresponsive dPG-based nanogels for targeted protein delivery ..... 101

2. HA hydrogels as dermal drug delivery vehicles for proteins ..... 102

3. Solid MN arrays for the intra-epidermal delivery of proteins ..... 103

4. Prospects ..... 105

5. References ..... 106

**Chapter 7** ..... 108

**Summary**

<b>Annex</b> .....	109
1. Biodegradable dendritic polyglycerol nanogels for encapsulation and release of pharmaceutical biomacromolecules.....	109
1.1 Experimental section – general considerations .....	109
1.2 Materials.....	109
1.3 Synthetic procedures.....	110
1.3.1 Preparation of p-propargyloxy-benzaldehyde (pPBA).....	110
1.3.2 Preparation of p-propargyloxy-benzdimethylacetale (pPBDMA).....	110
1.3.3 Preparation of fluorescent nanogels .....	110
1.3.4 GPC characterization of dPG7.7-10- p-PBDMA.....	111
1.3.5 Dynamic light scattering measurements .....	111
1.3.6 Circular dichroism (CD) measurements .....	111
1.4 Figures .....	112
1.4.1 NMR spectra.....	112
1.4.2 Asparaginase release measured by HPLC .....	113
1.4.3 Circular dichroism spectra of proteins.....	114
2. Thermosensitive dendritic polyglycerol-based nanogels for cutaneous delivery of biomacromolecules .....	115
2.1 Materials.....	115
2.2 Synthesis and fluorescence labeling of acrylated dPG (dPG-Ac 5 %).....	116
2.3 Skin penetration tests .....	116
2.4 Figures .....	117
3. Interactions of Hyaluronic Acid with the Skin and Implications for the Dermal Delivery of Biomacromolecules.....	119
3.1 Figures .....	119
4. References.....	121
<b>Publications and presentations associated with the thesis</b> .....	122

# Chapter 1

## Introduction

### 1. Human skin

#### 1.1 Anatomy and physiology

The skin is one of the human body's most mesmerizing components, as it combines several essential and vital functions. It is a sensitive sensory organ, regulates the body's temperature, controls the loss of water from the body and provides protection against external and environmental impacts like microorganisms, UV radiation or simple mechanical harm [1–3].

Mammalian skin is composed of three distinct layers, the epidermis, the dermis and the subcutis (Fig. 1-1) [1,4,5]. Starting on the outside, the epidermis with a thickness of up to 180  $\mu\text{m}$  plays an important part in the skin's regeneration process and barrier properties. With a thickness of 15 to 20  $\mu\text{m}$ , the outermost layer of the epidermis, the stratum corneum (SC), presents the main barrier towards exogenous impacts. The SC has a unique structure consisting of 10 to 15 layers of non-viable, flattened and tightly packed corneocytes which are embedded into a lipophilic lipid matrix. During the skin's life-cycle and regeneration, keratinocytes are developed by cell division in the stratum basale, the innermost layer of the viable epidermis. During their transition to the skin surface, the terminally differentiated keratinocytes undergo apoptosis, a process where they are transformed to corneocytes. These dead, anucleated and cornified cells are mainly built up from keratin filaments as well as lipids, fatty acids and ceramides. Cross-connected by corneodesmosomes, the overlapping corneocytes form a tightly arranged layer that further contributes to the extensive SC barrier characteristics [6]. In-between the corneocytes, a multilamellar matrix mainly composed of cholesterol (25%), cholesterol sulfate (less than 5%), free fatty acids (10 to 15%) and ceramides (45 to 50%) further defines the barrier properties [7]. Compared to other biological membranes, the lipid matrix does not contain phospholipids. The ceramides, which can be categorized into 9 sub-classes, are of special interest, as previous studies have demonstrated a relationship between ceramide composition and impaired skin barrier [8]. Because the ceramides and also the fatty acids are non-branched and without double bonds, the components are able to be laterally packed tightly, which leads to the formation of highly ordered bi-layered gel-phase membrane domains, as described by Madison et al. (2003). These membrane domains are less fluid and permeable than the typical phospholipid-based

biological membranes [7,9]. This intercellular lipid matrix is crucial for the formation of the skin barrier and also influences the percutaneous absorption of exogenous substances [7]. Next to the epidermis lies the dermis (up to 2000  $\mu\text{m}$ ). The dermis is a connective tissue that consists of elastic and collagen fiber networks. These networks provide and support the skin's elasticity, the epidermal structure and embed nerves as well as blood and lymphatic vessels, which are necessary for the skin's immune system and nutrition. In addition, the nerves and blood vessels are needed for the regulation of sensory sensations like pain, pressure or temperature [5,10,11]. Besides these components, the skin includes also appendages like hair follicles and sebaceous glands as well as apocrine and endocrine sweat glands [12]. Further specialized cells are located in the stratum basale of the epidermis, including melanocytes and Merkel cells. The melanocytes provide the skin with pigments, which play a role in UV radiation protection, and the Merkel cells are necessary for the skin's mechano-sensory system. Additionally, the macrophage-like antigen-presenting Langerhans cells and the dendritic epidermal T cells are essential to protect the body from allergens in terms of the skin's immune system [13].

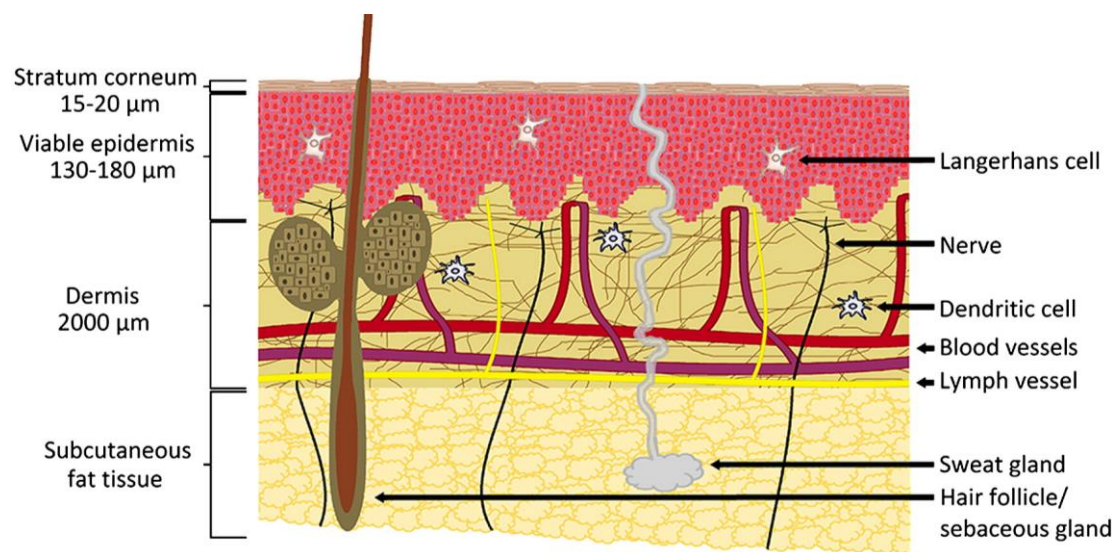


**Figure 1-1** Schematic depiction of the different skin layers, appendages and vessels (printed with permission from Van der Maaden et al., 2012 [11]).

## 1.2 Genetic skin disorders

Healthy skin is commonly characterized by a well-functioning skin barrier, regular skin shedding and moderate hydration, where the skin barrier prevents the intrusion of exogens and allergens as well as regulates the skin's water balance [1–3]. In case of an impaired skin barrier, severe consequences can occur that not only restrict an individual's well-being but

often also involve serious health implications. Classified as skin diseases, the different manifestations of impaired skin often have multifactorial causes and are frequently tied to genetic factors as well [14]. Two common and one rare but well discussed genetically derived skin diseases as well as their current treatment strategies are introduced below.

### **1.2.1 Atopic dermatitis**

Atopic dermatitis (AD) is one of the most common atopic and inflammatory skin diseases and even one of the most common chronic disorders in children besides allergic rhinitis and asthma [15]. Up to 20% of children and up to 3% of adults suffer from AD, commonly starting at an early age. Typical AD symptoms include for instance reddish or brownish scaly, dry, itchy and cracked skin patches, lesions and eczema [14]. The cause of AD is not fully understood yet. However, 50% of affected individuals show a genetic predisposition. It has been discovered that loss-of-function mutations in the *FLG* gene result in a reduced production of the epidermal barrier protein filaggrin and thus impair the skin barrier integrity. Furthermore, the lack of filaggrin negatively impacts the corneocyte and skin lipid formation as well as skin pH and hydration adjustment, as the filaggrin derived metabolites urocanic acid and pyrrolidonecarboxylic acid are likewise reduced [14,16]. However, environmental factors like nutrition and allergens seem to be of pivotal relevance for AD manifestation, too. [14]

### **1.2.2 Psoriasis**

Similarly to AD, the chronic inflammatory skin disorder psoriasis also derives from a mixture of genetic predisposition and exogenous triggers, but stays unraveled concerning its exact etiology. It affects about 2-3% of the European population and is characterized by a sporadic outbreak that typically is initialized in individuals in their twenties [17]. The most common form of psoriasis with approximately 90% sufferers is psoriasis vulgaris (PV) or plaque psoriasis. The PV symptoms include inflammations, extensive skin cell proliferation (leading to a desquamation every 6-8 days compared to the normal regeneration cycle of 40 days) and abnormal differentiation resulting in silvery skin plaques that are often found in the elbow and knee regions. In rare cases, the disease can spread systemically and causes synovitis or arthritis-like symptoms. 10-30% of the affected patients develop an inflammatory arthritis, psoriatic arthritis, which progressively destroys the joints if it is not treated correctly [17]. As the likeliness to develop the disease is 4 to 6 fold increased in individuals with a family history, a genetic or hereditary component is discussed [17]. Genes that are normally only expressed in the basal layer where found to be expressed also in the thickened spinous layer, e.g. the genes encoding for filaggrin, corneodesmosin, epidermal transglutaminase, involucrin or loricrin. Furthermore, an increased release of pro-inflammatory factors like interleukins, tumor necrosis factor  $\alpha$  and interferons is often observed [17,18].

### **1.2.3 Ichthyosis vulgaris**

Ichthyosis vulgaris (IV) is a severe skin disease that is characterized by hyperkeratosis, excessive scaling, xerosis (abnormally dry skin), keratosis pilaris, and palmar/plantar hyperlinearity. In addition, patients suffering from IV also express a strong association with further atopic disorders [19]. IV is genetically linked to a loss-of-function mutation in the filaggrin gene and that condition can be inherited in a semi dominant manner with 83 to 96% penetrance [19]. Here, the produced profilaggrin is truncated, which inhibits the further processing to functional filaggrin subunits. The reduced filaggrin level affects the formation of the cornified envelope of the corneocytes, the correct loading of lamellar bodies and the organization of the lipid bilayers. This ultimately leads to a destabilized and deranged stratum corneum skin barrier [19,20]. Furthermore, the amount of proteolysed filaggrin products like diverse amino acids, polycarboxylic acid and precursors to urocanic acid, which contribute to the natural moisturizing factor (NMF) of the skin, are reduced, which results in dry skin with increased UV sensitivity [19].

### **1.2.4 Current pharmacotherapy for PV, AD and IV**

The treatment of skin diseases is a complex and sometimes challenging task that often needs close collaboration between patients and physicians. Most often a chosen treatment might merely address the symptoms, as the route cause is either barely known or the cause itself can't be treated due to the skin disease complexity or its origin.

Hence, physicians and patients aim for a holistic treatment approach, where on one side external trigger factors need to be avoided and on the other side an optimal skin care needs to be combined with a suited pharmacotherapy [21]. Patients with a less severe course of the skin disease might only need topical treatment, whereas more severe cases may require a potent oral or intravenous therapy [22].

#### ***Atopic Dermatitis***

A basic skin care routine is advised for AD patients with an extra dry skin. Here, hydrating and moisturizing emollients with a high lipid content and ointments with urea (2 to 10%) and propylene glycol (10 to 25%) are recommended to restore and maintain a throughout moisturized skin [19,23]. Sometimes, combinations with UV phototherapy can additionally improve and ameliorate lighter AD courses [23].

Topical corticosteroids are the number one choice in medical treatment due to their efficiency. Used in acute and chronic inflammations, their immunosuppressive and anti-inflammatory properties are used to down-regulate the production of proinflammatory factors like the nuclear factor kappa-light-chain-enhancer of activated B cells and TNF $\alpha$  or to inhibit genes that code for the cytokines IL-1 to 6, IL-8 and IFN- $\gamma$ . The topical application of GCs is,

as said, very effective but also implies severe side effects upon long-term use like skin atrophy [24–27].

To further suppress the immune system and to circumvent skin atrophy, macrolide immunosuppressants like pimecrolimus or tacrolimus, also known as calcineurin-inhibitors, are used. They intervene by suppressing the transcription of cytokine (IL-2 to 5, TNF $\alpha$ ) producing genes and thus help normalizing the patient's immune system response [23,28]. For severe cases a systemic therapy might be necessary. Here, cyclosporin A is one of the best known calcineurin-inhibitor medications. For both short and long term therapy, Cyclosporin A shows a quick response, but needs to be closely monitored due to its nephron- and hepatotoxicity [23].

As a third choice medication, Mycophenolatmofetil is sometimes used in cases where patients didn't respond to any other medication. Despite its efficacy for severe AD, drawbacks are its teratogenicity, the often associated gastrointestinal implications as well as cytopenias [23].

### ***Ichthyosis vulgaris***

For patients with Ichthyosis vulgaris, therapy options are very limited and primarily focus on skin care and reduction of the skin areas with hyperkeratosis. Besides creams with keratolytic (salicylic acid) and hydrating (urea) agents, baths in sodium bicarbonate solution can help soften and remove the scales combined with mechanical exfoliation. For severe cases, the retinoid acitretin can be used for severe cases of skin hornification as well as the vitamin-A acid tretinoin [29].

### ***Psoriasis***

An adapted skin care regiment can help soothing the skin related symptoms like dryness, itchiness and hyperkeratosis. Using keratolytica such as salicylic, lactic or glycolic acid (5 up to 20%) can help shedding the excess skin. Anthralin (Anthra-Derm) creams can help reducing the cell growth of keratinocytes in addition [22].

For light to moderate severe cases, topical corticosteroids remain one of the most widely used treatment options for psoriasis [22]. Despite their usefulness due to a rapid onset, their application is strictly limited to certain doses throughout the week, as side effects like acne, tachyphylaxis and skin atrophy are very likely to occur [22].

Topical (tazaroten) and systemically applied (acitretin, isotretinoin) retinoids may further contribute, as they intervene with the epidermal proliferation and thus down regulate the hyperkeratinization. Another option is the use of vitamin D<sub>3</sub> analogues like calcipotriene, calcitriol and tacalcitol, as vitamin D<sub>3</sub> acts as both vitamin and hormone and thus is able to

regulate cell growth, differentiation, and immune function as well as calcium and phosphorus metabolism [30].

Functioning as a systemic administered immunosuppressant, Methotrexat is administered once-weekly and showed to be a safe, well-tolerated and effective medication. Due to its teratogenicity, strict contraception is inevitable [23,31].

Since patients with mild to severe PV are often struggling a lifetime, new targeted and sophisticated treatment options needed to be introduced that enabled a continuous and potentially more effective therapy with less side effects [18]. Biologic agents have been developed that target crucial biophysiological pathways and immune cells in the genesis of PV. Adalimumab (Humira®), a human monoclonal immunoglobulin G1 antibody against TNF $\alpha$ , is an approved biologic in the treatment of rheumatoid arthritis, psoriatic arthritis and chronic plaque psoriasis. It is administered every 2 weeks subcutaneously and, after systemic uptake, binds to TNF $\alpha$  and thus blocks the interaction with cell surface TNF $\alpha$  receptors with significant patient responses. Although adalimumab was able to relieve both skin and arthritis conditions, the general immunosuppressant properties and reactivated tuberculosis cases accompanied by the systemic administration need to be considered [18]. Similar to adalimumab further biologics targeting TNF $\alpha$  antibodies, e.g. etanercept (Enbrel®), infliximab (Remicade®), also achieve good results in PV treatment [32,33]. Etanercept, a fusion protein composed of human IgG1 Fc region and human TNF type II receptor (TNF-Rp75), binds to soluble TNF $\alpha$ , whereas the *i.v.* administered infliximab, a chimeric monoclonal antibody, also binds to membrane-bound TNF $\alpha$ . But as seen for adalimumab, etanercept and infliximab unfortunately also bear a high risk of opportunistic infections associated with the suppressed immune system [18,32,33]. Ustekinumab (Stelara®) is a relatively new developed monoclonal IgG1k antibody that binds to the p40 subunit of IL-12 and IL-23, thus blocking their interactions with their receptors[31]. Here, Ustekinumab is administered every 12 Weeks (after an initial application and a consecutive second dose after 4 weeks) and adverse effects were limited to minor infections [31].

Hence, biologically derived therapeutics and antibodies represent an important and constructive pillar in severe genetic skin disease treatment and need to be the focus of attention in future therapeutic development. To eradicate side effects associated with *s.c.* and *i.v.* administration, the application of these biologics could be shifted to topical and dermal administration options.

## 2. Dermal drug delivery and skin penetration

### 2.1 Characteristics of skin penetration

The increasing interest of the pharmaceutical industry in dermally applied products is reflected in the number of drugs that are investigated for topical application in clinical trials, which currently represent one third of all investigated drugs [34]. Although dermally applied drugs may offer many advantages, like by-passing the enterohepatic cycle, painless application, controlled drug release, dermal drug delivery and less systemic side effects, they also oppose some challenges [35,36].

The dermal penetration of a drug after topical application is highly dependent on the skin's main barrier, the SC and occurs mainly via passive diffusion [12]. As previously described, the dense packing of the corneocytes, their tight interconnection by desmosomes and the corneocyte surrounding lipid matrix are in charge for the restricted and limited uptake of applied substances [7,35,37]. In general, there are three pathways known through which a drug can penetrate into the skin: the shunt or transappendageal route (including the penetration through the sweat glands, the hair follicles, and the sebaceous glands, which is most suitable for hydrophilic compounds), the intercellular (for the mainly lipophilic compounds), and the transcellular route, which most of the hydrophilic compounds have to follow [5,38]. Furthermore, the penetration of a drug is highly dependent on the drug's physico-chemical properties. Concerning the size, small substances with a molecular weight of less than 500 Da are preferred due to the skin's distinct total cut-off of 800 Da [38]. For an easy passive diffusion, a moderate lipophilicity ( $\log P = 1$  to 3) is supportive. As the drugs mostly have to travel through the intercellular lipid matrix, water-soluble or hydrophilic compounds will be highly restricted in their penetration via certain routes [38]. On the other hand, high lipophilicity displayed by an octanol-water partitioning coefficient larger than  $\log P$  3 may eventually result in trapping of the drug in the intercellular matrix, as these high lipophilic compounds may be impeded by the hydrophilic regions in the lipid bilayer [5,38–41]. After the dermal application, the drugs penetrate depending on Fick's first law, which describes the passive diffusion of the drug across the skin with the following equation [5]:

$$J = \frac{(K \cdot D)}{h} \cdot \Delta c$$

*J* = diffusion velocity/ steady-state flux ( $\mu\text{g} / \text{cm}^2 \cdot \text{h}$ )

*K* = distribution coefficient (cm/h)

*D* = diffusion coefficient of the membrane ( $\text{cm}^2/\text{h}$ )

*h* = thickness of membrane (cm)

$\Delta c$  = concentration differences ( $\mu\text{g}/\text{cm}^3$ )

Hence, the permeation is determined by factors like the area of treated skin, the body region reflected in the skin thickness, the drug concentration and solubility in its vehicle and the release from it. Additionally, skin hydration, temperature, pH are also relevant influencing parameters that need to be considered [42].

Although the majority of drugs and substances penetrate the skin via the intercellular and transcellular route, the transappendageal route offers a potential alternative. Despite only 0.1 to 1% of the total skin surface is covered with hair follicles and sweat glands, especially the hair follicles are considered as potential “shunts”, areas that offer less resistance to the penetration of mainly hydrophilic compounds [12,37,38]. With a thinner SC layer at the base and a surrounding network of blood capillaries, a more rapid passage through the hair follicles and uptake into the blood stream is discussed for nanoparticles and liposomes [12]. The likeliness of a nanoparticle-based system to penetrate skin is not clearly revealed yet. But it is assumed that particles > 10 nm are unlikely to penetrate the SC directly. Instead they tend to accumulate in hair follicles and may enter or deliver the drug into the viable epidermis via the transappendageal route [12]. But as the number of those porous orifices is rather low, the quantitative benefit of the transappendageal route has to be questioned [43].

## **2.2 Systems for dermal drug delivery testing**

To evaluate skin permeation and penetration of drugs in order to study new dermal drug delivery systems, *in-vitro* experiments are an attractive alternative to *in-vivo* studies. The latter are often ethically questionable or need a safe and sound rationale to be fully acknowledged by the regulatory authorities. The validated approach for *in-vitro* set-ups is the use of diffusion cells (Franz diffusion cells) that can be either used in a static or flow-through mode. To mimic bio-physiological conditions, different types of membranes or barriers are used to study drug permeation / penetration [44]. Excised animal skin, most commonly from pigs or rats, can serve as cost effective and simple experimental model. Pig skin is favored as it has a similar structural composition as human skin and depicts the same epidermal properties as well as amount of hair coat in its morphology. Although pig skin is established for *in-vitro* testing [44–46], it still holds some disadvantages. Compared to human skin, pig skin has a higher degree of vascularization and sebaceous gland distribution. Furthermore, the SC is thicker, which may lead to altered diffusion characteristics compared to human conditions. The skin of furry animals, such as rats and mice, is also an alternative for testing, but is disadvised due to a different skin morphology including many skin appendages, hair follicles and different SC lipid composition, which makes the skin more permeable compared to pig or human skin [44]. Although working with human skin is preferred, the access to human skin is restricted since the main sources are limited and originate from skin removal surgery (breast or abdomen) or post-mortem skin donations. Therefore, reconstructed human skin is commonly used as a substitute and was developed to achieve skin models with

humanized features [44,45]. Reconstructed human skin can be divided into epidermal (SC and viable epidermis) and full thickness skin models (SC, viable epidermis and dermal equivalent) [44]. Some of the commercially available models were subjected to validation processes concerning phototoxicity, irritation and corrosion testing and are now implemented in the OECD (Organization for Economic Co-operation and Development) guidelines for these tests [44,47,48], e.g. EpiSkin™ SM (SkinEthic, Lyon, France) and EpiDerm™ SCT (MatTek, Ashland, MA). Unfortunately, these models are not yet fully acknowledged by the OECD for skin absorption testing [44]. One of the main reasons is the higher permeability of reconstructed human skin, as it still shows differences in the skin lipid composition and the skin barrier properties [44]. Compared to native human SC some of the models show significantly different lamellar ordering of SC lipids, the lack of polar ceramides or less triglycerides, which all contributes to an altered skin barrier. In addition, reduced expression of differentiation-related keratins was observed, leading to disturbed keratinocyte differentiation [44]. However, reconstructed human skin allows for specific alterations, e.g. gene modifications to mimic selected skin diseases like AD [16,49,50] or psoriasis [51]. This enables customized and patient oriented research towards the development of new therapeutics or therapeutic drug delivery systems.

### **2.3 Expectations and challenges of dermal biomacromolecule delivery**

Biomacromolecules as therapeutic compounds are very important and highly researched in pharmaceutical industry, as they often offer a higher efficiency, potency and specificity in the treatment of severe diseases with complex and heterogenic characteristics, e.g. infections, cancer or autoimmune diseases [36,52,53]. Marketed products like Herceptin® (trastuzumab), an antibody used in the successful treatment of HER2-positive breast cancer patients where it selectively blocks the overexpressed human epidermal growth factor receptor 2 (HER2) [54], Humira® (adalimumab), an inhibitor for the TNF $\alpha$  used in the treatment of chronic inflammatory diseases [55], and others [56] show the importance of this class of therapeutics for developing a patient oriented and personalized treatment [57,58].

But as promising biomacromolecules and specifically proteins are for fighting severe diseases, they are challenging due to their physicochemical characteristics. They are typically hydrophilic and complex structures with high molecular weights, starting for peptides at 300 Da and going up to 1000 kDa for proteins [36,59]. Because of their fragile nature, proteins often suffer from instability and are prone to chemical change, denaturation, and aggregation. Common risks are presented through factors like shear or agitation stress, pH or ionic strength changes, light and higher temperatures. Chemical modifications include processes like oxidation, disulfide bond breakage, hydrolysis, deamidation and N-terminal and C-terminal changes [60,61]. Upon unfolding, the higher order structure is changed and

proteins also become prone to form aggregates, which can lead to a loss in biological activity or may enhance the patients' immune response to the protein drug molecules [61–65].

Because of their size and hydrophilicity, biomacromolecules are classically administered parenterally. But for treatments of topical diseases, local dermal delivery of proteins proposes an appealing alternative. The dermal route shows an increased patient compliance due to the painless and easy application. The administered therapeutics can be actively controlled for sustained delivery or for a discontinuation of treatment. Additionally, the targeted administration of the drug into the skin tissue without systemic uptake reduces the associated side effects. But the mentioned physicochemical properties of proteins pose a significant problem for the penetration through biological barriers, especially the SC. With their high molecular weight they are clearly above the SCs cut-off (800 Da) and their hydrophilic properties almost completely restrict skin penetration or permeation [5,36,66,67].

In summary, as biomacromolecules are an essential source for the treatment of severe diseases, further research is necessary to develop smart drug delivery systems, which may enable to treat skin diseases locally instead of parenterally [55]. They could hypothetically benefit from locally applied protein drugs in terms of a low dose substitution therapy, by which disease specific deficient proteins could be replaced by administration without or with less systemic side effects compared to the i.v. route. Aufenvenne et al. (2013) investigated the efficacy of liposomes loaded with transglutaminase-1 (TGase-1) for local topical enzyme replacement in TGase-1 deficient skin grafts. The authors could show that the protein activity as well as the correct skin architecture and skin barrier could be restored upon enzyme replacement [68]. Similarly, Stout et al. (2013) developed a filaggrin-cell penetrating peptide conjugate, which was able to restore a normal phenotype in filaggrin-deficient flaky tail mice after application and uptake of the conjugate [69].

### **3. Systems for dermal drug delivery**

The main obstacle for an efficient protein delivery into human skin is to overcome of the skin barrier represented by the SC without damaging the biomacromolecules or compromising their biological activity. The most noteworthy formulation attempts and drug delivery systems or vehicles for this are summarized in figure 1-2 and representative systems are introduced below.

Delivery enhancers, which include chemical penetration enhancers and substances that increase the SC hydration, are a useful tool to increase a drugs' skin permeability, solubility and partitioning into the skin in general [66,67]. Alcohols (ethanol), surfactants (sodiumlaurylsulfate, N-decylmethyl sulfoxide), phospholipids, esters, amines, amides and fatty acids act by altering the SC lipid bilayer by either fluidizing or extracting the lipids. Co-

solvents like polypropylene glycol enhance these effects as they help dissolving the penetration enhancers in the SC [42,70,71]. Substances like paraffin, oils from emulsions, as well as gelling agents like hyaluronic acid act as a water reservoir and partially as occlusive agents on the SC surface and thus increase the SC hydration and consequently the permeability of mostly hydrophilic but also lipophilic drugs [5,72]. However, as proteins are rather large, a high quantity of chemical enhancers would be necessary to achieve penetration effects, which is a concern in terms of toxicity, skin irritation induction, and protein stability in the vehicle [71].

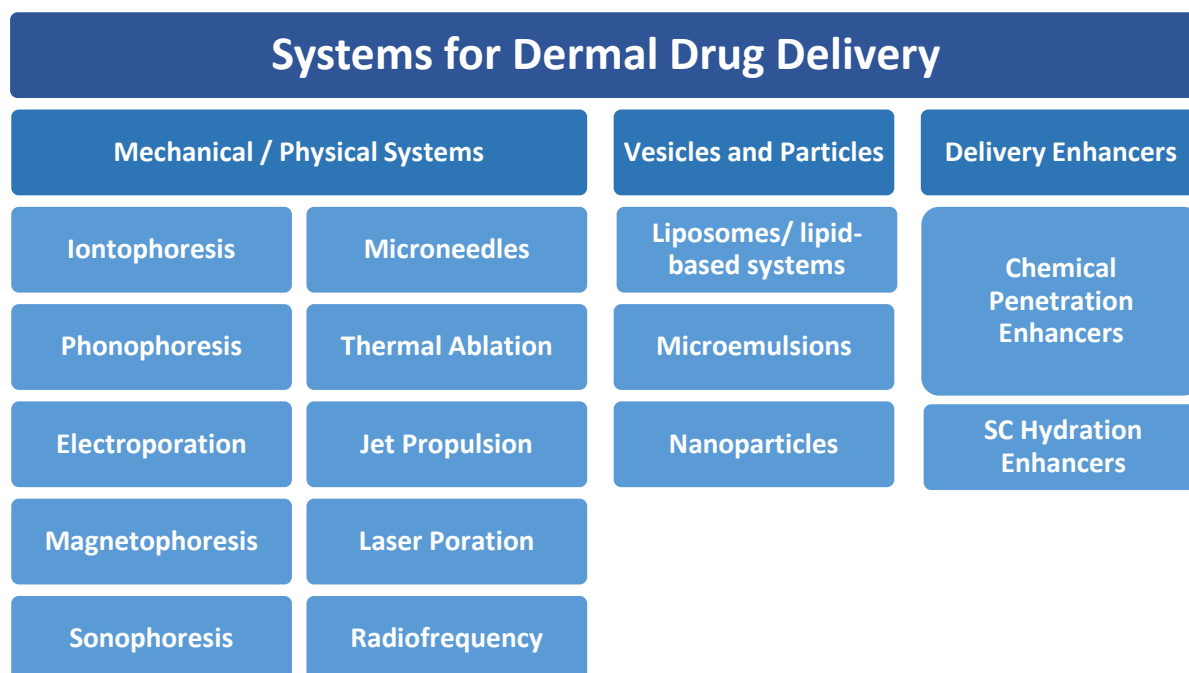


**Figure 1-2** Dermal drug delivery strategies for proteins.

Delivery enhancers, which include chemical penetration enhancers and substances that increase the SC hydration, are a useful tool to increase a drugs' skin permeability, solubility and partitioning into the skin in general [66,67]. Alcohols (ethanol), surfactants (sodiumlaurylsulfate, N-decylmethyl sulfoxide), phospholipids, esters, amines, amides and fatty acids act by altering the SC lipid bilayer by either fluidizing or extracting the lipids. Co-solvents like polypropylene glycol enhance these effects as they help dissolving the penetration enhancers in the SC [42,70,71]. Substances like paraffin, oils from emulsions, as well as gelling agents like hyaluronic acid act as a water reservoir and partially as occlusive agents on the SC surface and thus increase the SC hydration and consequently the permeability of mostly hydrophilic but also lipophilic drugs [5,72]. However, as proteins are rather large, a high quantity of chemical enhancers would be necessary to achieve penetration effects, which is a concern in terms of toxicity, skin irritation induction, and protein stability in the vehicle [71].

Colloidal carrier systems such as liposomes, solid lipid nanoparticles (SLN), dendrimer nanoparticles and microemulsions are considered to assist and enhance the localized delivery of biomacromolecules and have been in focus of research for many years [66,71]. For instance, liposomes and lipid-based carriers are known to interact with the SC lipids and have been shown to deposit their payload in the SC and the upper skin layers [12,66,70,71].

Within the group of the physical and mechanical systems, iontophoresis is one of the most extensively researched and more successful techniques for biomacromolecule delivery [67]. Iontophoresis has been investigated and established for small molecule drugs like lidocaine or fentanyl with good results in anesthesia and analgesia, where drug delivery is mediated by SC disruption caused by applying continuous low-voltage currents [66]. As iontophoresis offers a non-invasive and continuous skin delivery, its potential for protein and peptide skin delivery has also been investigated [67,73,74], but was restricted to molecules with sizes between 10 to 15 kDa and a high isoelectric point, as a positively charged protein is more effectively delivered into the negatively charged surface of the skin using anodal iontophoresis [67].

Dermal drug delivery systems and devices for proteins need to combine an easy preparation, easy application, good patient compliance, efficient and steady drug administration during the treatment, as well as protein stability. In the following sections, three different drug delivery vehicles and systems are introduced that include these attributes. To our knowledge, these systems have not been investigated in terms of localized and targeted dermal delivery of proteins with regard to replacement therapy in skin diseases yet and were selected as candidates for this thesis.

### **3.1 Nanoparticle-based release systems**

Nanoparticles and nanoparticle-based release systems have been increasingly used over the last thirty to fifty years due to their versatility and flexibility in preparation and use. Basically, nanoparticles vary broadly with respect to the used material, their morphology and in size. Popular nanoparticles include e.g. solid lipid nanoparticles, virus-like nanoparticles, quantum dots, liposomes and dendrimers [12,75]. Further diverse nanoparticulate carriers may also be prepared from natural polymers (ovalbumin, chitosan, hyaluronic acid, modified chondroitin sulfate) or synthetic polymers (poly (ethylene glycol)-b-poly (methacrylic acid), poly (N-isopropylacrylamide- co-acrylic acid), poly (N-isopropylacrylamide)) [76]. Recently, nanoparticles and nanogels based of dendritic or hyperbranched polyglycerol chains gained interest in the development of protein-compatible drug delivery systems [77].

### 3.1.1 Polyglycerol-based nanogels

Polyglycerol is a very versatile and flexible compound that can easily be modified to yield hyperbranched dendrimer-like structures. Its advantages for drug delivery include a very good biocompatibility, non-cytotoxicity, haemocompatibility, adjustability in size with narrow polydispersities, good solubility in polar and aqueous solutions and good compatibility with proteins [78–82]. Hyperbranched or dendritic polyglycerols (dPG) can be defined as globular PG structures that display a single core from which multiple branches radiate in a dandelion-like setting (Fig. 1-3).

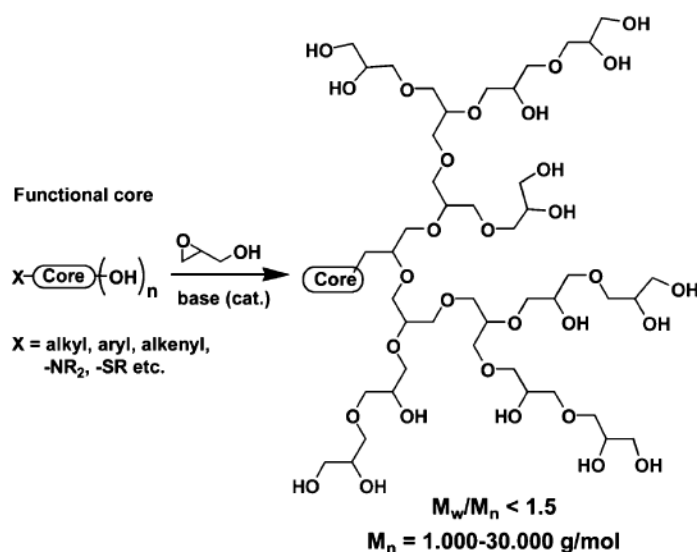


**Figure 1-3** Synthesis and schematic structure of dendritic polyglycerol (modified and reprinted with permission from [77]).

They are traditionally prepared by ring opening polymerization of glycidol by either anionic or cationic means. Polymers of 10 to 100 nm (diameter ~ 10nm) can be obtained [81,83]. In aqueous solution, dPGs take up water, swell and thus show the characteristics of both a hyperbranched polymer and a cross-linked macroscopic gel. Hence, dPG solutions can be classified as nanogels: nano scaled polymer networks that are able to absorb water into the network when surrounded by an aqueous environment. Additionally, the generally mild reaction conditions allow the incorporation of proteins without damage [79]. Hence, these dPG-based are suitable candidates for local topical delivery and other drug delivery applications of proteins [75,79,82].

### 3.1.2 Functionalization and targeted drug delivery

One of the most interesting characteristic of the dPG nanogels is the opportunity to introduce dPG-chain functionalization or macro-crosslinkers. Tackling the crosslinkers, a stimuli-responsive payload release can be achieved, e.g. upon change in pH, temperature, or by an

electrical or magnetic field [81,84–88]. Depending on the introduced functional group, the release kinetics of the dPG can be tuned. Whereas functional groups like acetals or ketals are cleaved by pH stimuli, reductive environments act on groups such as disulfide bridges [82]. Upon the stimuli, the dPGs respond with degradation into lower molecular weight fragments and release of the incorporated drug [89]. The pH triggered drug release is especially interesting for targeted drug delivery to inflamed or cancerous tissue, where the pH is slightly acidic (solid tumors ~ pH 6.0; inflamed tissues ~ pH 6.5-6.0; endosome/lysozyme cellular compartments ~ pH 5.0 -5.5) [82,90]. The nanogel degradation appears upon contact of the acetal or ketal macro-crosslinkers with peripheral protons present at the site of action by means of acid-catalyzed hydrolysis [82,91]. Introducing thermoresponsive polymers like poly(N-isopropylacrylamide) (PNIPAM), the dPG can be combined with a temperature trigger, where the dPG responds with a rapid change in conformation due to drastic swelling or de-swelling. In this case, the drug release kinetics depend highly on the rate at which the nanogel shrinks, as the drug is literally squeezed out from the network [83,84,92].

### **3.1.3 The potential of dPG-based nanogels in drug delivery**

The main therapeutic focus is application of dPG-based nanogels in cancer therapy. The nanogels loaded with cytotoxic drugs are administered *i.v.* and the release is triggered at the tumor tissue site [84,88,90,93]. Nagasaki et al. (2007) worked with core-shell type PEGylated nanogels made from core-cross-linked poly[2-(N,N-diethylamino)ethyl methacrylate] and tethered PEG chains for half-life extension. Equipped with a swelling mechanism upon pH trigger, they were able to demonstrate successful and controlled release of doxorubicin into endosomal compartments of a drug-resistant HuH-7 tumor cell line (hepatic cellular carcinoma) [94]. Combining PNIPAM with dPG-based polyglycerol, Cuggino et al. (2011) introduced a precipitation polymerization method for the preparation of thermoresponsive nanogel systems of 50 to 200 nm that showed structural phase transitions at a temperature of 32.5 to 34.6 °C. Although cell compatibility and viability tests revealed a non-cytotoxic and even cell-penetrating behavior, unfortunately no drug delivery experiments were carried out [84]. Steinhilber et al. (2011) demonstrated the biological compatibility for encapsulated biomaterials. The authors encapsulated yeast cells during the free-radical polymerization of dPG-decaacrylate and polyethylene glycol-diacrylate with cell viabilities up to 80% [79]. Furthermore, different research groups used diverse nanogels to incorporate proteins like insulin/ BSA/  $\beta$ -galactosidase [95], horseradish peroxidase [96], and lysozyme [97].

## 3.2 Hyaluronic acid for dermal drug delivery

### 3.2.1 Structure and physico-chemical characteristics of HA

Hyaluronic acid (HA), or hyaluronan when present as polyanion *in-vivo*, is a polysaccharide found in the intercellular matrix in vertebrates and bacteria [98,99]. Extracted from rooster combs, umbilical cords, or bacteria, HA is generated at various molecular weights (~ 5 kDa up to ~ 5 MDa) [99]. HA has many advantageous properties like good biocompatibility, non-immunogenicity, biodegradability and viscoelasticity. These properties render a perfect biomaterial for the pharmaceutical and cosmetic sector [99]

Built from repeating units of D-glucuronic acid and N-acetyl-D-glucosamine, HA's primary structure arranges into an unbranched linear chain with the monosaccharides linked together through alternating  $\beta_{1,3}$  and  $\beta_{1,4}$  glycosidic bonds (Fig. 1-4) [72,99].

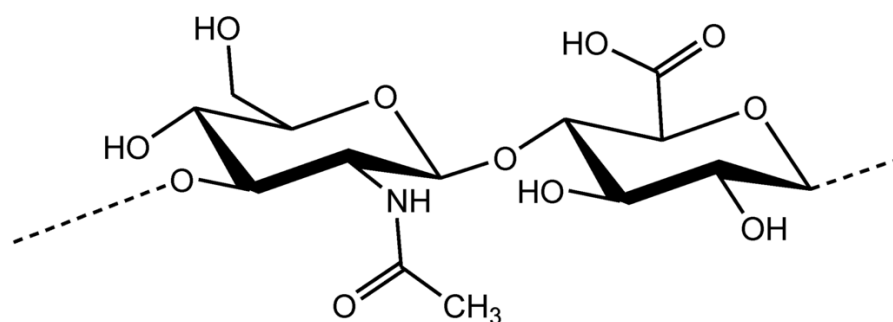


**Figure 1-4** Chemical structure of the disaccharide unit of hyaluronic acid (printed with permission from [100]).

In aqueous solution, HA molecules are suggested to assume an expanded random coil structure with a highly entangled network, which is strongly hydrated with up to 15 water molecules bound per disaccharide unit [99,101]. The swelling behavior depends on factors such as pH, ionic strength and degree of cross-linking [101]. With an isoelectric point of 8.6 and an intrinsic pK value of the carboxyl group of 3.21, HA gels reach their swelling equilibrium at pH 6, while they collapse at lower pH. With the addition of salt, the equilibrium swelling at pH 7 is decreased due to charge shielding. Looking at the temperature, the swelling behavior was only affected to minor degrees [101].

The viscosity of HA gels increases substantially with HA molecular weight and concentration and strongly depends on the pH. The addition of phospholipids, which compete with HA molecules for the hydrophobic binding sites, and sodium chloride, which shields electrostatic repulsion between HA molecules, decrease both the viscous and the elastic modulus. In contrast, sugars appear to promote the HA gel structure, enhancing the interaction between HA molecules and decreasing their hydrodynamic radius [99].

## **3.2.2 HA in drug delivery**

### **3.2.2.1 General drug delivery aspects of HA**

HA has found its way into many drug delivery areas including ophthalmic, nasal, pulmonary and parenteral drug delivery due to its either hydration-rendering, wound healing or lubricant properties, where HA was able to increase the bioavailability, e.g. for ophthalmically administered drugs like pilocarpine, and the local tissue adhesion of the incorporated drug [99]. In addition, HA also provides a stabilizing network surrounding [102,103].

Very unique is the use of HA conjugates in cancer treatment for specific site targeting into the lymphatic tissues [99,100]. Luo et al. (2005) report the use of a HA – taxol conjugate, which selectively targeted the cancer tissue in the breast, colon and ovarian cancer cells [104]. Other interesting approaches address the HA cell receptor CD44 that is often overexpressed in drug-resistant cancer cells and cancer stem cells [105]. Wei et al. (2012) investigated the efficiency of a cholesterol modified HA-drug conjugated nanogels using etoposide and salinomycin and curcumin. The small nanogel (20 to 40 nm) and a drug load of approx. 20% showed 2 to 7 times higher cytotoxicity in CD44-expressing drug-resistant breast and pancreatic cancer cell compared to the free drugs. Due to the binding of HA to the CD44 receptor and the sustained drug release following ester linkage hydrolysis, the drug accumulated to much higher extent in the cancer cells [105].

### **3.2.2.2 Transdermal and dermal drug delivery of HA**

HA is widely used as topical and dermal drug delivery vehicle and formulation excipient in the treatment of various skin conditions and diseases, providing improved skin hydration, regenerating skin elasticity and enhancing wound healing [72,98,106,107]. HA is also known to act as a topical drug delivery enhancer for NSAIDs like diclofenac. Solaraze® (3% diclofenac in 2.5 % HA), is an alternative to surgery in the treatment of actinic keratosis [72]. Concerning the mode of action, different hypotheses are discussed. Firstly, the skin absorption of diclofenac may be facilitated due to increased skin hydration through the swollen SC, providing an increased hydrophilic environment for the drug permeation [72]. Secondly, co-transport of the active and HA is discussed [108]. Additionally, HA and the drug may be actively transported via HA receptors (hyaladherins, CD44) expressed on the cell surface of keratinocytes [103]. The theory also provides the basis for the testing of a HA – human growth hormone conjugate (HA-hGH), which was investigated by Yang et al. (2012) [103]. Proliferative effects in keratinocytes and fibroblasts could be demonstrated and elevated levels of phosphorylated Janus kinase 2 (p-JAK2) also confirmed the biological activity of the HA-hGH conjugate in fibroblasts [103]. As these experiments were carried out in cultured cells, the efficacy of the HA conjugate still needs to be evaluated in dermal application. Concerning the HA mediated dermal delivery of high molecular weight

biomolecules into the skin, scarcely any research is published that does not include the use of microneedles (MN) or other penetration-facilitating devices. This highlights the need for further research on both the HA drug delivery vehicle and the mode of action of HA-mediated biomacromolecule delivery, which will be covered in this thesis.

### **3.3 Solid microneedles for dermal drug delivery**

#### **3.3.1 MN fabrication and characterization**

As mentioned earlier, dermal drug delivery is limited to a small group of drugs due to the extensive barrier properties of the SC. The easiest way to overcome the SC barrier is mechanical perforation. Besides techniques like electroporation, microdermabrasion or needle-free jet injectors, microneedles (MN) are a straightforward approach to selectively pierce the SC [66,109,110]. Shorter needles improve the patient's safety but still enable drug delivery to the target site. They are designed to avoid the stimulation of nociceptors, which are located in the upper dermis, making MN application practically pain free [110]. To increase the effectiveness of drug application, MNs are usually designed as arrays. As single-use units, the use of MN can help to prevent infections or the transfer of contagious diseases [111]. Many types of MN made of diverse materials emerged (Fig. 1-6), e.g. solid MN made of silicon, metal, glass, ceramics and polymers. They are classically produced by either lithographic, and wet or dry etching techniques [111].

#### **3.3.2 Drug application techniques and formulation aspects**

When the SC is pierced with a MN arrays, a micro channel is generated whose depth depends on the MN needle length and manner of application [112,113]. To deliver a drug, the drugs are either applied onto the skin before or after MN application as solutions, gels, creams, ointments or drug infused patches [111,113]. The drug reaches the epidermis and deeper dermal layers by diffusion into and through the microchannels [110]. Alternatively, the drug is directly coated onto the MNs. Upon application, the solid coatings dissolve in the interstitial fluid [110,111]. Typically, the coating is produced by dipping processes, generating a thin film on the needle tips. To achieve a uniform and reproducible coating, the appropriate excipients need to be selected [114]. Mixtures of different viscosity enhancers or gelling agents (e.g. carboxymethyl cellulose, hyaluronic acid, sodium alginate, xanthan gum), sugars (e.g. sucrose, saccharose, trehalose) and surfactants (e.g. diverse polysorbates and poloxamers) were successfully developed to form a reproducible coating providing adequate stability for incorporated proteins [114–117].

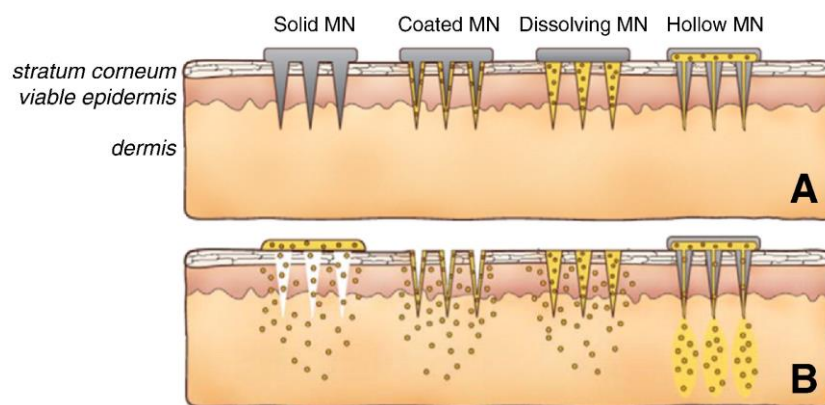


**Figure 1-5** Schematic display of four MN types after skin application (A) and their mode of action in drug delivery (B) (printed with permission from [110]).

Another different approach is the embedding of the drugs into dissolvable MN made of preferentially polymers (e.g. carboxymethyl cellulose, hyaluronic acid, poly(lactic-co-glycolic) acid) and sugars, such as dextrans, dextrans and sucrose. These MN are prepared commonly by micro-molding of polymer/sugar solutions or tip drawing of polymer/sugar melts [111,118,119]. As the amounts of drugs that can be delivered by these three described approaches are limited, hollow microneedles have been developed, which offer the opportunity to apply larger quantities. The application of 0.2 up to 15 mL drug solution may be possible as presented by Becton Dickinson Technologies (Microinfusor™) [111].

### 3.3.3 Dermal drug delivery mediated by MN

MNs offer a low-cost, easy-to-manufacture and flexible delivery device. Therefore, these devices are a promising option for the topical delivery of complex and sensitive biomacromolecules [110]. As protein mostly require low doses in the microgram range, MN are a suitable platform for their administration [110]. Consequently, MNs were recently studied to deliver diverse peptide hormones e.g. insulin [120,121], desmopressin [122], erythropoietin [123], or the human growth hormone [124]. Furthermore, the use of MN for intradermal vaccination against measles [125] or influenza [126,127] is very appealing. MN mediated vaccination is a particularly attractive approach since the vaccines can be directly administered into the viable epidermis resulting in a strong and more potent immune response due to the rapid targeting of Langerhans and dermal dendritic cells [114,128,129].

## 4. Objectives of the thesis

The goal of the thesis was the development and characterization of three different systems for local and targeted intraepidermal delivery of biomacromolecules. As incidences of skin diseases like atopic dermatitis are on the rise in the industrialized countries affecting especially children, adequate and effective therapies become more and more important.

Although the causes for the diseases are often multifactorial, a certain patient population suffers from genetic conditions that result in highly down regulated epidermal levels of functional proteins. Since these proteins are essential in the viable epidermis for the development of a healthy skin barrier, the substitution of the lacking proteins, such as transglutaminase or filaggrin, is an interesting starting-point for a new therapeutic concept.

Therefore, the presented thesis aims to introduce three delivery systems based on innovative concepts, which were either adapted or modified for topical and especially dermal protein delivery and intensively investigated for their intraepidermal delivery yields and mechanisms.

The three objectives of the thesis can be summarized as followed:

- 1.) In cooperation with the FU Berlin (AG Haag, AG Caldéron), dPG-based nanogels were developed and modified to suit the properties of protein encapsulated topical and dermal delivery systems. The process and release-trigger adapted dPG nanogels were characterized and investigated for controlled protein release and stability. The release yield was assessed as a function of skin barrier integrity. dPG nanogel-based transglutaminase-1 substitution in a deficient skin model was evaluated as proof-of-concept.
- 2.) HA, a versatile polysaccharide that already demonstrated to promote the dermal drug delivery of small-molecule drugs like diclofenac, was explored as topical protein delivery system with focus on the influence of HA molecular weight and concentration. The delivery yield was investigated as a function of skin barrier integrity. To unravel the mode of action, interactions of HA with protein and SC was studied.
- 3.) As solid stainless-steel MN established a reputation to be valuable tools in vaccine delivery, their potential for skin disease treatment was evaluated. Here, the feasibility and the adequate MN properties for localized intraepidermal protein application were investigated and the MN's potential for skin irritation was assessed. Furthermore, special attention was set on the in-process and storage stability of coated MN, an important factor that was thitherto sparsely regarded in literature.

## 5. References

1. Menon GK, Cleary GW, Lane ME. *The structure and function of the stratum corneum. Int. J. Pharm.* 435(1), 3–9 (2012).
2. Natarajan VT, Ganju P, Ramkumar A, Grover R, Gokhale RS. *Multifaceted pathways protect human skin from UV radiation. Nat. Chem. Biol.* 10(7), 542–51 (2014).
3. Pasparakis M, Haase I, Nestle FO. *Mechanisms regulating skin immunity and inflammation. Nat. Rev. Immunol.* 14(5), 289–301 (2014).
4. Wertz PW. *Current understanding of skin biology pertinent to skin penetration: Skin biochemistry. Skin Pharmacol. Physiol.* 26, 217–226 (2013).

5. Mbah CJ, Uzor PF, Omeje EO. Perspectives on transdermal drug delivery. *J. Chem. Pharm. Res.* 3(3), 680–700 (2011).
6. Norlén L. Stratum corneum keratin structure, function and formation – a comprehensive review. *Int. J. Cosmet. Sci.* 28(6), 397–425 (2006).
7. Madison KC. Barrier Function of the Skin: “La Raison d’EOE tre” of the Epidermis. *J. Invest. Dermatol.* 121(2), 231–241 (2003).
8. van Smeden J, Hoppel L, van der Heijden R, Hankemeier T, Vreeken RJ, Bouwstra JA. LC/MS analysis of stratum corneum lipids: ceramide profiling and discovery. *J. Lipid Res.* 52(6), 1211–1221 (2011).
9. Elias PM. Structure and Function of the Stratum Corneum Extracellular Matrix. *J. Invest. Dermatol.* 132(9), 2131–2133 (2012).
10. McGrath JA, Eady RAJ, Pope FM. Anatomy and Organization of Human Skin. In: *Rook’s Textbook of Dermatology.* , 45–128 (2004).
11. Van Der Maaden K, Jiskoot W, Bouwstra J. Microneedle technologies for (trans)dermal drug and vaccine delivery. *J. Control. Release.* 161(2), 645–655 (2012).
12. Prow TW, Grice JE, Lin LL, et al. Nanoparticles and microparticles for skin drug delivery. *Adv. Drug Deliv. Rev.* 63(6), 470–491 (2011).
13. Salmon JK, Armstrong CA, Ansel JC. The skin as an immune organ. *West. J. Med.* 160(2), 146–152 (1994).
14. Nutten S. Atopic Dermatitis: Global Epidemiology and Risk Factors. *Ann. Nutr. Metab.* 66(suppl 1(Suppl. 1), 8–16 (2015).
15. Stone KD. Atopic diseases of childhood. *Curr. Opin. Pediatr.* 15(5), 495–511 (2003).
16. Vávrová K, Henkes D, Strüver K, et al. Filaggrin deficiency leads to impaired lipid profile and altered acidification pathways in a 3D skin construct. *J. Invest. Dermatol.* 134(3), 746–53 (2014).
17. Roberson EDO, Bowcock AM. Psoriasis genetics: breaking the barrier. *Trends Genet.* 26(9), 415–423 (2010).
18. Alwawi EA, Mehlis SL, Gordon KB. Treating psoriasis with adalimumab. *Ther. Clin. Risk Manag.* 4(2), 345–351 (2008).
19. Thyssen JP, Godoy-Gijon E, Elias PM. Ichthyosis vulgaris: The filaggrin mutation disease. *Br. J. Dermatol.* 168(6), 1155–1166 (2013).
20. Smith FJD, Irvine AD, Terron-Kwiatkowski A, et al. Loss-of-function mutations in the gene encoding filaggrin cause ichthyosis vulgaris. *Nat. Genet.* 38(3), 337–342 (2006).
21. Hon K, Leung AC, Barankin B. Barrier Repair Therapy in Atopic Dermatitis: An Overview. *Am. J. Clin. Dermatol.* 14(5), 389–399 (2013).
22. Federman DG, Froelich CW, Kirsner RS. Topical psoriasis therapy. *Am. Fam. Physician.* 59(4), 957 (1999).
23. Deleuran MS, Vestergaard C. Therapie der schweren atopischen Dermatitis bei Erwachsenen. *JDDG J. der Dtsch. Dermatologischen Gesellschaft.* 10(6), 399–406 (2012).
24. Werfel T, Schwerk N, Hansen G, Kapp A. The Diagnosis and Graded Therapy of Atopic Dermatitis. *Dtsch. Arztebl. Int.* 111(29-30), 509–520 (2014).
25. Eichenfield LF, Tom WL, Berger TG, et al. GUIDELINES OF CARE FOR THE MANAGEMENT OF ATOPIC DERMATITIS: Part 2: Management and Treatment of Atopic Dermatitis with Topical Therapies. *J. Am. Acad. Dermatol.* 71(1), 116–132 (2014).
26. De Bosscher K, Vanden Berghe W, Haegeman G. The interplay between the glucocorticoid receptor and nuclear factor- $\kappa$ B or activator protein-1: molecular mechanisms for gene repression. *Endocr. Rev.* 24(4), 488–522 (2003).
27. Nelson HS, Leung DYM, Bloom JW. Update on glucocorticoid action and resistance. *J. Allergy Clin. Immunol.* 111(1), 3–22 (2015).
28. Carr WW. Topical Calcineurin Inhibitors for Atopic Dermatitis: Review and Treatment Recommendations. *Paediatr. Drugs.* 15(4), 303–310 (2013).
29. Küster W. Ichthyosen: Vorschläge für eine verbesserte Therapie. *Dtsch Arztebl Int.* 103(24), A–1684 (2006).
30. Kim GK. The Rationale Behind Topical Vitamin D Analogs in the Treatment of Psoriasis: Where Does Topical Calcitriol Fit In? *J. Clin. Aesthet. Dermatol.* 3(8), 46–53 (2010).
31. Chien AL, Elder JT, Ellis CN. Ustekinumab. *Drugs.* 69(9), 1141–1152 (2009).
32. Papp KA. Etanercept in psoriasis. *Expert Opin. Pharmacother.* 5(10), 2139–2146 (2004).
33. Saraceno R, Saggini A, Pietroleonardo L, Chimenti S. Infliximab in the treatment of plaque type psoriasis. *Clin. Cosmet. Investig. Dermatol.* 2, 27–37 (2009).
34. Paudel KS, Milewski M, Swadley CL, Brogden NK, Ghosh P, Stinchcomb AL. Challenges and opportunities in dermal/transdermal delivery. *Ther. Deliv.* 1(1), 109–131 (2010).

35. Jepps OG, Dancik Y, Anissimov YG, Roberts MS. Modeling the human skin barrier - Towards a better understanding of dermal absorption. *Adv. Drug Deliv. Rev.* 65(2), 152–168 (2013).
36. Mitragotri S, Burke P a., Langer R. Overcoming the challenges in administering biopharmaceuticals: formulation and delivery strategies. *Nat. Rev. Drug Discov.* 13(9), 655–672 (2014).
37. Berard F, Marty JP, Nicolas JF. Allergen penetration through the skin. *Eur. J. Dermatology.* 13(4), 324–330 (2003).
38. Bos JD, Meinardi MM. The 500 Dalton rule for the skin penetration of chemical compounds and drugs. *Exp. Dermatol.* 9(5), 165–169 (2000).
39. Brown MB, Traynor MJ, Martin GP, Akomeah FK. Transdermal drug delivery systems: Skin perturbation devices. *Methods Mol. Biol.* 437, 119–139 (2008).
40. Brown MB, Martin GP, Jones S a, Akomeah FK. Dermal and transdermal drug delivery systems: current and future prospects. *Drug Deliv.* 13(May 2005), 175–187 (2006).
41. Liu X, Testa B, Fahr A. Lipophilicity and its relationship with passive drug permeation. *Pharm. Res.* 28(5), 962–977 (2011).
42. Latheshjilal. L, P. Phanitejaswini, Y.Soujanya, U.Swapna, V. Sarika GM. Transdermal Drug Delivery Systems: An Overview. *Int.J. PharmTech Res.* 3(4), 2140–2148 (2011).
43. Tanner T, Marks R. Delivering drugs by the transdermal route: Review and comment. *Ski. Res. Technol.* 14(3), 249–260 (2008).
44. KÜchler S, Strüver K, Friess W. Reconstructed skin models as emerging tools for drug absorption studies. *Expert Opin. Drug Metab. Toxicol.* 9(10), 1255–1263 (2013).
45. Schäfer-Korting M, Mahmoud A, Borgia SL, et al. Reconstructed epidermis and full-thickness skin for absorption testing: Influence of the vehicles used on steroid permeation. *ATLA Altern. to Lab. Anim.* 36(4), 441–452 (2008).
46. Schaefer-Korting M, Bock U, Diembeck W, et al. The use of reconstructed human epidermis for skin absorption testing: Results of the validation study. *Altern. to Lab. Anim. ATLA.* 36(2), 161–187 (2008).
47. OECD. Test No. 439: In Vitro Skin Irritation Reconstructed Human Epidermis Test Method. .
48. OECD. Test No. 431: In Vitro Skin Corrosion: Reconstructed Human Epidermis Test Method. OECD Guidel. Test. Chem. Sect. 4 Heal. Eff. , 33 (2014).
49. KÜchler S, Henkes D, Eckl K, Ackermann K. KÜchler Hallmarks of Atopic Skin Mimicked In Vitro by Means of a Skin Disease Model Based on FLG Knock-down. *ATLA. ,* 2011 (2011).
50. Eckl KM, Weindl G, Ackermann K, et al. Increased cutaneous absorption reflects impaired barrier function of reconstructed skin models mimicking keratinisation disorders. *Exp. Dermatol.* 23(4), 286–288 (2014).
51. Tjabringa G, Bergers M, van Rens D, de Boer R, Lamme E, Schalkwijk J. Development and Validation of Human Psoriatic Skin Equivalents. *Am. J. Pathol.* 173(3), 815–823 (2008).
52. Lu Y, Sun W, Gu Z. Stimuli-responsive nanomaterials for therapeutic protein delivery. *J. Control. Release.* (2014).
53. Scott AM, Wolchok JD, Old LJ. Antibody therapy of cancer. *Nat. Rev. Cancer.* 12(4), 278–287 (2012).
54. Scholl S, Beuzeboc P, Pouillart P. Targeting HER2 in other tumor types. *Ann. Oncol.* 12 Suppl 1, S81–S87 (2001).
55. (Rob) Aggarwal S. What's fueling the biotech engine[mdash]2012 to 2013. *Nat Biotech.* 32(1), 32–39 (2014).
56. Van Der Walle CF, Olejnik O. An overview of the field of peptide and protein delivery. In: *Peptide and Protein Delivery.* , 1–22 (2011).
57. Marques AM, Turner A, de Mello RA. Personalizing medicine for metastatic colorectal cancer: Current developments. *World J. Gastroenterol.* 20(30), 10425–10431 (2014).
58. Sato AK, Viswanathan M, Kent RB, Wood CR. Therapeutic peptides: technological advances driving peptides into development. *Curr. Opin. Biotechnol.* 17, 638–642 (2006).
59. Benson HAE, Namjoshi S. Proteins and peptides: Strategies for delivery to and across the skin. *J. Pharm. Sci.* 97(9), 3591–3610 (2008).
60. Wang W. Instability, stabilization, and formulation of liquid protein pharmaceuticals. *Int. J. Pharm.* 185(2), 129–188 (1999).
61. Wang W. Protein aggregation and its inhibition in biopharmaceutics. *Int. J. Pharm.* 289(1-2), 1–30 (2005).
62. Cromwell MEM, Hilario E, Jacobson F. Protein aggregation and bioprocessing. *AAPS J.* 8(3), E572–E579 (2006).
63. Frokjaer S, Otzen DE. Protein drug stability: a formulation challenge. *Nat. Rev. Drug Discov.* 4(4), 298–306 (2005).

64. Mahler HC, Friess W, Grauschopf U, Kiese S. Protein aggregation: Pathways, induction factors and analysis. *J. Pharm. Sci.* 98(9), 2909–2934 (2009).
65. Werner BP, Winter G. Particle contamination of parenterals and in-line filtration of proteinaceous drugs. *Int. J. Pharm.* 496(2), 250–267 (2015).
66. Prausnitz MR, Langer R. Transdermal drug delivery. *Nat. Biotechnol.* 26(11), 1261–1268 (2008).
67. Kalluri H, Banga AK. Transdermal delivery of proteins. *AAPS PharmSciTech.* 12(1), 431–441 (2011).
68. Aufenvenne K, Larcher F, Hausser I, et al. Topical enzyme-replacement therapy restores transglutaminase 1 activity and corrects architecture of transglutaminase-1-deficient skin grafts. *Am. J. Hum. Genet.* 93(4), 620–630 (2013).
69. Stout TE, McFarland T, Mitchell JC, Appukuttan B, Timothy Stout J. Recombinant Filaggrin Is Internalized and Processed to Correct Filaggrin Deficiency. *J. Invest. Dermatol.* 134(2), 423–429 (2013).
70. Mbah CJ, Uzor PF, Omeje EO. Perspectives on transdermal drug delivery. *J. Chem. Pharm. Res.* 3(3), 680–700 (2011).
71. Herwadkar A, Banga AK. Transdermal Delivery of Peptides and Proteins. In: . Walle CVDBT-P and PD (Ed.). . Academic Press, Boston, 69–86 (2011).
72. Brown MB, Jones SA. Hyaluronic acid: A unique topical vehicle for the localized delivery of drugs to the skin. *J. Eur. Acad. Dermatology Venereol.* 19(3), 308–318 (2005).
73. Pillai, O., Nair, V., Poduri, R., Panchagnula R. Transdermal iontophoresis. Part II: Peptide and protein delivery. *Methods Find Exp Clin Pharmacol.* 21(3), 229 (1999).
74. Bai Y, Sachdeva V, Kim H, Friden PM, Banga AK. Transdermal delivery of proteins using a combination of iontophoresis and microporation. *Ther. Deliv.* 5(5), 525–536 (2014).
75. Rigogliuso S, Sabatino MA, Adamo G, Grimaldi N, Dispenza C, Ghersi G. Polymeric nanogels: Nanocarriers for drug delivery application. *Chem. Eng.* 27 (2012).
76. Maya S, Sarmiento B, Nair A, Rejinold NS, Nair S V, Jayakumar R. Smart stimuli sensitive nanogels in cancer drug delivery and imaging: A review. *Curr. Pharm. Des.* 19(41), 7203–7218 (2013).
77. Frey H, Haag R. Dendritic polyglycerol: A new versatile biocompatible material. *Rev. Mol. Biotechnol.* 90(3-4), 257–267 (2002).
78. Sisson AL, Haag R. Polyglycerol nanogels: highly functional scaffolds for biomedical applications. *Soft Matter.* 6, 4968 (2010).
79. Steinhilber D, Seiffert S, Heyman JA, Paulus F, Weitz DA, Haag R. Hyperbranched polyglycerols on the nanometer and micrometer scale. *Biomaterials.* 32(5), 1311–1316 (2011).
80. Sisson AL, Steinhilber D, Rossow T, Welker P, Licha K, Haag R. Biocompatible Functionalized Polyglycerol Microgels with Cell Penetrating Properties. *Angew. Chemie Int. Ed.* 48(41), 7540–7545 (2009).
81. Steinhilber D, Sisson AL, Mangoldt D, Welker P, Licha K, Haag R. Synthesis, reductive cleavage, and cellular interaction studies of biodegradable, polyglycerol nanogels. *Adv. Funct. Mater.* 20(23), 4133–4138 (2010).
82. Steinhilber D, Witting M, Zhang X, et al. Surfactant free preparation of biodegradable dendritic polyglycerol nanogels by inverse nanoprecipitation for encapsulation and release of pharmaceutical biomacromolecules. *J. Control. Release.* 169(3), 289–295 (2013).
83. Sisson AL, Haag R. Polyglycerol nanogels: highly functional scaffolds for biomedical applications. *Soft Matter.* 6(20), 4968 (2010).
84. Cuggino JC, Alvarez I. Cl, Strumia MC, et al. Thermosensitive nanogels based on dendritic polyglycerol and N-isopropylacrylamide for biomedical applications. *Soft Matter.* 7(23), 11259 (2011).
85. Fleige E, Quadir MA, Haag R. Stimuli-responsive polymeric nanocarriers for the controlled transport of active compounds: Concepts and applications. *Adv. Drug Deliv. Rev.* 64(9), 866–884 (2012).
86. Soussan E, Cassel S, Blanzat M, Rico-Lattes I. Drug delivery by soft matter: Matrix and vesicular carriers. *Angew. Chemie - Int. Ed.* 48, 274–288 (2009).
87. Tan ML, Choong PFM, Dass CR. Recent developments in liposomes, microparticles and nanoparticles for protein and peptide drug delivery. *Peptides.* 31, 184–193 (2010).
88. Calderón M, Quadir MA, Sharma SK, Haag R. Dendritic polyglycerols for biomedical applications. *Adv. Mater.* 22(2), 190–218 (2010).
89. Haag R, Kratz F. Polymer therapeutics: Concepts and applications. *Angew. Chemie - Int. Ed.* 45(8), 1198–1215 (2006).
90. Asadian-Birjand M, Sousa-Herves A, Steinhilber D, Cuggino JC, Calderon M. Functional nanogels for biomedical applications. *Curr. Med. Chem.* 19(29), 5029–43 (2012).

91. Cordes EH, Bull HG. Mechanism and catalysis for hydrolysis of acetals, ketals, and ortho esters. *Chem. Rev.* 74(5), 581–603 (1974).
92. Oh JK, Drumright R, Siegwart DJ, Matyjaszewski K. The development of microgels/nanogels for drug delivery applications. *Prog. Polym. Sci.* 33(4), 448–477 (2008).
93. Khandare J, Calderón M, Dagia NM, Haag R. Multifunctional dendritic polymers in nanomedicine: opportunities and challenges. *Chem. Soc. Rev.* 41(7), 2824 (2012).
94. Oishi M, Nagasaki Y. Synthesis, characterization, and biomedical applications of core–shell-type stimuli-responsive nanogels – Nanogel composed of poly[2-(N,N-diethylamino)ethyl methacrylate] core and PEG tethered chains. *React. Funct. Polym.* 67(11), 1311–1329 (2007).
95. Bhuchar N, Sunasee R, Ishihara K, Thundat T, Narain R. Degradable thermoresponsive nanogels for protein encapsulation and controlled release. *Bioconjug. Chem.* 23, 75–83 (2012).
96. Wu C, Bottcher C, Haag R. Enzymatically crosslinked dendritic polyglycerol nanogels for encapsulation of catalytically active proteins. *Soft Matter.* 11(5), 972–980 (2015).
97. Pan G, Guo Q, Cao C, Yang H, Li B. Thermo-responsive molecularly imprinted nanogels for specific recognition and controlled release of proteins. *Soft Matter.* 9(14), 3840–3850 (2013).
98. Necas J, Bartosikova L, Brauner P, Kolar J. Hyaluronic acid (hyaluronan): A review. *Vet. Med. (Praha).* 53(8), 397–411 (2008).
99. Liao Y-H, Jones SA, Forbes B, Martin GP, Brown MB. Hyaluronan: pharmaceutical characterization and drug delivery. *Drug Deliv.* 12(6), 327–342 (2005).
100. Mero A, Campisi M. Hyaluronic acid bioconjugates for the delivery of bioactive molecules. *Polymers (Basel).* 6(1), 346–369 (2014).
101. Shah CB, Barnett SM. Swelling behavior of hyaluronic acid gels. *J. Appl. Polym. Sci.* 45(2), 293–298 (1992).
102. Meyer J, Whitcomb L, Treuheit M, Collins D. Sustained in vivo activity of recombinant human granulocyte colony stimulating factor (rHG-CSF) incorporated into hyaluronan. *J. Control. Release.* 35(1), 67–72 (1995).
103. Yang J-A, Kim E-S, Kwon JH, et al. Transdermal delivery of hyaluronic acid – Human growth hormone conjugate. *Biomaterials.* 33(25), 5947–5954 (2012).
104. Luo Y, Ziebell MR, Prestwich GD. A hyaluronic acid-taxol antitumor bioconjugate targeted to cancer cells. *Biomacromolecules.* 1(2), 208–218 (2000).
105. Wei X, Senanayake TH, Warren G, Vinogradov S V. Hyaluronic acid-based nanogel-drug conjugates with enhanced anticancer activity designed for the targeting of cd44-positive and drug-resistant tumors. *Bioconjug. Chem.* 24(4), 658–668 (2013).
106. Jin Y, Ubonvan T, Kim D. Hyaluronic Acid in Drug Delivery Systems. *J. Pharm. Investig.* 40, 33–43 (2010).
107. Burdick JA, Prestwich GD. Hyaluronic acid hydrogels for biomedical applications. *Adv. Mater.* 23(12), H41–H56 (2011).
108. Brown TJ, Alcorn D, Fraser JRE. Absorption of hyaluronan applied to the surface of intact skin. *J. Invest. Dermatol.* 113(5), 740–746 (1999).
109. Sachdeva V, Banga AK. Microneedles and their applications. *Recent Pat. Drug Deliv. Formul.* 5, 95–132 (2011).
110. Kim YC, Park JH, Prausnitz MR. Microneedles for drug and vaccine delivery. *Adv. Drug Deliv. Rev.* 64, 1547–1568 (2012).
111. Indermun S, Luttge R, Choonara YE, et al. Current advances in the fabrication of microneedles for transdermal delivery. *J. Control. Release.* 185, 130–138 (2014).
112. Mohammed YH, Yamada M, Lin LL, et al. Microneedle enhanced delivery of cosmeceutically relevant peptides in human skin. *PLoS One.* 9(7), 1–9 (2014).
113. Cheung K, Han T, Das DB. Effect of Force of Microneedle Insertion on the Permeability of Insulin in Skin. *J. Diabetes Sci. Technol.* 8(3), 444–452 (2014).
114. Gill HS, Prausnitz MR. Coating formulations for microneedles. *Pharm. Res.* 24(7), 1369–1380 (2007).
115. Quan F-S, Kim Y-C, Yoo D-G, Compans RW, Prausnitz MR, Kang S-M. Stabilization of Influenza Vaccine Enhances Protection by Microneedle Delivery in the Mouse Skin. *PLoS One.* 4(9), e7152 (2009).
116. Kim YC, Quan FS, Compans RW, Kang SM, Prausnitz MR. Formulation and coating of microneedles with inactivated influenza virus to improve vaccine stability and immunogenicity. *J. Control. Release.* 142(2), 187–195 (2010).
117. Choi HJ, Yoo DG, Bondy BJ, et al. Stability of influenza vaccine coated onto microneedles. *Biomaterials.* 33(14), 3756–3769 (2012).
118. Zhu Z, Luo H, Lu W, et al. Rapidly Dissolvable Microneedle Patches for Transdermal Delivery of Exenatide. *Pharm. Res.* (2014).

119. McGrath MG, Vucen S, Vrdoljak A, et al. Production of dissolvable microneedles using an atomised spray process: Effect of microneedle composition on skin penetration. *Eur. J. Pharm. Biopharm.* 86(2), 200–211 (2014).
120. Cheung K, Han T, Das DB. Effect of Force of Microneedle Insertion on the Permeability of Insulin in Skin. *J. Diabetes Sci. Technol.* 8, 444–452 (2014).
121. Martanto W, Davis SP, Holiday NR, Wang J, Gill HS, Prausnitz MR. Transdermal delivery of insulin using microneedles in vivo. *Pharm. Res.* 21, 947–952 (2004).
122. Cormier M, Johnson B, Ameri M, et al. Transdermal delivery of desmopressin using a coated microneedle array patch system. *J. Control. Release.* 97, 503–511 (2004).
123. Peters EE, Ameri M, Wang X, Maa YF, Daddona PE. Erythropoietin-coated ZP-microneedle transdermal system: Preclinical formulation, stability, and delivery. *Pharm. Res.* 29, 1618–1626 (2012).
124. Ameri M, Kadkhodayan M, Nguyen J, et al. Human growth hormone delivery with a microneedle transdermal system: Preclinical formulation, stability, delivery and PK of therapeutically relevant doses. *Pharmaceutics.* 6, 220–234 (2014).
125. Edens C, Collins ML, Ayers J, Rota PA, Prausnitz MR. Measles vaccination using a microneedle patch. *Vaccine.* 31, 3403–3409 (2013).
126. Quan FS, Kim YC, Song JM, et al. Long-term protective immunity from an influenza virus-like particle vaccine administered with a microneedle patch. *Clin. Vaccine Immunol.* 20, 1433–1439 (2013).
127. Kang S-M, Song J-M, Kim Y-C. Microneedle and mucosal delivery of influenza vaccines. *Expert Rev. Vaccines.* 11, 547–560 (2012).
128. Prausnitz M, Mikszta J, Cormier M, Andrianov A. Microneedle-Based Vaccines. In: *Vaccines for Pandemic Influenza SE - 18.* Compans RW, Orenstein WA (Eds.). . Springer Berlin Heidelberg, 369–393 (2009).
129. Van Damme P, Oosterhuis-Kafeja F, Van der Wielen M, Almagor Y, Sharon O, Levin Y. Safety and efficacy of a novel microneedle device for dose sparing intradermal influenza vaccination in healthy adults. *Vaccine.* 27(3), 454–459 (2009).

## Chapter 2

### Biodegradable dendritic polyglycerol nanogels for encapsulation and release of pharmaceutical biomacromolecules

The following chapter has been published as peer-reviewed article in the Journal of Controlled Release and appears in this thesis with the journal's permission:

Dirk Steinhilber, Madeleine Witting, Xuejiao Zhang, Michael Staegemann, Florian Paulus, Wolfgang Friess, Sarah Kuchler, Rainer Haag

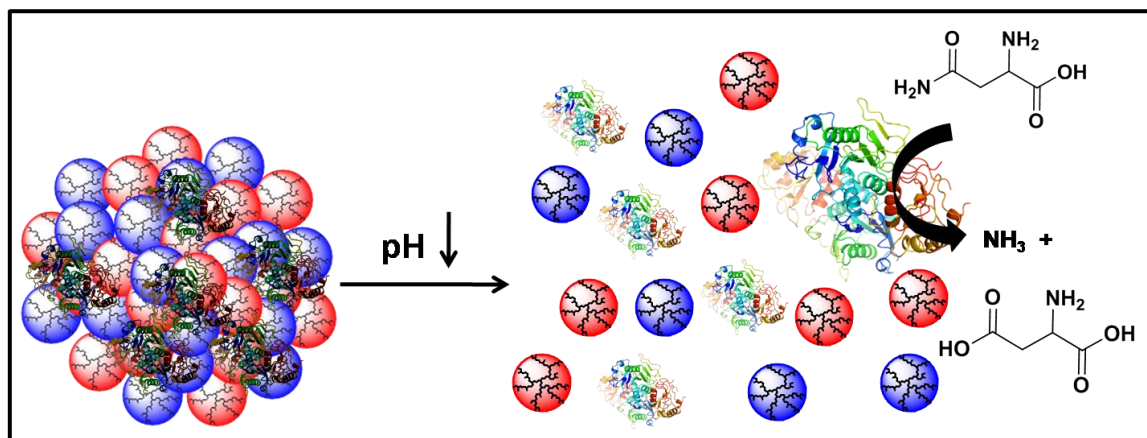
*Surfactant free preparation of biodegradable dendritic polyglycerol nanogels by inverse nanoprecipitation for encapsulation and release of pharmaceutical biomacromolecules*

J. Control. Release 169, 3, (2013) 289 – 295

Online available: <http://www.sciencedirect.com/science/article/pii/S016836591200836X>

The personal contribution covers the experimental set-up and contribution to the written parts concerning the nanogel degradation, protein release and characterization. The correspondent chapters are: **2.4 / 2.5 / 2.6 / 2.7 / 2.8 / 3.4**

#### Graphical Abstract



## **Abstract**

In this paper we report a novel approach to generate biodegradable polyglycerol nanogels on different length scales. We developed a mild, surfactant free inverse nanoprecipitation process to template hydrophilic polyglycerol nanoparticles. In situ crosslinking of the precipitated nanoparticles by bio-orthogonal copper catalyzed click chemistry allows us to obtain size defined polyglycerol nanogels (100 - 1000 nm). Biodegradability was achieved by the introduction of benzacetal bonds into the net points of the nanogel. Interestingly, the polyglycerol nanogels quickly degraded into low molecular weight fragments at acidic pH values, which are present in inflamed and tumor tissues as well as intracellular organelles, and they remained stable at physiological pH values for a long time. This mild approach to biodegradable polyglycerol nanogels allows us to encapsulate model proteins, including the therapeutic relevant enzyme asparaginase, into the protein resistant polyglycerol network. Enzymes were encapsulated with an efficacy of almost 100 % and after drug release, full enzyme activity and structural integrity were observed. This new inverse nanoprecipitation procedure allows the efficient encapsulation and release of various biomolecules including proteins and could find broad applications in polymer therapeutics and nanomedicine.

**Keywords:** Polyglycerol Nanogel, Nanoprecipitation, Biodegradability, Surfactant Free, Protein Encapsulation, Stimuli-Responsive Release

## 1. Introduction

Therapeutically relevant proteins such as antibodies, cytokines, growth factors, and enzymes are playing an increasing role in the treatment of viral, malignant, and autoimmune diseases [1,2]. Therapeutic proteins, however, often suffer from insufficient stability and shelf-life, costly production, immunogenic and allergic potential, as well as poor bioavailability and sensitivity towards proteases [3]. An elegant method to overcome most of these problems is the attachment of polyethylene glycol (PEG) chains onto the surface of the protein [4–7]. Covalent PEGylation of the native protein increases its molecular weight and as a result prolongs the half-life in vivo [3]. By the molecular weight elevation passive targeting to solid tumors can be achieved by the enhanced permeation and retention effect [8,9]. Additionally, the resistance to proteases and immunogenic responses is increased by the PEG coating. PEGylation of proteins, however, still suffer from the loss of biological activity [5].

These problems can be circumvented, when proteins are encapsulated non-covalently into nanogels [10,11]. Nanogels, which are hydrogel particles on the nanometer scale, are highly water swollen scaffolds that exhibit similar properties as many biological objects, thus making them excellent candidates for biomedical applications [12–16]. Within the past few years, two strategies have evolved for the encapsulation of biomolecules into nanogels. They can be encapsulated after nanogel formation by the diffusion of the guest into the nanogel due to specific interactions of the guest with the nanogels [17]. Strong interactions with the gel matrix, however, might cause denaturation of the encapsulated payloads and diffusion limitations lead to low encapsulation efficiencies. Another strategy entraps the encapsulated payloads in-situ to the nanogel formation process, which ensures high encapsulation efficiencies and a homogenous distribution of the guest within the entire gel particle [11]. Additionally, the encapsulated payloads can be embedded very tightly in the gel matrix by tuning the degree of crosslinking. Thus, the guest can be transported to the target site without any loss of payload by leaching.

For drug release, nanogels require external stimuli to achieve a controlled release of the guests at the target site. Guest liberation by nanogel degradation and resulting network dissolution is the most promising strategy. Release kinetics can be tuned by the degradation kinetics and the generated low molecular weight degradation fragments can be cleared by the kidneys, which reduces the possibility of long term toxicity by organ accumulation [5]. Various chemical bonds such as disulfides [18,19], acetals [20,21], ketals [22,23], phosphate esters [24], silyl ethers [25], and esters [26] have been introduced into nanogel networks which are cleaved in response to specific biological stimuli including pH or reductive environments [27].

In-situ encapsulation, however, requires mild nanogel preparation conditions to retain high biomolecule activity especially when dealing with sensitive substances such as proteins.

Nanogels are usually prepared by the templation of reactive monomers on the nanometer scale and subsequent crosslinking of the templates to obtain hydrogel nanoparticles. The most frequently used methods are templations in mini- [26,28–32] and microemulsion droplets [33–35]. High energy input by ultrasonication, which is required for the formation of miniemulsions, prevents the encapsulation of labile compounds by this technique. The formation of microemulsions requires high surfactant loadings, which lead to purification problems and thereby also limit applications of this technique.

Another approach which has been developed by Whitesides et al. [36] and further improved by the De Simone group [37] is the templation of polymer macromonomers in soft lithography templates. Clean room conditions, however, are required for this approach possibly limiting the broad application of this technique. Another widely used approach is based on the crosslinking of polymeric micelles [15]. Even though this approach is often called “surfactant free” in literature, amphiphilic polymers are required which might interact and denature the encapsulated payloads. Additionally, material parameters like size, elasticity and shape are difficult to influence. The nanoprecipitation technique has evolved as a powerful tool for the preparation of hard polymer nanoparticles built from polystyrene (PS) [38], polymethyl methacrylate (PMMA) [39,40], and polylactic acid /polylactic-co-glycolic acid (PLA/PLGA) [41–43]. Particles prepared by nanoprecipitation avoids the above mentioned downsides and allows hydrophobic drugs to be encapsulated [43]. To our knowledge, however, the nanoprecipitation technique has not been applied for the preparation of nanogels, made from hydrophilic polymers.

In this paper we describe for the first time the templation of hydrophilic polyglycerol-macromonomers by nanoprecipitation and subsequent chemical crosslinking of the precipitated particles. We use dendritic polyglycerol (dPG) as nanogel scaffold material, due to its outstanding multifunctionality [44,45] and protein resistance [46–48]. Minimal interaction with the polymer matrix provides maximal protein stabilization. Additionally, the rigidity of dendritic macromolecules generates high diffusion barriers for the encapsulated proteins, thereby facilitating stable transport behavior. We call this novel approach inverse nanoprecipitation due to the inversion of polarity in the nanoprecipitation process. The combination of the mild nanogel preparation method with the biocompatible nature of polyglycerol material allows us to encapsulate therapeutic enzymes with encapsulation efficacies higher than 99% under full retention of activity and structural integrity. Finally we show that the incorporation of pH labile, cyclic benzacetal bonds into the nanogel network leads to degradation triggered controlled enzyme release at acidic pH values. This novel approach to enzyme loaded and protein resistant nanogel particles is an important alternative for traditional PEGylation strategies and may find broad application in nanomedicine and polymer therapeutics.

## 2. Methods

### 2.1 Preparation of dPG<sub>7.7</sub> functionalized with 10 p-PBDMA units (dPG<sub>7.7</sub>-10-p-PBDMA)

dPG<sub>7.7</sub> (1g, 0.13 mmol) and *p*-PBDMA (250 mg, 1.3 mmol) were dissolved in NMP (4 mL) and anhydrous PTSA (22 mg, 0.13 mmol) was added. The reaction was heated to 120 °C for 3h and the condensed methanol was removed from the reaction equilibrium by cryodistillation. After cooling down to room temperature (RT) the reaction was quenched by the addition of aqueous ammonia (1 mL). NMP was evaporated by cryodistillation and the residue was re-dissolved in basified water (0.05 wt% aqueous ammonia). The solution was dialyzed in basified water (0.05 wt% aqueous ammonia) for 2 d, changing the dialysate every 3 h. After freeze-drying, dPG<sub>7.7</sub>-10- p-PBDMA was obtained as a viscous wax (conversion 99 %, yield 80 %). GPC/SEC:  $M_n=6.5$  kDa,  $M_w=8.9$  kDa, PDI=1.4. Hydrodynamic diameter by DLS: 3.8 nm. IR [ $\text{cm}^{-1}$ ]: 3385, 2871, 1613, 1513, 1456, 1304, 1221, 1067, 830. <sup>1</sup>H NMR (400 MHz, CD<sub>3</sub>OD, 25 °C):  $\delta$  (ppm) = 7.51–7.32 (broad, aromatic), 7.09–6.95 (broad, aromatic), 5.91–5.72 (d, broad, acetal-H), 4.74 (s, aromatic-O-CH<sub>2</sub>), 4.46–3.39 (PG backbone), 2.99 (s, CCH).

### 2.2 Preparation of polyglycerol nanogels by nanoprecipitation

dPG<sub>7.7</sub>-10-p-PBDMA (5 mg, 0.6  $\mu\text{mol}$ ) and dPG<sub>7.7</sub>[N<sub>3</sub>]<sub>7</sub> (7 mg, 0.9  $\mu\text{mol}$ ) were dissolved separately in Mili-Q-water (0.5 mL). THPTA (500  $\mu\text{g}$ , 1.15  $\mu\text{mol}$ ), CuSO<sub>4</sub> (72  $\mu\text{g}$ , 0.3  $\mu\text{mol}$ ) and NaAsc (228  $\mu\text{g}$ , 1.15  $\mu\text{mol}$ ) were added exactly in this sequence to the dPG<sub>7.7</sub>-7- p-PBDMA solution. The solutions were cooled down to 4°C, mixed and added quickly to magnetically stirred acetone (20 mL). Precipitated polyglycerol nanoparticles were obtained as blue shining dispersions and the particle size was determined by DLS (Table 2-1). After 3 h the reaction was quenched by the addition of excess azidoglycerol (50 mg, 893  $\mu\text{mol}$ ). After 12 h Mili-Q-water (20 mL) was added and acetone was evaporated to obtain blue shining nanogel dispersions in water. The nanogels were collected by centrifugation (4000 rpm) and washed 5 times with Mili-Q-water. The nanogels were characterized by DLS (Table 2-1) optical- and fluorescence microscopy and transmission electron microscopy.

**Table 2-1** Size and PDI by dynamic light scattering (DLS). Measurements were performed in triplicate; intensity average mean value and standard deviation from the mean value are presented.

$C_{\text{Macromonomer}}$ [mg/mL]	$d$ [nm] acetone	PDI	$d$ [nm] water	PDI
12	580	0.03	820	0.07
6	440	0.02	610	0.03
3	310	0.06	430	0.08
1.5	102	0.04	145	0.07

### 2.3 Encapsulation of asparaginase into the nanogels

dPG<sub>7.7</sub>-10-p-propargyloxy-benzacetale (2 mg, 0.2 µmol) and dPG<sub>7.7</sub>[N<sub>3</sub>]<sub>7</sub> (3 mg, 0.3 µmol) were dissolved separately in Mili-Q-water (0.5 mL). THPTA (500 µg, 1.15 µmol), CuOAc (37 µg, 0.3 µmol) were added to the dPG<sub>7.7</sub>-10-p-propargyloxy-benzacetale solution and asparaginase was added to the dPG<sub>7.7</sub>[N<sub>3</sub>]<sub>7</sub> solution. The solutions were cooled down to 4 °C, mixed and added quickly to magnetically stirred acetone (20 mL). After 3 h the gelation reaction was quenched by the addition of excess azidoglycerol (50 mg, 893 µmol). After 12 h the nanogels were collected by centrifugation (4000 rpm) and washed 5 times with Mili-Q-water.

### 2.4 Determination of nanogel degradation kinetics

Nanogel dispersions were incubated at 37 °C and at different pH values (pH 4, 5 and 7.4). Between 30 min and 48 h, the nanogels were separated from degraded fragments by centrifugation (4000 rpm, 30 min) and the UV-absorbance was measured at 350 nm (Fig. 2-3A). Complete nanogel degradation was confirmed by DLS size measurements.

### 2.5 Determination of proteins' secondary structure - Fourier-transformed-infrared spectroscopy (FT-IR)

Experiments were recorded using a Bruker Tensor 27 FTIR spectrometer (Ettlingen, Germany) equipped with a Bio ATR measuring cell and a MCT detector. The cell was connected to a water bath (Haake, Pfintzal, Germany) for a constant cell temperature of 25 °C. 25 µL of the sample was spread under dry nitrogen to ensure an equal distribution on the crystal surface and analyzed against PBS buffer (pH 5) or water as blank. For each experiment, 120 scans were set for the blank and sample with a resolution of 4 cm<sup>-1</sup> and water vapor correction. The data were analyzed with the OPUS 6.5 software for second derivative spectra and vector normalization.

### 2.6 Determination of asparaginase activity

The activity of asparaginase was determined as the specific activity [U/mg] of the enzyme according to published procedures [49]. The units of enzyme activity were defined as micromoles of ammonia released per minute.

$$\text{Units / mg} = \frac{\text{micromoles ammonia released}}{10 \text{ minutes} \times \text{mg enzyme in reaction}}$$

A mixture of 50 µl asparaginase, 100 µl Tris-HCl buffer pH 8.6 and 850 µl L-asparagine monohydrate buffer solution was incubated at 37 °C for 10 min. After adding 50 µl 1.5 M

trichloroacetic acid solution and centrifugation, 100  $\mu$ l of the supernatant was added to Nessler's solution. After 10 min, the optical density was assessed at 436 nm, compared with the standard curve and corrected for total enzyme amount.

## **2.7 Drug release study**

The polyglycerol nanogels (10 mg/mL polymer and 0.5 mg/mL asparaginase) were acidified with HCl to pH 5 and 4, respectively. The samples were incubated at room temperature ( $25 \pm 2$  °C) under mild agitation (300 rpm). Samples were collected for up to 3 days and subsequently analyzed with size exclusion HPLC. To stop the particle degradation, the samples were neutralized with 0.1M KOH prior to HPLC analysis.

## **2.8 Size exclusion HPLC (SE-HPLC) analysis**

To analyze the drug release of degraded polyglycerol nanogels, 50  $\mu$ l of the neutralized samples were injected into the HPLC system equipped with a TSKgel<sup>®</sup> G4000 PWXL column (dimensions: 300 x 7.8 mm, 10  $\mu$ m particle size; TOSOH Bioscience, Stuttgart, Germany). Isocratic elution with 20 mM Na<sub>2</sub>HPO<sub>4</sub>, 150mM NaCl, pH 7.4, 0.003 mM NaN<sub>3</sub> was performed with a flow-rate of 0.4 ml/min. The concentration of asparaginase was determined using UV (280 nm) and fluorescence (ex. 295 nm, em. 348 nm) detection.

# **3. Results and discussion**

## **3.1 Nanogel preparation by inverse nanoprecipitation and in situ gelation**

When biomolecules are encapsulated into nanogels insitu to network formation, mildest reaction conditions are required. The nanoprecipitation technology, which has been successfully applied for several years, is based on the injection of highly diluted polymer solutions into polymer non solvents. This technique is surfactant free and works without high energy input such as ultrasonication and is therefore an excellent candidate for the encapsulation of labile enzymes.

To our knowledge, however, this technique has not been applied for the preparation of hydrophilic nanogel particles. These water swollen polymer networks are highly interesting for the stabilization of labile enzymes. We chose dPGs as nanogel building blocks, because of its excellent protein resistant properties [46–48]. In such water swollen networks, enzymes are entrapped without any interaction with the polymer matrix. Additionally, enzyme diffusion is strongly reduced due to the rigid conformation of dPGs, which ensures stable guest encapsulation. Another outstanding property of dPG is its multivalent polyhydroxylated

surface, which allows the modification with cross-linkable groups under full retention of water solubility.

Copper catalyzed Huisgen 2+3 cycloaddition as model crosslinking reaction due to its bio-orthogonality, high conversions and fast reaction kinetics. We selected pHBA as a core building block for the acid labile crosslinker because it is known that degradation kinetics of the corresponding benzacetals is interesting for many biomedical applications. Additionally, phenol groups can easily be modified by ether bond formation. After the propargylation of pHBA we activated the aldehyde by the formation of the dimethylacetal. Final acid catalyzed dPG-acetal formation was achieved under methanol evaporation by cryo-distillation to obtain acid labile dPG-crosslinker (Fig. 2-1). DPG, functionalized with 7 azide functionalities was prepared according to a modified procedure established in our group.

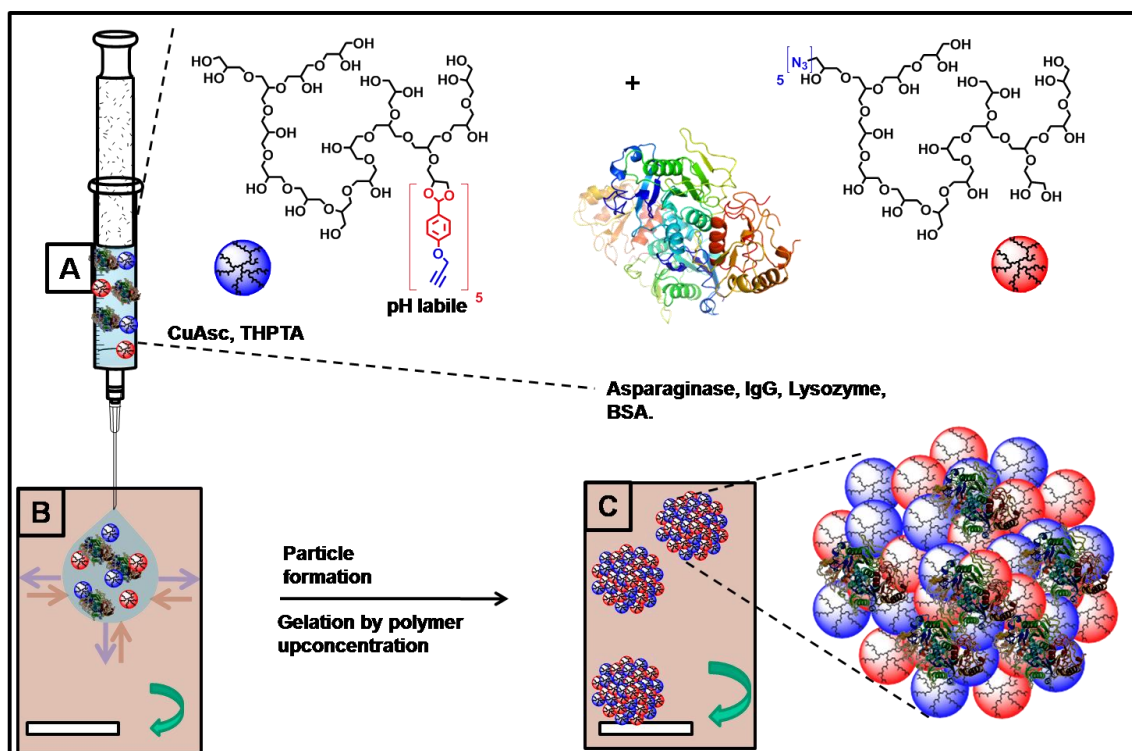


**Figure 2-1** Schematic representation of the nanoprecipitation process. A: Injection of aqueous solution of alkyne functionalized polyglycerol macromonomers, (blue spheres), azide functionalized polyglycerol macromonomers (red spheres) and proteins asparaginase, IgG, Lysozyme and BSA (3D structure of  $\alpha$ -helices and  $\beta$ -turns). B: Particle templation by diffusion of aqueous phase (blue arrow) into acetone phase (brown). C: Particle gelation by azide alkyne 2+3 cycloaddition.

With this novel pH sensitive dPG-alkyne and the azide functionalized counterpart we prepared highly diluted aqueous solutions. After cooling to 4°C and adding a catalytic amount of CuAsc/THPA, dPG nanotemplates were formed by precipitation into acetone nonsolvent. The fast diffusion of the aqueous phase into the acetone phase causes the collapse of dPGs

into nanoaggregates. During this process the polymer concentration increases drastically, which induces gelation reactions and dPG network formation. Gelation prior to nanoprecipitation can be excluded as no size change was observed by dynamic light scattering (DLS). Interestingly, the polydispersity index (PDI) of the formed nanoaggregates is low narrow and diameters directly correlate with the macromonomer concentration in aqueous phase. Hence, we are able to modulate the particle size, which has proven to be one of the most important parameter for many biomedical applications [50,51], in a broad range between 100 – 1000 nm (Table 2-1).

Interestingly, the polydispersity index (PDI) of the formed nanoaggregates is low narrow and diameters directly correlate with the macromonomer concentration in aqueous phase. Hence, we are able to modulate the particle size, which has proven to be one of the most important parameter for many biomedical applications [50,51], in a broad range between 100 – 1000 nm (Table 2-1).

After gelation, remaining surface reactive alkyne groups were quenched by adding azidoglycerol. Finally, we harvest polyglycerol nanogels are harvested by the evaporation of acetone. When nanoparticles are transferred to the aqueous phase the diameter increases significantly, which is attributed to nanogel swelling. Interestingly, polydispersities remain low in the aqueous phase, which is a strong indication that nanogels are freely dispersible without aggregation (Table 2-1, Fig. 2-2). The simple reaction setup allows us to upscale the reaction to obtain polyglycerol nanogels in gram quantities.

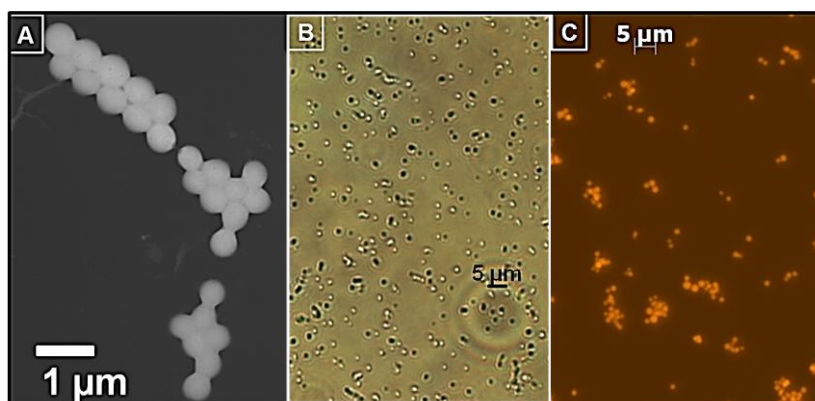


**Figure 2-2** Visualization of polyglycerol nanogels by electron microscopy (A), optical microscopy (B) and fluorescence microscopy (C).

### 3.2 Enzyme encapsulation by co-precipitation

The traditional nanoprecipitation technique is based on organic polymer solutions, from which the polymers are precipitated mostly into water. Because the used polymers like PS, PLA and PLGA are only soluble in organic solvents like acetone, dichloromethane and dimethylformamide, mostly hydrophobic small molecule drugs were encapsulated by this

approach. There are many water soluble biomacromolecular drugs like proteins, DNA and RNA. These labile biomacromolecules need to be protected from the harsh environment present at many administration sites. Pharmaceutical enzymes in particular show important characteristics, which make them superior from small molecule drugs. Their high affinity and specificity on their targets as well as their catalytic activity, which enables the conversion of multiple target molecules, makes them excellent drug molecules [1].

To encapsulate, stabilize and transport this important class of therapeutics, we applied our inverse nanoprecipitation polymerization technique which allows the co-precipitation and encapsulation of biomolecules from aqueous solutions, thus preserving their three-dimensional structure. As a model enzyme we selected asparaginase, which is an important therapeutic enzyme for the treatment of acute lymphocytic leukemia [52–54]. Co-precipitation of the enzyme in presence of the PG macromonomers yielded enzyme loaded nanogels. We determined the encapsulation efficacy to be almost 100 % as no free enzyme could be detected by HPLC analysis.

### **3.3 Degradation triggered release under acidic conditions**

Cargo liberation triggered by degradation in acidic environments is one of the most promising release strategies. Many interesting biomedical targets like inflamed- and tumor tissue (pH 6.5 – 6), intracellular endosomes (pH 5) and lysosomes (pH 4) can be used for pH dependent release. Protons, which can catalyze hydrolysis reaction, have high diffusion rates because of their small size and show high accessibility at the cleavage site. Hence, degradability limitations due to diffusion barriers are not an issue in this degradation process. In this study we prepared cyclic PG-benzacetals as degradable macro-crosslinkers. While other pH labile groups like imines, hydrazones often generate toxic polyamine degradation products, polyhydroxylated dPG is reformed after acetal cleavage. In contrast to traditional approaches to pH cleavable materials, in which low molecular weight degradable monomers are used [20], we use biocompatible macromonomers to build gel networks. By this strategy we can minimize the total amount of crosslinking units in the gel, which ensures maximal biocompatibility. Our polyglycerol nanogels degrade quickly at pH 4 and pH 5, with degradation half-lives of 2 h and 11 h respectively (Fig. 2-3A, Fig. 2-4). Interestingly, nanogel degradation kinetics and enzyme release kinetics are almost identical (Fig. 2-3B), which proves that release is only triggered by degradation. Additionally, the asparaginase is released without interactions between degraded dPG, which proves that these protein resistant materials are excellent scaffolds for the encapsulation, transport and release of proteins.

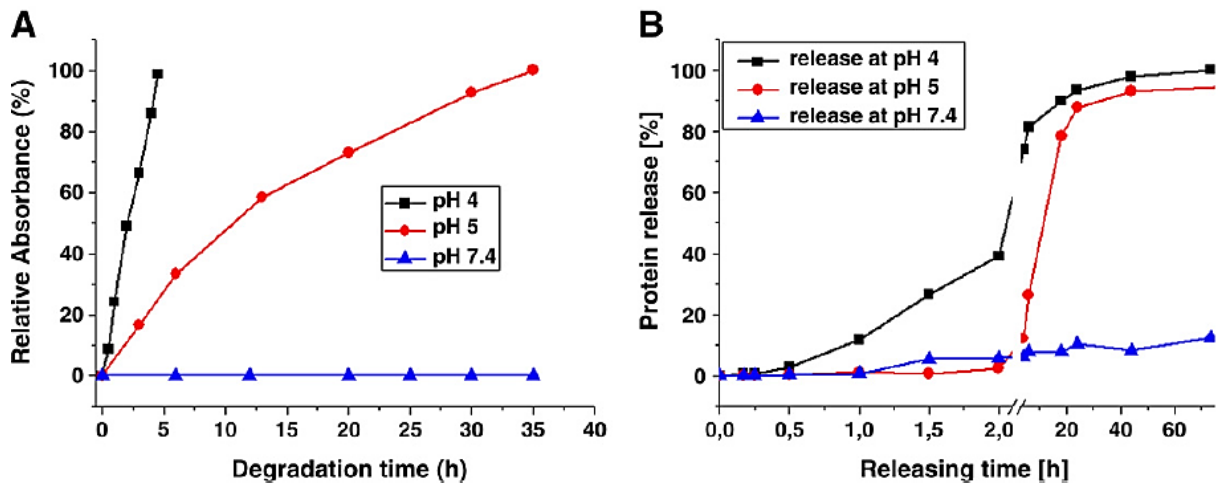


**Figure 2-3** A: Degradation kinetics of polyglycerol nanogels determined by UV/Vis absorption in the supernatant at pH 4 (black squares), pH 5 (red circles) and pH 7.4 (blue triangles) at 37 °C. B: Protein release kinetics determined by HPLC at pH 4 (black squares), pH 5 (red circles), and pH 7.4 (blue triangles) at 25°C.

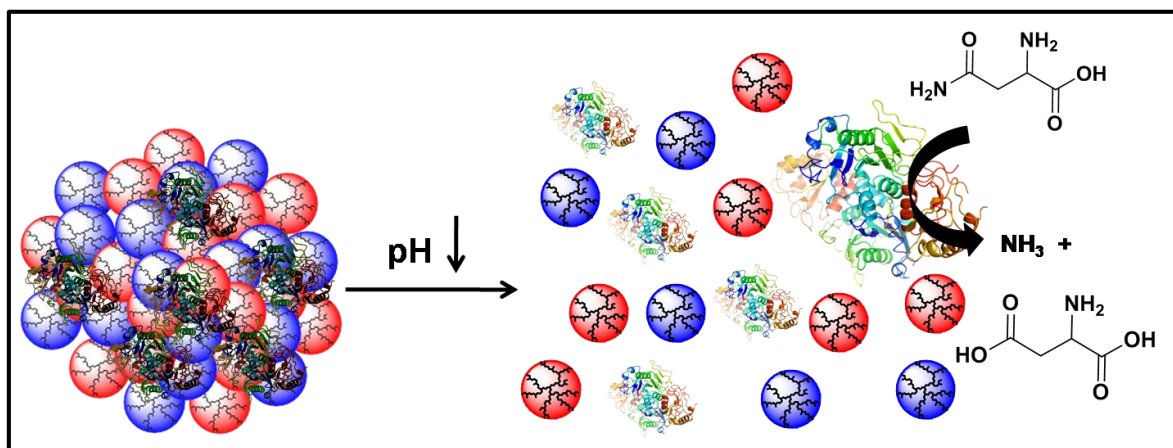


**Figure 2-4** Schematic representation of degradation triggered release of a therapeutic relevant enzyme and its catalytic conversion of asparagine to aspartic acid under ammonia generation.

### 3.4 Structure-activity assay of encapsulated and released asparaginase

#### 3.4.1 Determination of proteins' secondary structure by Fourier-transformed-infrared spectroscopy (FT-IR)

To determine the structural composition and especially the secondary structure of the model protein asparaginase before and after encapsulation in the polyglycerol nanogels, FT-IR spectra were recorded.

Several bands can be used for structural analysis of asparaginase [55]. The most sensitive spectral region for protein secondary structure analysis is the amide I band (1700-1600 cm<sup>-1</sup>), which results mainly from C=O stretch vibrations of the peptide linkages [56]. The major component of the native protein belongs to a band at approximately 1657 cm<sup>-1</sup>,

corresponding to a helical conformation. The band at  $\sim 1653\text{ cm}^{-1}$  corresponds to a disordered/irregular part of the molecule. Extended  $\beta$  strands can be found at  $\sim 1637\text{ cm}^{-1}$  [57]. Comparable spectra for amide I ( $\sim 1662\text{-}1648\text{ cm}^{-1}$ ) and II ( $\sim 1580\text{-}1510\text{ cm}^{-1}$ ) band were obtained with the encapsulated and the native protein when evaluating the second derivative spectra of the FT-IR measurements (Fig. 2-5A/B, Table 2-2)

In general, no significant changes of the secondary structure of asparaginase were detected after encapsulation and release from the PG nanogels. For the amide I band, the peak intensities around  $1660\text{ cm}^{-1}$  and  $1635\text{ cm}^{-1}$  are the same, no significant changes were detected (Table 2-2). The same holds true for the negative  $\beta$ -sheet peak of the formerly encapsulated protein at  $1637.3\text{ cm}^{-1}$  which is slightly shifted  $2\text{ cm}^{-1}$  to the left (compared to the native proteins at  $1635.4\text{ cm}^{-1}$ ).

The amide II spectral region from  $1575\text{ -}1480\text{ cm}^{-1}$  gives information about the out-of-phase combinations of N-H, the in-plane N-H bending, and also about the C-N stretching vibrations. In general, this region exhibits much less protein conformational sensitivity compared to the amide I region [55,56]. The second derivative of the amide II spectra (Fig. 2-5B) shows no significant differences in secondary structures of the native protein and the released asparaginase (Table 2-2).

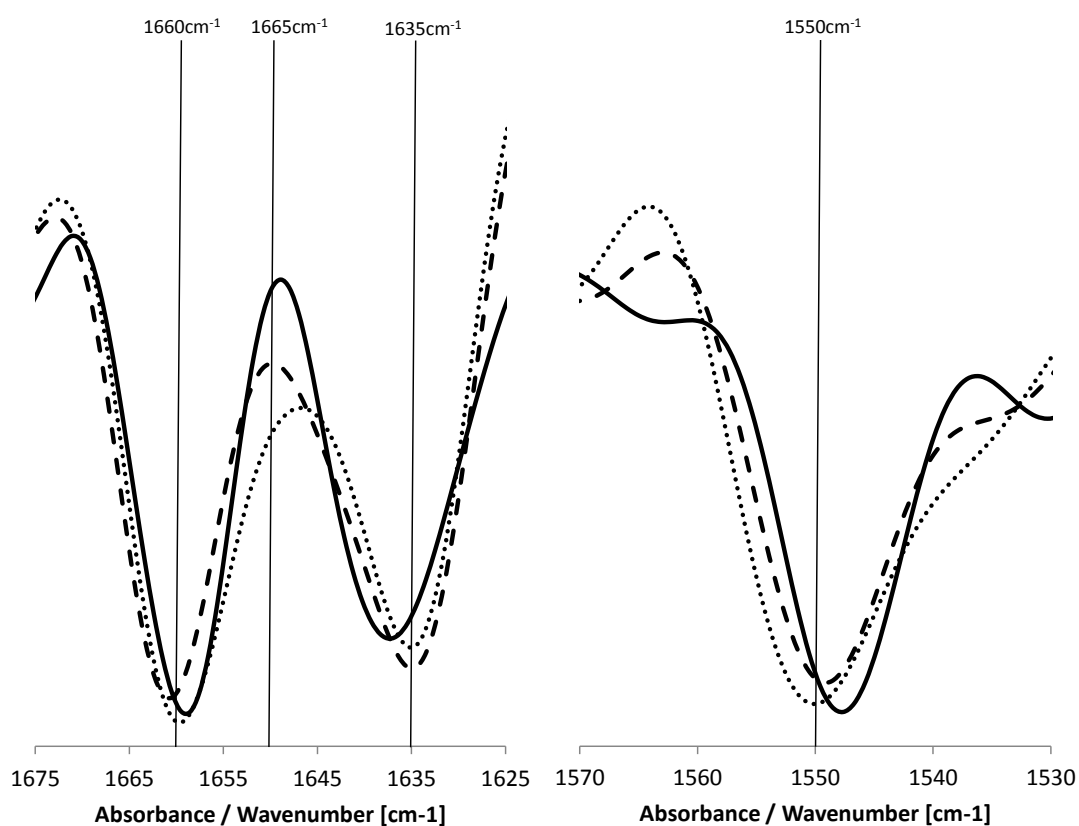


**Figure 2-5** The second derivative spectra of the amide I (left) and II (right) region of the ATR-FT-IR spectra of asparaginase in water (freshly prepared; dashed line), in PBS buffer pH 5 (stored for 1 week; dotted line) and after release from polyglycerol nanogels (stored for 1 week; connected line)

**Table 2-2** Comparison of peak positions (second derivative FT-IR spectra, wavenumbers [ $\text{cm}^{-1}$ ])

	Amide I band		Amide II band	
<b>Asparaginase in water (freshly prepared)</b>	1660.5	1649.9	1634.4	1549.6
<b>Asparaginase in PBS pH 5.0 (7d storage)</b>	1659.5	1646.9	1635.4	1550.5
<b>Asparaginase after release (7d storage)</b>	1659.0	1648.9	1637.3	1547.6

### 3.4.2 Determination of asparaginase activity

The asparaginase activity assay assessed the protein activity of the freshly prepared solution in water with 98.6 U/mg, the same as declared by the supplier (98.2 U/mg). Looking at the asparaginase in PBS pH 5.0 a slightly decreased activity (-12.5%) was found (86.1 U/mg, Fig. 2-6, Table 2-2).

For the asparaginase released from the polyglycerol nanogels, the activity (86.2 U/mg) is the same as for the non-treated and, thus, native protein in PBS pH 5.0 (Table 2-2). The activity assay for the intact PG nanogel with encapsulated asparaginase revealed an enzyme activity of  $38.9 \pm 4.1$  U/mg. Based on the former data (asparaginase activity after PG-encapsulation and release at pH 5, 87.5 U/mg) this value refers to 44.5 %. As no free asparaginase was detectable, it can be concluded that the substrate is able to interact with the asparaginase molecules located at the surface of the PG nanogel particles.

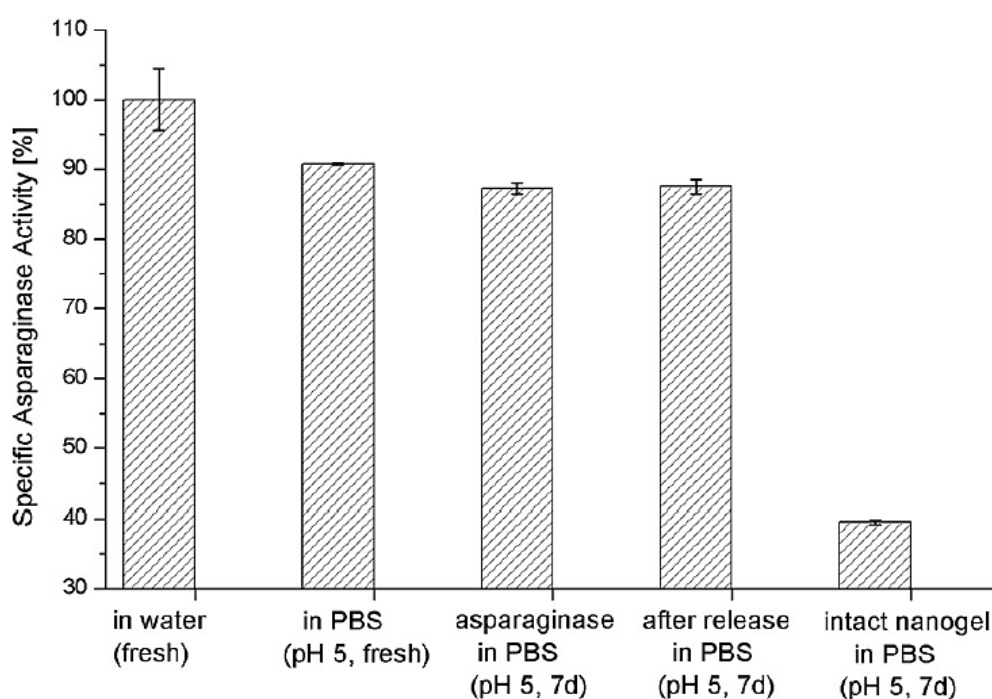


**Figure 2-6** Specific enzyme activity  $\pm$  SD [U/mg] determined with an asparaginase activity assay.

FT-IR measurements of the asparaginase showed no significant changes in secondary structure after protein encapsulation in the PG nanogels and subsequent release in a slightly acidified buffer (pH 5). As shown in Table 2-1, the peak shifts of our samples (amide I and II bands) range between 2 and 3  $\text{cm}^{-1}$ . In general, shifts up to 3  $\text{cm}^{-1}$  are inevitable and normal due to handling and measurement inaccuracies. Thus, for FT-IR spectra literature often refers to peak ranges, due to variations between different proteins, batch variability and measurement inaccuracies [56].

The asparaginase activity assay showed excellent results concerning the maintenance of the protein activity after encapsulation and protein release. Comparing the stored samples to freshly prepared asparaginase solution, a lower enzyme activity (- 12.5%) was found. Most likely, this decrease is related to a loss of active enzyme due to the storage in PBS pH 5. Nevertheless, as the encapsulated and released asparaginase had the same activity as the non-processed sample in PBS pH 5.0, it can be concluded that the encapsulation and release does not impair enzyme activity.

## 4. Conclusion

We have developed a new approach to dendritic polyglycerol nanogels by surfactant free, inverse nanoprecipitation. Size defined nanogels were observed, while diameters were freely adjustable between 100 and 1000 nm. Applying mild encapsulation conditions we were able to encapsulate the enzyme asparaginase with an efficacy of almost 100 %. After degradation triggered release in acidic environments no structural changes in the released cargo were observed and full enzyme activity was retained. Future work will be directed to the encapsulation of various biomacromolecules such as DNA, RNA, and proteins.

## 5. Acknowledgements

We thank Aileen Justies and Dr. Maximilian Zieringer for the help with fluorescence and optical microscopy correspondingly. We also thank Cathleen Schlesener for size exclusion measurements. This work was supported by the Helmholtz Virtuelles Institut / Helmholtz-Zentrum and the Focus Area Nanoscale of the Free University Berlin.

## 6. References

1. Steinman L, Merrill JT, McInnes IB, Peakman M. Optimization of current and future therapy for autoimmune diseases. *Nat. Med.* 18(1), 59–65 (2012).
2. Caspi RR. Immunotherapy of autoimmunity and cancer: the penalty for success. *Nat. Rev. Immunol.* 8(12), 970–976 (2008).

3. Jiskoot W, Randolph TW, Volkin DB, et al. Protein instability and immunogenicity: Roadblocks to clinical application of injectable protein delivery systems for sustained release. *J. Pharm. Sci.* 101(3), 946–954 (2012).
4. Caliceti P, Veronese FM. Pharmacokinetic and biodistribution properties of poly(ethylene glycol)-protein conjugates. *Adv. Drug Deliv. Rev.* 55(10), 1261–1277 (2003).
5. Haag R, Kratz F. Polymer therapeutics: Concepts and applications. *Angew. Chemie - Int. Ed.* 45(8), 1198–1215 (2006).
6. Banerjee SS, Aher N, Patil R, Khandare J. Poly(ethylene glycol)-Prodrug Conjugates: Concept, Design, and Applications. *J. Drug Deliv.* 2012, 1–17 (2012).
7. Knop K, Hoogenboom R, Fischer D, Schubert US. Poly(ethylene glycol) in drug delivery: Pros and cons as well as potential alternatives. *Angew. Chemie - Int. Ed.* 49(36), 6288–6308 (2010).
8. Matsumura Y, Maeda H. A new concept for macromolecular therapeutics in cancer chemotherapy: Mechanism of tumorotropic accumulation of proteins and the antitumor agent smancs. *Cancer Res.* 46(12 I), 6387–6392 (1986).
9. Jain RK. Transport of Molecules in the Tumor Interstitium: A Review. *Cancer Res.* . 47 (12 ), 3039–3051 (1987).
10. Nochi T, Yuki Y, Takahashi H, et al. Nanogel antigenic protein-delivery system for adjuvant-free intranasal vaccines. *Nat. Mater.* 9(7), 572–578 (2010).
11. Vermonden T, Censi R, Hennink WE. Hydrogels for protein delivery. *Chem. Rev.* 112, 2853–2888 (2012).
12. Kabanov A V., Vinogradov S V. Nanogels as pharmaceutical carriers: Finite networks of infinite capabilities. *Angew. Chemie - Int. Ed.* 48(30), 5418–5429 (2009).
13. Nayak S, Andrew Lyon L. Soft nanotechnology with soft nanoparticles. *Angew. Chemie - Int. Ed.* 44(47), 7686–7708 (2005).
14. Oh JK, Drumright R, Siegwart DJ, Matyjaszewski K. The development of microgels/nanogels for drug delivery applications. *Prog. Polym. Sci.* 33(4), 448–477 (2008).
15. Chacko RT, Ventura J, Zhuang J, Thayumanavan S. Polymer nanogels: A versatile nanoscopic drug delivery platform. *Adv. Drug Deliv. Rev.* 64(9), 836–851 (2012).
16. Asadian-Birjand M, Sousa-Herves A, Steinhilber D, Cuggino JC, Calderon M. Functional nanogels for biomedical applications. *Curr. Med. Chem.* 19(29), 5029–43 (2012).
17. Censi R, Di Martino P, Vermonden T, Hennink WE. Hydrogels for protein delivery in tissue engineering. *J. Control. Release.* 161(2), 680–692 (2012).
18. Oh JK, Tang C, Gao H, Tsarevsky N V., Matyjaszewski K. Inverse miniemulsion ATRP: A new method for synthesis and functionalization of well-defined water-soluble/cross-linked polymeric particles. *J. Am. Chem. Soc.* 128(16), 5578–5584 (2006).
19. Steinhilber D, Sisson AL, Mangoldt D, Welker P, Licha K, Haag R. Synthesis, reductive cleavage, and cellular interaction studies of biodegradable, polyglycerol nanogels. *Adv. Funct. Mater.* 20(23), 4133–4138 (2010).
20. Murthy N, Xu M, Schuck S, Kunisawa J, Shastri N, Fréchet JMJ. A macromolecular delivery vehicle for protein-based vaccines: acid-degradable protein-loaded microgels. *Proc. Natl. Acad. Sci. U. S. A.* 100(9), 4995–5000 (2003).
21. Paramonov SE, Bachelier EM, Beaudette TT, et al. Fully acid-degradable biocompatible polyacetal microparticles for drug delivery. *Bioconjug. Chem.* 19(4), 911–919 (2008).
22. Zhang J, Jia Y, Li X, Hu Y, Li X. Facile Engineering of Biocompatible Materials with pH-Modulated Degradability. *Adv. Mater.* 23(27), 3035–3040 (2011).
23. Shenoi RA, Lai BFL, Kizhakkedathu JN. Synthesis, characterization, and biocompatibility of biodegradable hyperbranched polyglycerols from acid-cleavable ketal group functionalized initiators. *Biomacromolecules.* 13(10), 3018–3030 (2012).
24. Yuan Y-Y, Du J-Z, Song W-J, et al. Biocompatible and functionalizable polyphosphate nanogel with a branched structure. *J. Mater. Chem.* 22(18), 9322–9329 (2012).
25. Parrott MC, Luft JC, Byrne JD, Fain JH, Napier ME, Desimone JM. Tunable bifunctional silyl ether cross-linkers for the design of acid-sensitive biomaterials. *J. Am. Chem. Soc.* 132(50), 17928–17932 (2010).
26. Klinger D, Landfester K. Enzymatic- and light-degradable hybrid nanogels: Crosslinking of polyacrylamide with acrylate-functionalized Dextrans containing photocleavable linkers. *J. Polym. Sci. Part A Polym. Chem.* 50(6), 1062–1075 (2012).
27. Fleige E, Quadir MA, Haag R. Stimuli-responsive polymeric nanocarriers for the controlled transport of active compounds: Concepts and applications. *Adv. Drug Deliv. Rev.* 64(9), 866–884 (2012).
28. Landfester K, Musyanovych A. Hydrogels in miniemulsions. *Adv. Polym. Sci.* 234, 39–63 (2010).

29. Sisson AL, Steinhilber D, Rossow T, Welker P, Licha K, Haag R. Biocompatible Functionalized Polyglycerol Microgels with Cell Penetrating Properties. *Angew. Chemie Int. Ed.* 48(41), 7540–7545 (2009).
30. Sisson AL, Papp I, Landfester K, Haag R. Functional Nanoparticles from Dendritic Precursors: Hierarchical Assembly in Miniemulsion. *Macromolecules.* 42(2), 556–559 (2009).
31. Steinhilber D, Seiffert S, Heyman JA, Paulus F, Weitz DA, Haag R. Hyperbranched polyglycerols on the nanometer and micrometer scale. *Biomaterials.* 32(5), 1311–1316 (2011).
32. Zhou H, Steinhilber D, Schlaad H, Sisson AL, Haag R. Glycerol based polyether-nanogels with tunable properties via acid-catalyzed epoxide-opening in miniemulsion. *React. Funct. Polym.* 71(3), 356–361 (2011).
33. Antonietti M. Microgels—Polymers with a Special Molecular Architecture. *Angew. Chemie Int. Ed. English.* 27(12), 1743–1747 (1988).
34. Du JZ, Sun TM, Song WJ, Wu J, Wang J. A tumor-acidity-activated charge-conversional nanogel as an intelligent vehicle for promoted tumoral-cell uptake and drug delivery. *Angew. Chemie - Int. Ed.* 49(21), 3621–3626 (2010).
35. McAllister K, Sazani P, Adam M, et al. Polymeric nanogels produced via inverse microemulsion polymerization as potential gene and antisense delivery agents. *J. Am. Chem. Soc.* 124(51), 15198–15207 (2002).
36. Xia Y, Whitesides GM. SOFT LITHOGRAPHY. *Annu. Rev. Mater. Sci.* 28(1), 153–184 (1998).
37. Rolland JP, Maynor BW, Euliss LE, Exner AE, Denison GM, DeSimone JM. Direct fabrication and harvesting of monodisperse, shape-specific nanobiomaterials. *J. Am. Chem. Soc.* 127(28), 10096–10100 (2005).
38. Zhang C, Pansare VJ, Prud'homme RK, Priestley RD. Flash nanoprecipitation of polystyrene nanoparticles. *Soft Matter.* 8(1), 86–93 (2012).
39. Schubert S, Delaney, Jr JT, Schubert US. Nanoprecipitation and nanoformulation of polymers: from history to powerful possibilities beyond poly(lactic acid). *Soft Matter.* 7(5), 1581 (2011).
40. Perevyazko IY, Delaney JT, Vollrath A, Pavlov GM, Schubert S, Schubert US. Examination and optimization of the self-assembly of biocompatible, polymeric nanoparticles by high-throughput nanoprecipitation. *Soft Matter.* 7(10), 5030 (2011).
41. Sussman EM, Clarke MB, Shastri VP. Single-step process to produce surface-functionalized polymeric nanoparticles. *Langmuir.* 23(24), 12275–12279 (2007).
42. Tong R, Yala L, Fan TM, Cheng J. The formulation of aptamer-coated paclitaxel-poly(lactide) nanoconjugates and their targeting to cancer cells. *Biomaterials.* 31(11), 3043–3053 (2010).
43. Zhang L, Chan JM, Gu FX, et al. Self-assembled lipid-polymer hybrid nanoparticles: A robust drug delivery platform. *ACS Nano.* 2(8), 1696–1702 (2008).
44. Sisson AL, Haag R. Polyglycerol nanogels: highly functional scaffolds for biomedical applications. *Soft Matter.* 6(20), 4968 (2010).
45. Khandare J, Calderón M, Dagia NM, Haag R. Multifunctional dendritic polymers in nanomedicine: opportunities and challenges. *Chem. Soc. Rev.* 41(7), 2824 (2012).
46. Siegers C, Biesalski M, Haag R. Self-assembled monolayers of dendritic polyglycerol derivatives on gold that resist the adsorption of proteins. *Chem. - A Eur. J.* 10(11), 2831–2838 (2004).
47. Weinhart M, Grunwald I, Wyszogrodzka M, Gaetjen L, Hartwig A, Haag R. Linear poly(methyl glycerol) and linear polyglycerol as potent protein and cell resistant alternatives to poly(ethylene glycol). *Chem. - An Asian J.* 5(9), 1992–2000 (2010).
48. Ekinci D, Sisson AL, Lendlein A. Polyglycerol-based polymer network films for potential biomedical applications. *J. Mater. Chem.* 22(39), 21100 (2012).
49. Mashburn LT, Wriston JC. Tumor inhibitory effect of L-asparaginase from *Escherichia Coli*. *Arch. Biochem. Biophys.* 105, 450–452 (1964).
50. Mitragotri S, Lahann J. Physical approaches to biomaterial design. *Nat. Mater.* 8(1), 15–23 (2009).
51. Papp I, Sieben C, Sisson AL, et al. Inhibition of Influenza Virus Activity by Multivalent Glycoarchitectures with Matched Sizes. *ChemBioChem.* 12(6), 887–895 (2011).
52. Pui C-H, Evans WE. Treatment of acute lymphoblastic leukemia. *N. Engl. J. Med.* 354(2), 166–178 (2006).
53. Patil S, Coutsouvelis J, Spencer A. Asparaginase in the management of adult acute lymphoblastic leukaemia: Is it used appropriately? *Cancer Treat. Rev.* 37(3), 202–207 (2011).
54. Sabu A. Sources, properties and applications of microbial therapeutic enzymes. *Indian J. Biotechnol.* 2(3), 334–341 (2003).
55. Adeishvili K. Glycerol-induced aggregation of the oligomeric L-asparaginase II from *E. coli* monitored with ATR-FTIR. *Int. J. Mol. Sci.* 2(2), 109–120 (2001).

56. Kong J, Yu S. *Fourier transform infrared spectroscopic analysis of protein secondary structures. Acta Biochim. Biophys. Sin. (Shanghai).* 39(8), 549–559 (2007).
57. Vellard M. *The enzyme as drug: Application of enzymes as pharmaceuticals. Curr. Opin. Biotechnol.* 14(4), 444–450 (2003).

## Chapter 3

### Thermosensitive dendritic polyglycerol-based nanogels for cutaneous delivery of biomacromolecules

The following chapter has been published as peer-reviewed article in the Journal of Controlled Release and appears in this thesis with the journal's permission:

Madeleine Witting<sup>1</sup>, Maria Molina<sup>1</sup>, Katja Obst, Roswitha Plank, Katja Martina Eckl, Hans Christian Hennies, Marcelo Calerón, Wolfgang Frieß, Sarah Hedtrich

*Thermosensitive dendritic polyglycerol-based nanogels for cutaneous delivery of biomacromolecules*

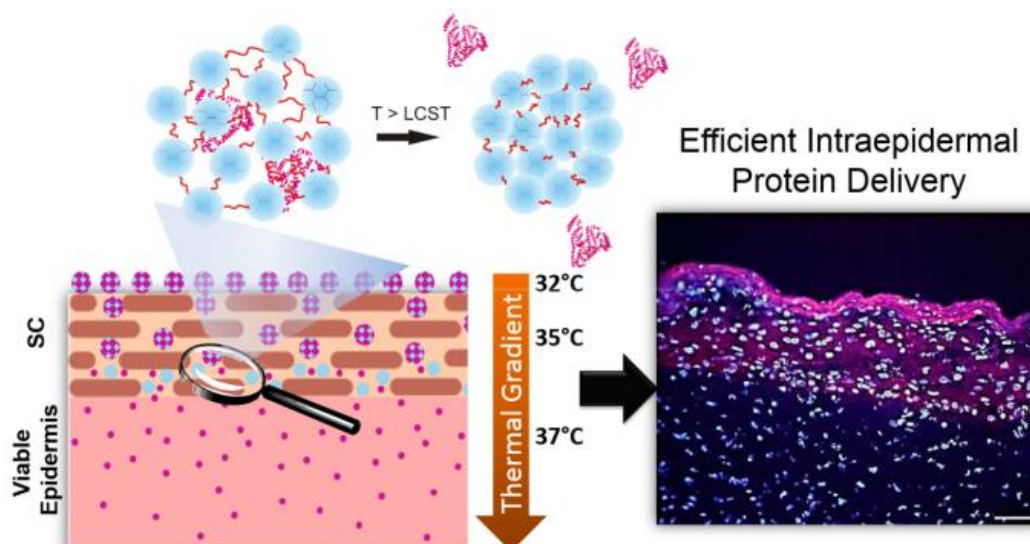
<sup>1</sup> both authors contributed equally

Nanomedicine 11, 5, (2015) 1179-1187

Online available: [http://www.nanomedjournal.com/article/S1549-9634\(15\)00067-2/abstract](http://www.nanomedjournal.com/article/S1549-9634(15)00067-2/abstract)

The personal contribution covers the written parts of the introduction, the results and discussion as well as the experimental set-up and execution with exception of the following chapters: **2.1 / 2.2 / 2.7.2 / 2.7.3 / 2.8 / 3.1 / 3.3** (personal contribution only covers the pig skin experiments)

#### Graphical Abstract



## Abstract

Genetic skin diseases caused by mutations resulting in diminished protein synthesis could benefit from local substitution of the missing protein. Proteins, however, are excluded from topical applications due to their physicochemical properties.

We prepared protein-loaded thermoresponsive poly(N-isopropylacrylamide)-polyglycerol-based nanogels exhibiting a thermal trigger point at 35°C, which is favorable for cutaneous applications due to the native thermal gradient of human skin. At  $\geq 35^\circ\text{C}$ , the particle size ( $\sim 200$  nm) was instantly reduced by 20% and 93% of the protein were released; no alterations of protein structure or activity were detected. Skin penetration experiments demonstrated efficient intraepidermal protein delivery particularly in barrier deficient skin, penetration of the nanogels themselves was not detected. The proof of concept was provided by transglutaminase1-loaded nanogels which efficiently delivered the protein into transglutaminase1-deficient skin models resulting in a restoration of skin barrier function.

In conclusion, thermoresponsive nanogels are promising topical delivery systems for biomacromolecules.

Keywords: reconstructed human skin, cutaneous protein delivery, thermoresponsive nanogels, dendritic polyglycerol, skin barrier restoration

## 1. Introduction

At present, nanotechnology is one of the incessantly and fastest growing areas of current pharmaceutical research with an enormous potential to generate diverse and efficient drug delivery systems [1, 2]. Skin health maintenance benefits from nanotechnology, because materials on the nanometer scale are potent tools for dermal and transdermal drug delivery enabling specific, effective, and customized treatment options and the diagnosis of cutaneous diseases [3, 4].

A well-defined, monodisperse and stable nanostructure is crucial for biomedical applications. This has been achieved by dendritic polymers such as hyperbranched or dendritic polyglycerol (dPG) [5]. dPG allows easy preparation combined with good aqueous solubility, high biocompatibility, multifunctionality, and protein stabilization against degradation and denaturation [6-9]. Fabricated as nanogels, which can be described as a cross-linked hydrophilic three-dimensional polymer network, dPG nanomaterials yield useful size ranges between 20 to 350 nm [7, 10].

Stimuli-responsive dPG-based nanogels became of special interest as they respond rapidly when being exposed to certain environmental conditions such as changes in temperature, pH, electrical or magnetic fields [10-14]. Thermoresponsive nanogels can be obtained by combining dPG with thermoresponsive linkers such as poly(N-isopropylacrylamide) (PNIPAM). PNIPAM-dPG nanogels undergo a reversible phase-transition at 32-33 °C, the lower critical solution temperature (LCST) of PNIPAM. When LCST is exceeded, the nanogels decrease in size due to changes in the local environment around the hydrophobic isopropyl domains, resulting in the expelling of water and loaded drugs [15]. Since the LCST is close to the physiological skin surface temperature (32 °C) which steadily increases with skin depth, these thermoresponsive PNIPAM-dPG nanogels may have a potential for topical applications [16-18].

Particularly for severe genetic skin diseases, with the underlying cause often located in the viable epidermis, the use of nanocarriers allow new therapeutic options [19]. Examples for these genodermatoses are the more common ichthyosis vulgaris caused by loss-of-function mutations in the gene encoding for filaggrin (*FLG*) [20], and the rare autosomal recessive congenital ichthyosis which can be caused by mutations in the transglutaminase gene (*TGM1*) [21]. Filaggrin is a highly repetitive structural protein expressed in the stratified layers of the skin and a lack in filaggrin impairs the barrier function and results in dryness and scaling and often atopic manifestations. *TGM1* codes for the enzyme transglutaminase 1 (TGase-1); a key player in the formation of the skin barrier. So far, therapeutic options only allow an alleviation of the symptoms using topically applied creams and ointments. Therefore, local substitution of the missing proteins presents an interesting treatment option which eliminates the need of parenteral application and high systemic drug levels. For this

approach, however, specific drug delivery systems are required as the excellent barrier properties of the human skin almost completely restrict the absorption of biomacromolecules due to their high molecular weight and hydrophilicity [22, 23].

To our best knowledge, PNIPAM-dPG nanogels for the delivery of biomacromolecules into the skin have not yet been explored. In the present study, we describe the synthesis of PNIPAM-dPG nanogels that encapsulate the model proteins bovine serum albumin (BSA) and L-asparaginase II (Asp) as well as the therapeutic protein candidate TGase-1. The PNIPAM-dPG nanogels were characterized for loading efficiency, protein release, and protein stability. UV-Vis spectroscopy, high performance size exclusion chromatography (HP-SEC), Fourier transformed infrared spectroscopy (FT-IR) measurements and specific activity assays were used to determine the protein concentration, protein stability, and to assess the bioactivity. To evaluate the cutaneous protein delivery efficiency, penetration studies in excised pig skin and reconstructed human skin were performed. Reconstructed human skin is increasingly important for skin absorption studies as it resembles native human skin well and offers several advantages over *in vivo* studies which are mostly performed in rodents. Rodent skin differs considerably from human skin since, e.g., the respective skin layers are significantly thinner and the abundance of hair follicles in rodents result in a distinct overestimation of skin absorption [24, 25]. Here, to mimic diseased and impaired skin barriers, the pig skin was tape-stripped 30 times [26] and the genes encoding for filaggrin and TGase-1, respectively, were knocked down in reconstructed human skin models [27-29].

## 2. Methods

### 2.1 Synthesis, characterization, and protein encapsulation of PNIPAM-dPG nanogels

PNIPAM-dPG nanogels were synthesized according to previously reported methods [10]. Briefly, 100 mg of NIPAM, 33 wt% of acrylated dPG (please see *Supplementary Materials* for the synthesis and fluorescent labeling), SDS (1.8 mg), and APS (2.8 mg) were dissolved in 5 mL of distilled water. Argon was bubbled into the reaction mixture for 15 min. The mixture was stirred under argon atmosphere for another 15 min. The reaction mixture was transferred into a hot bath at 68 °C and polymerization was activated after 5 min with the addition of catalytic amount of TEMED (120 µL). The mixture was stirred at 500 rpm for at least 4 h. The products were purified by dialysis membrane (MWCO 50000) in water for 48 h then lyophilized to yield the nanogels as a white solid (total yield 90 %). Alternatively, nanogels with MIA/MANT label were synthesized in the similar manner as described above using MIA labeled dPG-Ac as cross-linker.

<sup>1</sup>H-NMR of PNIPAM-dPG nanogels: (500 MHz, D<sub>2</sub>O),  $\delta$ : 1.13 (s, 6H, isopropyl groups of NIPAM), 1.57 (2 H, polymer backbone), 2.00 (1 H, polymer backbone), 3.35 – 4.10 (6 H, polyglycerol scaffold protons + 1H NIPAM).

For protein encapsulation, PNIPAM-dPG nanogels (10 mg mL<sup>-1</sup>) were swollen in a protein solution (10 mg mL<sup>-1</sup>) for 24 h at 4 °C. The solutions were purified using Vivaspins 300000, (10 min at 6000 rpm; Sartorius AG, Göttingen, Germany). The concentration of the BSA, Asp, and TGase-1 was determined by UV measurements at 280 nm and 350 nm (which served for background correction). Additionally, the amount of loaded protein was determined by a Micro BCA™ Protein Assay Kit following an incubation of the loaded nanogels at 37 °C for 1 h.

For nanogel characterization, <sup>1</sup>H NMR spectra was measured by a Bruker DRX 400 (400 MHz spectra) spectrometer. Typically 10-30 mg of compound was used and deuterated solvents were used as standardized procedure. All spectra were recorded at room temperature and were analyzed with MestReNova software.

## 2.2 Fluorescence labeling of bovine serum albumin (BSA)

For skin penetration experiments, BSA was labeled with RhB ITC. A 1 mg mL<sup>-1</sup> RhB ITC solution in DMSO was added to a 6 mg mL<sup>-1</sup> BSA solution in 0.1 M sodium bicarbonate buffer (pH 9.0) at a ratio of 1:170 w/w (dye : protein). After 2 hours stirring under light protection, the labeled BSA was purified and concentrated to 20-25 mg mL<sup>-1</sup> using Vivaspins 30000. The absence of free dye was confirmed by HP-SEC (TSKgel® SWXL guard column (dimensions: 6.0 mm x 4.0 cm), TSKgel® G4000 PWXL column (dimensions: 300 x 7.8 mm, 10  $\mu$ m particle size; TOSOH Bioscience, Stuttgart), isocratic elution at 0.4 mL min<sup>-1</sup>, 100 mM Na<sub>2</sub>HPO<sub>4</sub>, 150 mM NaCl, pH 7.4) with UV and fluorescence detection (protein <sub>UV</sub> = 280 nm, dye <sub>UV</sub> = 555 nm; protein fluorescence = exc. 280/ em. 350 nm, dye fluorescence = exc. 540 nm/em. 580 nm). The degree of labeling (0.95 - 1.3) was assessed according to manufacturer protocols. The lysine-dye bond between BSA and RhB ITC is stable up to 10 days [30].

## 2.3 PNIPAM-dPG nanogel size, thermosensitive kinetics, and protein release

The PNIPAM-dPG nanogel size and dispersity were determined by dynamic light scattering (DLS, scattering angle 173°) upon heating from 25 °C to 42 °C at 1 °Cmin<sup>-1</sup> using a Zetasizer Nano-ZS90 equipped with a He-Ne laser ( $\lambda$  = 633 nm) (Malvern Instruments, Herrenberg, Germany). The nanogel stock solutions (protein concentration: 3 - 5 mg mL<sup>-1</sup>) were diluted to a concentration of 1 mg mL<sup>-1</sup>. To evaluate the release of BSA-RhB ITC, the loaded nanogels (1 mg mL<sup>-1</sup>) were incubated under mild stirring (100 rpm) at 25 °C, 32 °C, and 37 °C for up to 4 h, respectively. The released amount of protein was measured at UV<sub>protein</sub> = 280 nm and UV<sub>dye</sub> = 558 nm using a UV spectrometer equipped with a heatable cuvette chamber (Agilent

8453 UV-Vis Spectrophotometer, Frankfurt, Germany). The UV absorption was background (UV = 350 nm) and nanogel blank corrected. Additionally, the samples were analyzed via HP-SEC (see 2.2)

## **2.4 Protein stability testing**

Protein stability over time was investigated by storing Asp loaded nanogels at 2-8 °C and 25 °C for 2 and 4 weeks. To study the effects of freeze-thaw stress, Asp-loaded nanogels (1 mg mL<sup>-1</sup>), blank nanogel, and Asp solution (1 mg mL<sup>-1</sup>) were subjected to 4 freeze-thaw cycles (-20 °C; 1 hour of freezing and 1 h of thawing). Subsequently, the samples were analyzed for Asp activity (see 2.6), Asp degradation and aggregate formation via HP-SEC (see 2.2).

## **2.5 Determination of protein secondary structure - Fourier transformed infrared spectroscopy (FT-IR)**

To investigate the structural integrity of the proteins after nanogel loading and release, FT-IR measurements using a Bruker Tensor 27 FTIR spectrometer (Ettlingen, Germany) equipped with a Bio-ATR measuring cell were performed. The samples were measured at 25 °C (120 scans, resolution of 4 cm<sup>-1</sup>, water vapor correction) using water for reference. The data were analyzed with the OPUS 6.5 software for second derivative spectra after vector normalization.

## **2.6 Asparaginase (Asp) activity**

Asp activity was determined as specific enzyme activity [U mg<sup>-1</sup>] [7, 31]. Briefly, 50 µl of sample were mixed with 100 µl Tris-HCl buffer (pH 8.6) and 850 µl 0.01 M L-asparagine monohydrate in 50 mM Tris-HCL buffer (pH 8.6) and incubated at 37 °C for 10 min. After adding 50 µl 1.5 M trichloroacetic acid solution, 100 µl of the supernatant was added to 200 µL Nessler's solution. After 10 min at 22 °C, the optical density was measured at 436 nm, compared with the standard curve and corrected for total enzyme amount determined by Micro BCA™ Protein Assay Kit. The units of activity were defined as micromoles of ammonia released per minute. Freshly prepared Asp solution served for reference.

## **2.7 Skin penetration experiments**

### **2.7.1 Cutaneous protein delivery efficiency - pig skin**

To investigate the influence of the thermoresponsive PNIPAM-dPG nanogels on the skin penetration of BSA-RhB ITC, initial absorption studies using pig skin were performed according to validated test procedures (for detailed description see Supplementary Information) [16]. Pig skin of the axillary region from donor animals (breed: "Deutsche

Landrasse", 12-20 weeks old) was provided by the Clinic for Swine, Center for Clinical Veterinary Medicine, LMU Munich, Germany (DE091620017X-1).

To induce an impaired skin barrier, tape-stripping was performed (10 cm length; tesapack® 4120 PVC, Tesa SE, Hamburg). The stripping was repeated 30 times [26] and SC thickness was subsequently measured using an image analysis software showing a SC thickness reduction from  $13 \pm 0.6 \mu\text{m}$  to  $6 \pm 0.4 \mu\text{m}$ .

### **2.7.2 Cutaneous protein delivery efficiency - normal and filaggrin-deficient reconstructed skin**

Normal and filaggrin-deficient reconstructed human skin models were generated according to previously published procedures [27]. To determine the protein delivery efficiency of the thermoresponsive nanogels, first we assessed the activity and delivery of the model protein Asp in the skin models. Secondly, the effects of the therapeutic protein candidate TGase-1 in TGase-1-deficient skin models were evaluated.

For Asp activity assay, the skin models were mounted onto static-type Franz cells equipped with Teflon inserts (diameter: 15 mm, volume 12 mL, 0.385 cm<sup>2</sup> application area, Gauer Glas, Püttlingen, Germany). PBS (pH 7.4) served as acceptor medium. After 30 min, 44  $\mu\text{L}$  of the Asp-loaded PNIPAM-dPG nanogels (23  $\mu\text{g cm}^{-2}$ ) were applied onto the skin models for 3 h applying a temperature ramp from 32 °C to 37 °C. Subsequently, the epidermis of the skin models was gently peeled off from the collagen matrix, transferred to Eppendorf tubes (Eppendorf, Hamburg, Germany) and 200  $\mu\text{L}$  Tris-HCl buffer pH 8.6 were added. The protein was extracted from the epidermis using a TissueLyser (Qiagen, Venlo, Netherlands). The specific Asp activity was determined as described in 2.6.

To semi-quantitatively analyze the skin absorption of Asp in normal and barrier-deficient skin models, the Franz cells could not be applied. Instead, the skin models were incubated in a transwell setup for 3 h in an incubator applying a temperature gradient from 32 °C to 37 °C. Afterwards, the skin models were snap frozen using liquid nitrogen and 10  $\mu\text{m}$  cryosections were prepared. Subsequently, immuno-staining against Asp (sc-130472, Santa Cruz Biotechnology, Heidelberg, Germany) was performed according to standard protocols. After staining, the sections were embedded in antifading mounting medium (Dianova, Hamburg, Germany) and analyzed under normal and fluorescence light (BZ-8000; Keyence, Neu-Isenburg, Germany).

### **2.7.3 Cutaneous delivery of therapeutic protein TGase-1 in TGase-1-deficient reconstructed skin**

Control and TGase-1-deficient reconstructed human skin were generated as described previously [32]. To investigate the effects of the therapeutic protein TGase-1, 50  $\mu\text{L}$  of protein-loaded nanogels were applied (5  $\mu\text{g cm}^{-2}$  TGase-1) at day 5, 7, 9, and 11 of tissue

cultivation, respectively. At day 13, the skin sections were stained against TGase1 as described above (TGase-1 antibody sc-166467, Santa Cruz Biotechnology, Heidelberg, Germany) and skin permeability was assessed.

## 2.8 Skin permeability testing

To assess the barrier function, skin absorption tests with radiolabeled testosterone were performed according to validated procedures [16, 25]. Briefly, a stock solution of testosterone (40  $\mu\text{g ml}^{-1}$ , 2 % [v/v] Igepal<sup>®</sup> CA-630) was spiked with an appropriate amount of the radiolabelled compound to a total radioactivity of 2  $\mu\text{Ci ml}^{-1}$ . By using the static setup and the infinite dose approach, skin permeability tests (Franz diffusion cells, diameter 15 mm, volume 12 ml; PermeGear, Bethlehem, PA, USA) were performed in triplicate.

## 2.9 Statistical analysis

Statistical analysis is based on the Wilcoxon-Mann-Whitney test and the unpaired t-test; \* $p \leq 0.05$  indicates a statistically significant difference.

# 3. Results

## 3.1 Particle synthesis and characterization

The nanogels were prepared by precipitation polymerization with PNIPAM as thermoresponsive polymer, 33 % acrylated dPG as macro-crosslinker, SDS as colloidal stabilizer, and PS/TEMED as redox radical initiator (Figure 3-1) [10].

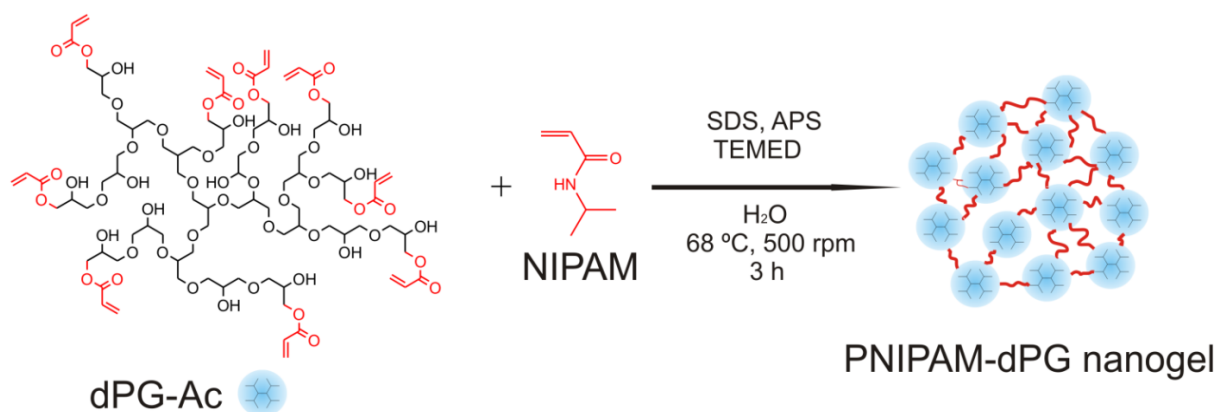


**Figure 3-1** Synthesis and chemical structure of the PNIPAM-dPG nanogels.

PNIPAM-dPG nanogels were subsequently characterized by DLS, NMR, and UV-Vis spectroscopy. To monitor temperature-related size changes, a temperature ramp was

applied during DLS heating the samples from 25 °C to 42 °C. The proteins BSA, Asp, and TGase-1 were encapsulated into the nanogels by swelling/diffusion at 4 °C. Table 3-1 lists the properties of the protein-loaded nanogels; zeta potential measurements revealed a neutral surface charge.

**Table 3-1** Characteristics of protein loaded nanogels.

Nanogel / protein	Loading capacity [%]	Diameter (nm) at 25 °C (PDI) / 37 °C (PDI) <sup>(a)</sup>	Thermal Trigger Point T <sub>p</sub> (°C) <sup>(b)</sup>
PNIPAM-dPG	-	192 (0.26) / 118 (0.09)	33.0
PNIPAM-dPG/BSA	70	207 (0.36) / 170 (0.19)	35.0
PNIPAM-dPG/Asp	30	205 (0.14) / 170 (0.14)	34.5

<sup>a</sup> determined by DLS, average of 3 measurements from the intensity distribution curves

<sup>b</sup> determined by UV-Vis transmittance ( $\lambda = 500$  nm)

### 3.2 Protein Release, structural integrity, and maintenance of bioactivity

The temperature-triggered decrease in nanogel size induced the release of the cargo. At 25 °C and 32 °C, only minimal amounts of BSA-RhB-ITC were released after 1 h ( $1.5 \pm 0.3$  % and  $4.8 \pm 0.8$  %, respectively) (Figure 3-2). In contrast,  $90.6 \pm 0.5$  % of the protein was released within 1 h at 37 °C; incubation for 4 h did not result in higher release rates (Figure S1). No protein aggregation was observed as determined by SEC measurements, no visible particles were detected.

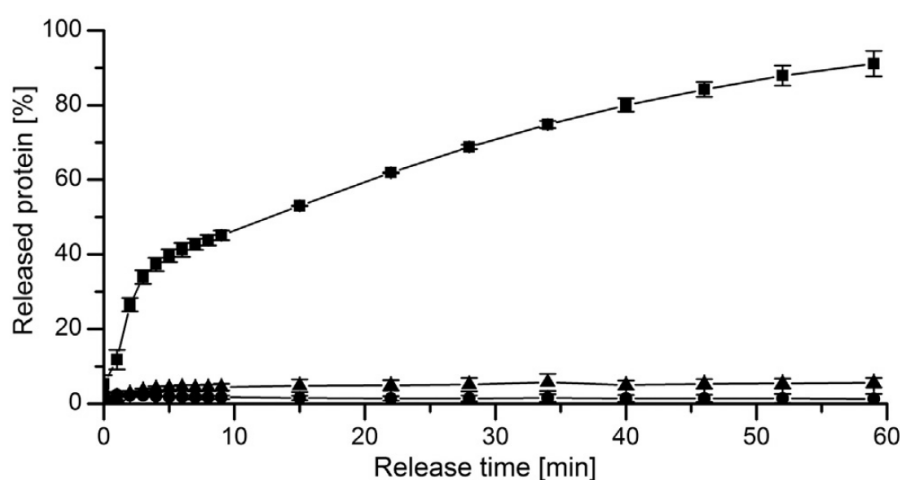


**Figure 3-2:** Release of bovine serum albumin from PNIPAM-dPG nanogels over 1 h at 25 °C (●), 32 °C (▲), and 37 °C (■) measured with UV-Vis spectroscopy. n=3, mean  $\pm$  SD

We also performed structural analysis of released BSA to exclude potential detrimental effects of the encapsulation and release process. Figure 3-3 displays the perfect overlay of

the spectra of fresh BSA solution and BSA released from the nanogels, including two additional controls. With peak positions at  $\sim 1657\text{ cm}^{-1}$  and  $\sim 1549\text{ cm}^{-1}$  and some smaller bands between  $1613$  and  $1637\text{ cm}^{-1}$ , BSA shows  $\sim 66\%$  alpha helix and  $\sim 20\%$  beta sheet structure, which is in accordance with the literature [33].

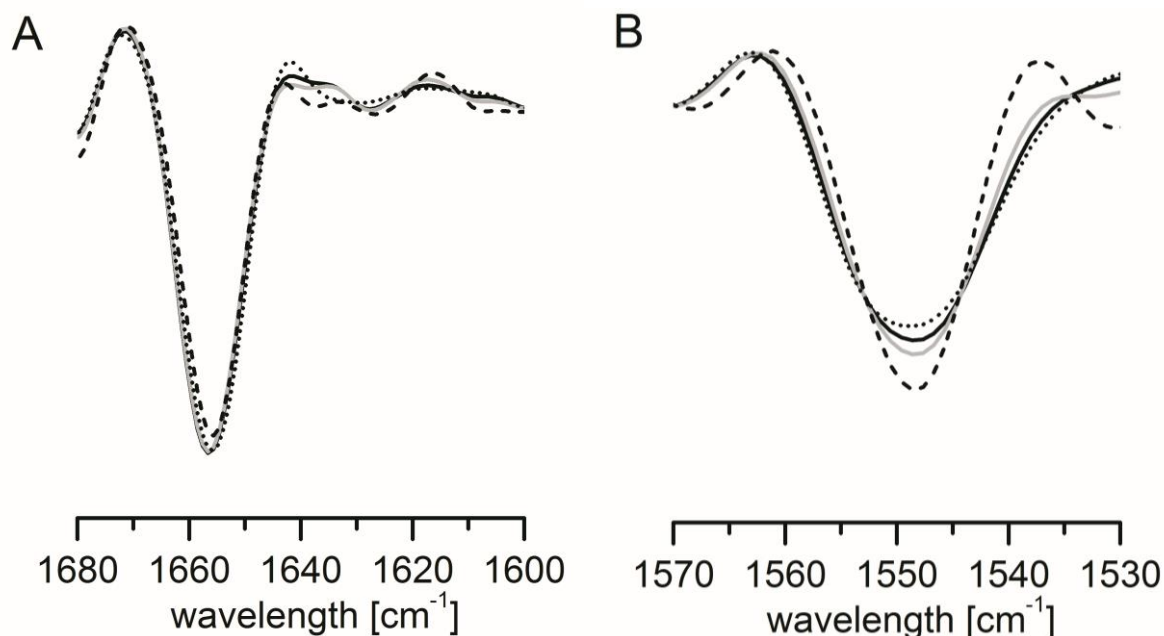


**Figure 3-3:** Second derivative ATR-FT-IR spectra of the (A) amide I ( $\sim 1650\text{ cm}^{-1}$ ) and (B) amide II ( $\sim 1550\text{ cm}^{-1}$ ) region of BSA in water, freshly prepared (solid line), BSA in water, 22 h at  $37\text{ }^{\circ}\text{C}$  (grey line), BSA loaded PNIPAM-dPG nanogel in water, freshly prepared (dotted line) and BSA after the release treatment for 22 h at  $37\text{ }^{\circ}\text{C}$  (dashed line).

Furthermore, released Asp did not show significant loss in bioactivity ( $98.5 \pm 4.1\%$ ) compared to freshly prepared Asp solution ( $100.0 \pm 4.4\%$ ) and Asp solution after 4 h incubation at  $37\text{ }^{\circ}\text{C}$  ( $100.6 \pm 5.0\%$ ). As an additional control, unloaded PNIPAM-dPG-nanogel was spiked with free Asp and incubated at  $37\text{ }^{\circ}\text{C}$ . Again, the bioactivity was not reduced.

To investigate potential protein stabilizing effects of the nanogels, freeze-thaw studies were performed. Freeze-thawing is an important stress factor for proteins since cold temperatures, ice formation, changes in solute concentrations, and pH can induce protein degradation or aggregation [34]. Asp in solution substantially lost bioactivity already after one freeze-thaw cycle ( $95.3 \pm 2.8\%$ ) which was further reduced to  $92.1 \pm 2.2\%$  after 4 cycles. In contrast, for loaded Asp only a slight decrease to  $96.3 \pm 0.5\%$  was observed following 4 freeze-thaw cycles (Figure 3-4A). Loading of Asp onto the nanogels also preserved its active tetramer form upon freeze-thaw stress, whereas Asp in solution experienced a distinct loss of the tetramers and a corresponding increase in aggregates and fragments (Figure S2). Similarly, storage of free Asp for 2 and 4 weeks at  $25\text{ }^{\circ}\text{C}$  resulted in significantly reduced bioactivity

(Figure 3-4B), less tetramers, and increased aggregation compared to nanogel-loaded Asp (Figure S3). No differences were observed at 4 °C.

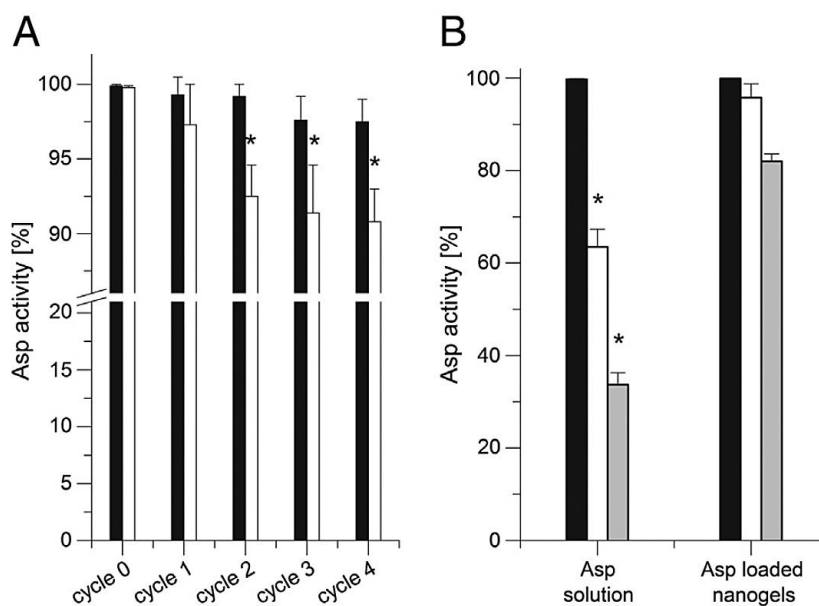


**Figure 3-4** A) Bioactivity of loaded asparaginase (Asp) (black bars) and free Asp in an aqueous solution (white bars) following 4 freeze-thaw cycles.  $n = 3$ , mean  $\pm$  SD. \*  $p < 0.05$  B) Bioactivity of loaded Asp and free Asp in an aqueous solution of freshly prepared samples (black bars), after 2 weeks (white bars), and 4 weeks (grey bars) storage at 25 °C.  $n = 3$ , mean  $\pm$  SD. \*  $p < 0.05$

### 3.3 Cutaneous protein delivery efficiency of PNIPAM-dPG nanogels

First, we investigated the protein delivery efficiency of BSA-RhB ITC loaded nanogels, nanogels spiked with free BSA-RhB ITC, and BSA-RhB ITC control solution in normal and tape-stripped pig skin. To elucidate whether the nanogels themselves are able to overcome the SC, the nanogels were fluorescently labeled with N-methylisatoic anhydride dye, resulting in a blue fluorescent N-methylantraniloyl group (MANT) [35].

In normal pig skin, no epidermal protein delivery was observed for all samples; the protein exclusively accumulated in the SC (Figure S4, A-C). In tape-stripped skin, however, the PNIPAM-dPG nanogels significantly enhanced intraepidermal protein delivery indicated by a distinct red staining of the viable epidermis (Figure S4, E). Again, no penetration was detected with the BSA-RhB ITC control solution and the spiked nanogel. The visual differences were substantiated by semi-quantitative image analysis (Table S1). Here, the fluorescence brightness evaluated as arbitrary brightness units (ABU) revealed a fourfold ABU increase in the epidermis of tape-stripped skin for BSA-loaded nanogels. The nanogels themselves were not able to overcome the SC even in damaged skin (data not shown).

In the next step, we studied the absorption of Asp in normal and filaggrin deficient skin models. Therefore, we applied Asp loaded PNIPAM-dPG nanogels and Asp control solution

onto normal and filaggrin deficient skin models for 3 h. To obtain comparable results to the pig skin experiment, the incubation time was reduced since skin models have a higher permeability due to a weaker skin barrier function [25, 36]. Subsequently, to get a rough estimation about the delivery efficiency of the nanogels, we determined the amount of Asp in the SC and viable epidermis by assessing the specific Asp activity present in the skin models [7]. Following the application of Asp loaded nanogels,  $9.5 \pm 0.1 \mu\text{g}$  Asp were detected in the SC and viable epidermis. In skin models incubated with the Asp solution, 30 % less protein was recovered ( $6.3 \pm 0.1 \mu\text{g}$ ).

Since this experimental setup did not allow the discrimination of the protein content in the SC and the viable epidermis, we subsequently performed immunohistology. The application of Asp solution did not result in intraepidermal penetration in normal (Figure 3-5 A) or barrier-deficient (Figure 3-5 C) skin models. In contrast, significant amounts of Asp were detected in the viable epidermis of barrier-deficient skin models following the application of the loaded nanogels (Figure 3-5 D) indicated by a marked red staining of the viable epidermis and the SC. No penetration was seen in normal skin models (Figure 3-5 B).

Consistently, the application of TGase-1-loaded nanogels also resulted in efficient protein delivery into the viable epidermis of TGase-1-deficient skin models as indicated by a distinct red staining (Figure 3-6 C). Immunostaining visualized the physiological distribution of TGase-1 in normal skin models (Figure 3-6 A) and its severely reduced expression in untreated TGase-1-deficient skin models (Figure 3-6 B).

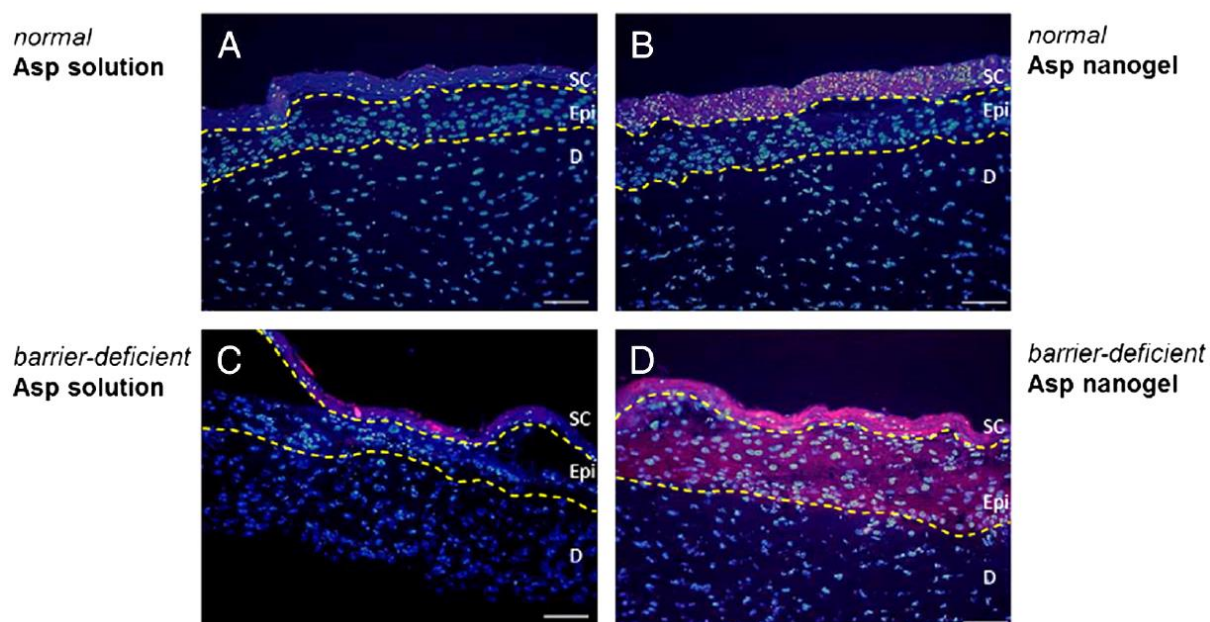


**Figure 3-5:** Skin penetration of asparaginase (Asp) in normal and barrier-deficient skin models following the application of Asp loaded PNIPAM-dPG nanogels and the Asp control solution. SC = stratum corneum, Epi = viable epidermis, D = dermis. Scale bar = 100  $\mu\text{m}$ .

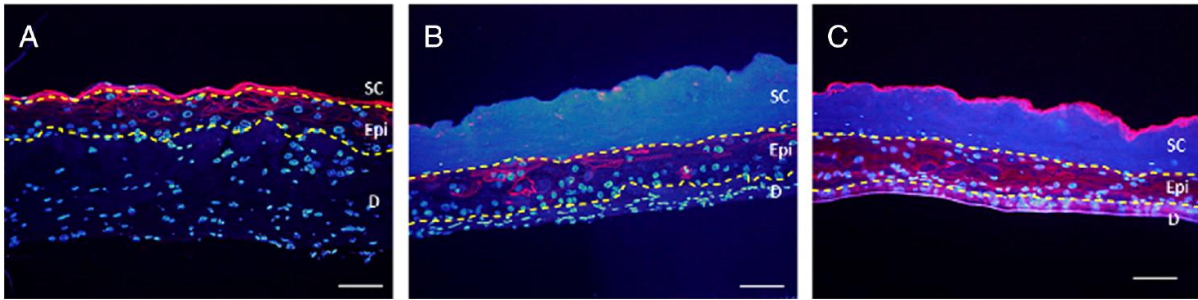


**Figure 3-6:** Immunostaining of transglutaminase 1 (TGase-1) in normal skin models (A), TGase-1-deficient skin models (B), and TGase-1-deficient skin models following the application of TGase-1-loaded nanogels (C). SC = stratum corneum, Epi = viable epidermis, D = dermis. Scale bar = 100 μm.

Finally, to provide the proof of concept of the local protein substitution approach, the skin barrier function of normal, untreated skin models, TGase-1-deficient skin models, and TGase-1-deficient skin models after treatment with TGase-1-loaded nanogels was determined. In normal skin models with a functional skin barrier, about  $\sim 1.5 \mu\text{g}\cdot\text{cm}^{-2}$  testosterone permeated through the skin. In TGase-1-deficient skin models, about 5-fold higher concentrations were measured ( $\sim 7.5 \mu\text{g}\cdot\text{cm}^{-2}$ ) reflecting the disturbed skin barrier function due to the lack of TGase-1 (Figure 3-7). Following the treatment with TGase-1-loaded nanogels, however, significantly reduced testosterone permeation ( $\sim 2 \mu\text{g}\cdot\text{cm}^{-2}$ ) was observed.

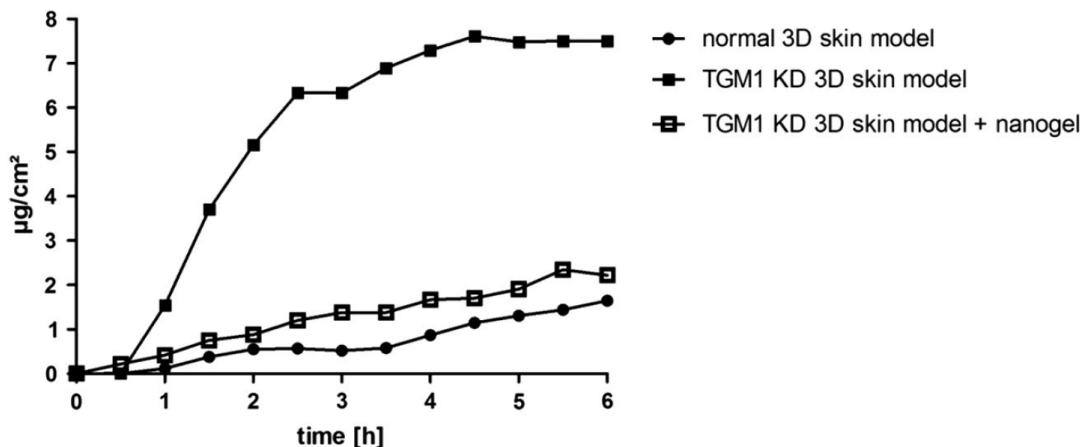


**Figure 3-7:** Permeation of testosterone through normal and TGase-1-deficient skin models treated with TGase-1-loaded nanogels (□).

## 4. Discussion

We successfully loaded different proteins onto thermoresponsive, dendritic nanogels and systematically investigated them for their suitability and efficiency as topical delivery system for labile biomacromolecules. The nanogels were thoroughly characterized for protein loading and release. Unloaded PNIPAM-dPG nanogels showed an average diameter of  $192 \pm 2 \text{ nm}$

(PDI 0.26) and underwent size reduction to  $118 \pm 1$  nm (PDI 0.09) at the thermal trigger point ( $T_P$ ) of 33 °C. After loading the nanogels with BSA or Asp, the nanogel size increased to  $207 \pm 3$  nm (PDI 0.36) and  $205 \pm 2$  nm (PDI 0.14), respectively (Table 3-1). Although the size increase was similar for Asp and BSA, the loading capacity was different with 70 % for BSA and only 30 % for Asp due to the different molecular weights (BSA 66 kDa vs. Asp ~140 kDa). Above  $T_P$ , the particle size of loaded nanogels was reduced to ~170 nm compared to ~118 nm of the unloaded nanogels. This can be explained by a higher rigidity of the loaded nanogels, as they have to work against a higher inner density resulting from the protein load. The thermally triggered size reductions result from the physicochemical characteristics of PNIPAM, which exhibits a LCST at 31 - 32 °C [10, 12, 37]. When exceeding the LCST, PNIPAM undergoes a reversible phase transition and water is simultaneously expelled. Unloaded PNIPAM-dPG nanogels exhibited a slightly higher phase transition at ~33 °C compared to pure PNIPAM caused by the dPG fraction which increases the nanogels' hydrophilicity [10]. Loading of the protein resulted in a slight shift of  $T_P$  to temperatures about ~35 °C most likely due to hydrophilic interactions between the nanogels and the proteins [7, 12]. This increased  $T_P$  can be beneficial for dermal applications. The skin temperature is 32 °C at the surface and raises constantly with increasing depth [17, 18]. By applying the nanogels onto the skin, the surface temperature prevents the immediate drug release and the nanogels may interact intensively with the skin surface as previously described for other dPG-based nanocarriers [36]. We hypothesize that the nanogels finally reach deeper layers of the stratum corneum where the trigger point temperature of ~35 °C is exceeded and ultimately the protein is released.

Since proteins are sensitive molecules, the investigation of potential detrimental effects on the structural integrity or bioactivity was crucial in which no negative effects of the nanogels were observed (Figure 3-4). In contrast, encapsulating the proteins in the nanogels even protected them from freeze-thaw stress and extended their storage stability (Figure 3-4, S3). To assess the efficiency of the thermoresponsive nanogels in dermal protein delivery, skin penetration experiments using pig skin and reconstructed human skin were performed. Pig skin is an accepted alternative for human skin [38]. Although the anatomical and physiological properties of pig and human skin are similar, the skin barrier of pigs is stronger, which typically leads to underestimation of skin absorption. To overcome this drawback, and to study the nanogels in viable skin, selected experiments were carried out in reconstructed human skin. These skin models resemble anatomical and physiological properties of native human skin [24, 39] and are advantageous over *in vivo* studies often performed in rodents due to the avoidance of interspecies-related variability. Moreover, a knock down of ichthyosis-associated genes in keratinocytes used for the reconstructed human skin enables the generation of diseased skin [27, 29, 40]. Consequentially, we opted for filaggrin- and TGase-1-deficient skin models. Filaggrin deficiency is the underlying cause for ichthyosis

vulgaris [20] and a major predisposing factor for the manifestation of atopic dermatitis [41]. Filaggrin deficiency causes disturbed epidermal maturation and differentiation, altered skin lipid composition and organization, and an impaired skin barrier [27, 28]. TGase-1 is a key enzyme in the formation of the cornified envelope of the human epidermis and mutations in the gene encoding for TGase-1 are the underlying cause for autosomal-recessive congenital ichthyosis which is also characterized by an impaired skin barrier function and generalized hyperkeratosis [42, 43]. Hence, these skin disease models mimic barrier-impaired skin which is important to consider since the barrier function of diseased skin differs significantly from normal skin [44, 45].

Our data clearly showed efficient cutaneous delivery of BSA, Asp, and the therapeutic protein candidate TGase-1 particularly in barrier deficient skin. Immunostaining of the skin models impressively visualized the extent of skin penetration of the different proteins (Figure 3-5, 3-6, S4).

In contrast, cutaneous absorption of the nanogels themselves was not observed. Whether nanocarriers are able to penetrate into normal or damaged skin is still up to debate as many studies with differing outcome are published [46-48]. For example, Zvyagin et al. [49] showed that zinc oxide particles (20-30 nm) stayed in the SC of normal skin and only accumulated in skin folds and hair follicles [49] which is also consistent with Luengo et al. [50]. Moreover, Ostrowski et al. demonstrated that skin barrier disruptions by either tape-stripping or skin diseases had no effect on the penetration of silica nanoparticles [51]. In contrast, Alnasif et al. showed pronounced penetration of dendritic core-multishell nanotransporters in damaged skin [36].

Since our results showed no penetration of the nanogels themselves, the mode of enhanced protein delivery is still ambiguous. Some studies highlighted the influence of surface charges on skin penetration and demonstrated that charged nanoparticles were more efficient due to better skin adhesion [52]. Since our nanogels exhibited no surface charge, electrostatic interactions can be excluded. As discussed earlier, we hypothesize that the nanogels interact intensively with the skin surface most likely due to the amphiphilic polyglycerol-based structure which also proved to be beneficial in previous studies [3, 53]. The nanogels finally reached deeper layers of the SC that exhibited temperatures  $\geq 33$  °C and the protein release was induced. Another possibility is that the nanogels act as drug release modifiers. Chauhan et al. described that poly(amido amines) were able to form stable drug-polymer complexes and the resulting solubility enhancement effectively increased the drug flux across the skin [54]. Furthermore, nanogels might be penetration enhancers by interacting with the skin surface lipids and proteins and, thus, loosening the tightly packed SC structure [55]. Clearly, further studies are required to unravel the mode of delivery.

To provide the proof of concept for the protein substitution approach, nanogel mediated delivery of the therapeutic protein candidate TGase-1 into TGase-1-deficient skin models

was tested. Following the application of TGase-1-loaded nanogels, the protein was efficiently delivered into the viable epidermis of TGase-1-deficient skin models (Figure 3-6) and the skin barrier function was restored indicated by a significant reduction of skin permeability (Figure 3-7).

Aufvenne et al., also aimed for a topical enzyme-replacement therapy to restore TGase-1 activity and correct the architecture of TGase-1-deficiency in skin grafts [42]. Treatment with 40 ng cm<sup>-2</sup> TGase-1 encapsulated in sterically stabilized liposomes resulted in considerable improvement of the ichthyosis phenotype and restored TGase-1 activity and epidermal barrier function. A further study which underlines the huge potential of a topical protein substitution therapy for severe skin diseases was published by Stout et al. [56]. Here, *in vivo* application of a “filaggrin - cell penetrating peptide conjugate” in filaggrin deficient flaky tail mice resulted in internalization and processing of the conjugate and a restoration of the normal phenotype. However, the carrier systems of both studies clearly have limitations such as physical instability and low loading capacities for the liposomes [57, 58] or potential irritant or toxic effects of cell penetrating peptides [59, 60]. In contrast, thermoresponsive nanogels offer several advantages such as good biocompatibility, high loading capacities, and triggered payload release.

In conclusion, we describe a thermoresponsive PNIPAM-dPG nanogel for cutaneous protein delivery, which is particularly applicable for human skin due to its native thermal gradient. We demonstrated that the delivery of TGase-1 loaded onto PNIPAM-dPG nanogels into TGase-1-deficient skin restored the skin barrier function. Although the protein delivery into the viable epidermis of normal skin appeared to be insufficient, the nanogels were superior in barrier-deficient skin (tape-stripped, filaggrin and TGase-1 deficient). Therefore, these nanogels have great potential for the approach of local protein substitution. Stress testing also revealed the ability of the nanogels to stabilize and maintain the biological function of labile proteins. Hence, PNIPAM-dPG nanogels are capable to load sensitive biomacromolecules and deliver them in therapeutically relevant concentrations into the viable epidermis of barrier-deficient skin without loss of protein integrity and bioactivity.

## 5. Acknowledgement

The authors state no conflict of interest and declare no commercial interests related to this work.

This project was financially supported by the German Research Foundation (DFG; KU 2904/2-1, S.K.; HE 3119/9-1, H.C.H.) and the Bundesministerium für Bildung und Forschung (BMBF) through the NanoMatFutur award (ThermoNanogele 13N12561, M.C.). Furthermore, we greatly acknowledge the financial support of the SFB 1112, projects A04 and C02. Dr.

Molina gratefully acknowledges to the Alexander von Humboldt Foundation for a postdoctoral fellowship.

## 6. References

1. Bamrungsap, S., Z. Zhao, T. Chen, L. Wang, C. Li, T. Fu, et al., *Nanotechnology in therapeutics: a focus on nanoparticles as a drug delivery system*. *Nanomedicine*, 2012. 7(8): p. 1253-1271.
2. Duncan, R., *Polymer therapeutics as nanomedicines: new perspectives*. *Current Opinion in Biotechnology*, 2011. 22(4): p. 492-501.
3. KÜchler, S., M.R. Radowski, T. Blaschke, M. Dathe, J. Plendl, R. Haag, et al., *Nanoparticles for skin penetration enhancement – A comparison of a dendritic core-multishell-nanotransporter and solid lipid nanoparticles*. *European Journal of Pharmaceutics and Biopharmaceutics*, 2009. 71(2): p. 243-250.
4. Gupta, S., R. Bansal, S. Gupta, N. Jindal, and A. Jindal, *Nanocarriers and nanoparticles for skin care and dermatological treatments*. Vol. 4. 2013.
5. Asadian-Birjand, M., A. Sousa-Herves, D. Steinhilber, J.C. Cuggino, and M. Calderon, *Functional nanogels for biomedical applications*. *Curr Med Chem*, 2012. 19(29): p. 5029-43.
6. Calderón, M., M.A. Quadir, S.K. Sharma, and R. Haag, *Dendritic Polyglycerols for Biomedical Applications*. *Advanced Materials*, 2010. 22(2): p. 190-218.
7. Steinhilber, D., M. Witting, X. Zhang, M. Staegemann, F. Paulus, W. Friess, et al., *Surfactant free preparation of biodegradable dendritic polyglycerol nanogels by inverse nanoprecipitation for encapsulation and release of pharmaceutical biomacromolecules*. *Journal of Controlled Release*, 2013. 169(3): p. 289-295.
8. Khandare, J., M. Calderon, N.M. Dagia, and R. Haag, *Multifunctional dendritic polymers in nanomedicine: opportunities and challenges*. *Chemical Society Reviews*, 2012. 41(7): p. 2824-2848.
9. Höger, K., T. Becherer, W. Qiang, R. Haag, W. Frieß, and S. KÜchler, *Polyglycerol coatings of glass vials for protein resistance*. *European Journal of Pharmaceutics and Biopharmaceutics*, 2013. 85(3, Part A): p. 756-764.
10. Cuggino, J.C., C.I. Alvarez I, M.C. Strumia, P. Welker, K. Licha, D. Steinhilber, et al., *Thermosensitive nanogels based on dendritic polyglycerol and N-isopropylacrylamide for biomedical applications*. *Soft Matter*, 2011. 7(23): p. 11259-11266.
11. Giulbudagian, M., M. Asadian-Birjand, D. Steinhilber, K. Achazi, M.A. Molina, and M. Calderón, *Fabrication of Thermoresponsive Nanogels by Thermo-Nanoprecipitation and in situ Encapsulation of Bioactives*. *Polymer Chemistry*, in press.
12. Bhuchar, N., R. Sunasee, K. Ishihara, T. Thundat, and R. Narain, *Degradable Thermoresponsive Nanogels for Protein Encapsulation and Controlled Release*. *Bioconjugate Chemistry*, 2011. 23(1): p. 75-83.
13. Molina, M., M. Giulbudagian, and M. Calderón, *Positively Charged Thermoresponsive Nanogels for Anticancer Drug Delivery*. *Macromolecular Chemistry and Physics*, in press.
14. Bergueiro, J. and M. Calderon, *Thermoresponsive Nanodevices in Biomedical Applications*. *Macromol Biosci*, 2014.
15. Fleige, E., M.A. Quadir, and R. Haag, *Stimuli-responsive polymeric nanocarriers for the controlled transport of active compounds: Concepts and applications*. *Advanced Drug Delivery Reviews*, 2012. 64(9): p. 866-884.
16. OECD, *Test No. 428: Skin Absorption: In Vitro Method*. OECD Publishing.
17. Benedict, F.G., W.R. Miles, and A. Johnson, *The Temperature of the Human Skin*. *PNAS*, 1919. 5(6): p. 218-222.
18. Aizawa, S. and M. Cabanac, *Temperature gradient across the skin's layers has no influence on local skin vasomotor responses*. *Journal of Thermal Biology*, 2000. 25(4): p. 313-316.
19. Prow, T.W., J.E. Grice, L.L. Lin, R. Faye, M. Butler, W. Becker, et al., *Nanoparticles and microparticles for skin drug delivery*. *Advanced Drug Delivery Reviews*, 2011. 63(6): p. 470-491.
20. Smith, F.J., A.D. Irvine, A. Terron-Kwiatkowski, A. Sandilands, L.E. Campbell, Y. Zhao, et al., *Loss-of-function mutations in the gene encoding filaggrin cause ichthyosis vulgaris*. *Nat Genet*, 2006. 38(3): p. 337-342.

21. Aufenvenne, K., F. Larcher, I. Hausser, B. Duarte, V. Oji, H. Nikolenko, et al., *Topical Enzyme-Replacement Therapy Restores Transglutaminase 1 Activity and Corrects Architecture of Transglutaminase-1-Deficient Skin Grafts*. *American Journal of Human Genetics*, 2013. 93(4): p. 620-630.
22. Herwadkar, A. and A.K. Banga, *Peptide and protein transdermal drug delivery*. *Drug Discovery Today: Technologies*, 2012. 9(2): p. e147-e154.
23. Schoellhammer, C.M., D. Blankschtein, and R. Langer, *Skin permeabilization for transdermal drug delivery: recent advances and future prospects*. *Expert Opinion on Drug Delivery*, 2014. 11(3): p. 393-407.
24. KÜchler, S., K. Strüver, and W. Friess, *Reconstructed skin models as emerging tools for drug absorption studies*. *Expert Opinion on Drug Metabolism & Toxicology*, 2013. 9(10): p. 1255-1263.
25. Schäfer-Korting, M., U. Bock, W. Diembeck, H.J. Dusing, A. Gamer, E. Haltner-Ukomadu, et al., *The use of reconstructed human epidermis for skin absorption testing: Results of the validation study*. *Altern Lab Anim*, 2008. 36(2): p. 161-87.
26. Gao, Y., X. Wang, S. Chen, S. Li, and X. Liu, *Acute skin barrier disruption with repeated tape stripping: an in vivo model for damage skin barrier*. *Skin Research and Technology*, 2013. 19(2): p. 162-168.
27. KÜchler, S., D. Henkes, K. Eckl, K. Ackermann, J. Plendl, H. Korting, et al., *Hallmarks of Atopic Skin In Vitro - Mimicked by the Means of a Skin Disease Model based on FLG Knock Down*. *ATLA*, 2011. 39: p. 471-480.
28. Vávrová, K., D. Henkes, K. Strüver, M. Sochorova, B. Skolova, M.Y. Witting, et al., *Filaggrin Deficiency Leads to Impaired Lipid Profile and Altered Acidification Pathways in a 3D Skin Construct*. *J Invest Dermatol*, 2014. 134(3): p. 746-753.
29. Mildner, M., J. Jin, L. Eckhart, S. Kezic, F. Gruber, C. Barresi, et al., *Knockdown of Filaggrin Impairs Diffusion Barrier Function and Increases UV Sensitivity in a Human Skin Model*. *J Invest Dermatol*, 2010. 130(9): p. 2286-2294.
30. Banks, P.R. and D.M. Paquette, *Comparison of Three Common Amine Reactive Fluorescent Probes Used for Conjugation to Biomolecules by Capillary Zone Electrophoresis*. *Bioconjugate Chemistry*, 1995. 6(4): p. 447-458.
31. Mashburn, L.T. and J.C. Wriston Jr, *Tumor inhibitory effect of L-asparaginase*. *Biochemical and Biophysical Research Communications*, 1963. 12(1): p. 50-55.
32. Eckl, K.M., T. Alef, S. Torres, and H.C. Hennies, *Full-thickness human skin models for congenital ichthyosis and related keratinization disorders*. *The Journal of investigative dermatology*, 2011. 131(9): p. 1938-42.
33. Maruyama, T., S. Katoh, M. Nakajima, and H. Nabetani, *Mechanism of bovine serum albumin aggregation during ultrafiltration*. *Biotechnology and Bioengineering*, 2001. 75(2): p. 233-238.
34. Hawe, A., J.C. Kasper, W. Friess, and W. Jiskoot, *Structural properties of monoclonal antibody aggregates induced by freeze-thawing and thermal stress*. *Eur J Pharm Sci*, 2009. 38(2): p. 79-87.
35. DeAngelis, P.L., *Polysaccharide Labeling with N-Methylisatoic Anhydride: Generation of Ultraviolet Chromophores and Blue Fluorophores*. *Analytical Biochemistry*, 2000. 284(1): p. 167-169.
36. Alnasif, N., C. Zoschke, E. Fleige, R. Brodewolf, A. Boreham, E. Rühl, et al., *Penetration of normal, damaged and diseased skin — An in vitro study on dendritic core-multishell nanotransporters*. *Journal of Controlled Release*, 2014. 185(0): p. 45-50.
37. Pelton, R., *Poly(N-isopropylacrylamide) (PNIPAM) is never hydrophobic*. *Journal of Colloid and Interface Science*, 2010. 348(2): p. 673-674.
38. Diembeck, W., H. Beck, F. Benech-Kieffer, P. Courtellemont, J. Dupuis, W. Lovell, et al., *Test Guidelines for In Vitro Assessment of Dermal Absorption and Percutaneous Penetration of Cosmetic Ingredients*. *Food and Chemical Toxicology*, 1999. 37(2-3): p. 191-205.
39. Carlson, M.W., A. Alt-Holland, C. Egles, and J.A. Garlick, *Three-Dimensional Tissue Models of Normal and Diseased Skin, in Current Protocols in Cell Biology*. 2001, John Wiley & Sons, Inc.
40. Oji, V., K.-M. Eckl, K. Aufenvenne, M. Nätebus, T. Tarinski, K. Ackermann, et al., *Loss of Corneodesmosin Leads to Severe Skin Barrier Defect, Pruritus, and Atopy: Unraveling the Peeling Skin Disease*. *The American Journal of Human Genetics*, 2010. 87(2): p. 274-281.
41. Palmer, C.N., A.D. Irvine, A. Terron-Kwiatkowski, Y. Zhao, H. Liao, S.P. Lee, et al., *Common loss-of-function variants of the epidermal barrier protein filaggrin are a major predisposing factor for atopic dermatitis*. *Nat Genet*, 2006. 38(4): p. 441-446.
42. Aufenvenne, K., F. Larcher, I. Hausser, B. Duarte, V. Oji, H. Nikolenko, et al., *Topical Enzyme-Replacement Therapy Restores Transglutaminase 1 Activity and Corrects Architecture of*

- Transglutaminase-1-Deficient Skin Grafts. *The American Journal of Human Genetics*, 2013. 93(4): p. 620-630.
43. Eckl, K.-M., T. Alef, S. Torres, and H.C. Hennies, Full-Thickness Human Skin Models for Congenital Ichthyosis and Related Keratinization Disorders. *J Invest Dermatol*, 2011. 131(9): p. 1938-1942.
  44. Gattu, S. and H.I. Maibach, Enhanced Absorption through Damaged Skin: An Overview of the *in vitro* Human Model. *Skin Pharmacology and Physiology*, 2010. 23(4): p. 171-176.
  45. Chiang, A., E. Tudela, and H.I. Maibach, Percutaneous absorption in diseased skin: an overview. *Journal of Applied Toxicology*, 2012. 32(8): p. 537-563.
  46. Watkinson, A., A. Bunge, J. Hadgraft, and M. Lane, Nanoparticles Do Not Penetrate Human Skin—A Theoretical Perspective. *Pharmaceutical Research*, 2013. 30(8): p. 1943-1946.
  47. Campbell, C.S., L.R. Contreras-Rojas, M.B. Delgado-Charro, and R.H. Guy, Objective assessment of nanoparticle disposition in mammalian skin after topical exposure. *Journal of Controlled Release*, 2012. 162(1): p. 201-207.
  48. Baroli, B., Penetration of nanoparticles and nanomaterials in the skin: Fiction or reality? *Journal of Pharmaceutical Sciences*, 2010. 99(1): p. 21-50.
  49. Zvyagin, A.V., X. Zhao, A. Gierden, W. Sanchez, J.A. Ross, and M.S. Roberts, Imaging of zinc oxide nanoparticle penetration in human skin *in vitro* and *in vivo*. *Journal of Biomedical Optics*, 2008. 13(6): p. 064031-9.
  50. Luengo, J., B. Weiss, M. Schneider, A. Ehlers, F. Stracke, K. König, et al., Influence of Nanoencapsulation on Human Skin Transport of Flufenamic Acid. *Skin Pharmacology and Physiology*, 2006. 19(4): p. 190-197.
  51. Ostrowski, A., D. Nordmeyer, A. Boreham, R. Brodewolf, L. Mundhenk, J.W. Fluhr, et al., Skin barrier disruptions in tape stripped and allergic dermatitis models have no effect on dermal penetration and systemic distribution of AHAPS-functionalized silica nanoparticles. *Nanomedicine: Nanotechnology, Biology and Medicine*, 2014: p. in press.
  52. Abdel-Mottaleb, M.M.A., B. Moulari, A. Beduneau, Y. Pellequer, and A. Lamprecht, Surface-charge-dependent nanoparticles accumulation in inflamed skin. *J Pharm Sci*, 2012. 101(11): p. 4231-4239.
  53. Alnasif, N., C. Zoschke, E. Fleige, R. Brodewolf, A. Boreham, E. Ruhl, et al., Penetration of normal, damaged and diseased skin - An *in vitro* study on dendritic core-multishell nanotransporters. *J Control Release*, 2014(185): p. 45-50.
  54. Chauhan, A.S., S. Sridevi, K.B. Chalasani, A.K. Jain, S.K. Jain, N.K. Jain, et al., Dendrimer-mediated transdermal delivery: enhanced bioavailability of indomethacin. *J Control Release*, 2003. 90(3): p. 335-43.
  55. Venuganti, V.V. and O.P. Perumal, Poly(amidoamine) dendrimers as skin penetration enhancers: Influence of charge, generation, and concentration. *Journal of Pharmaceutical Sciences*, 2009. 98(7): p. 2345-2356.
  56. Stout, T.E., T. McFarland, J.C. Mitchell, B. Appukuttan, and J. Timothy Stout, Recombinant Filaggrin Is Internalized and Processed to Correct Filaggrin Deficiency. *J Invest Dermatol*, 2014. 134(2): p. 423-429.
  57. Sabin, J., G. Prieto, J.M. Ruso, R. Hidalgo-Álvarez, and F. Sarmiento, Size and stability of liposomes: A possible role of hydration and osmotic forces. *The European Physical Journal E*, 2006. 20(4): p. 401-408.
  58. Akbarzadeh, A., R. Rezaei-Sadabady, S. Davaran, S.W. Joo, N. Zarghami, Y. Hanifehpour, et al., Liposome: classification, preparation, and applications. *Nanoscale Research Letters*, 2013. 8(1): p. 102.
  59. Farkhani, S.M., A. Valizadeh, H. Karami, S. Mohammadi, N. Sohrabi, and F. Badrzadeh, Cell penetrating peptides: Efficient vectors for delivery of nanoparticles, nanocarriers, therapeutic and diagnostic molecules. *Peptides*, 2014(57): p. 78-94.
  60. Lee, S.H., B. Castagner, and J.-C. Leroux, Is there a future for cell-penetrating peptides in oligonucleotide delivery? *European Journal of Pharmaceutics and Biopharmaceutics*, 2013. 85(1): p. 5-11.

# Chapter 4

## Interactions of Hyaluronic Acid with the Skin and Implications for the Dermal Delivery of Biomacromolecules

The following chapter has been published as peer-reviewed article in the journal Molecular Pharmaceutics and appears in this thesis with the journal's permission:

Madeleine Witting, Alexander Boreham, Robert Brodewolf, Kateřina Vávrová, Ulrike Alexiev, Wolfgang Friess, Sarah Hedtrich

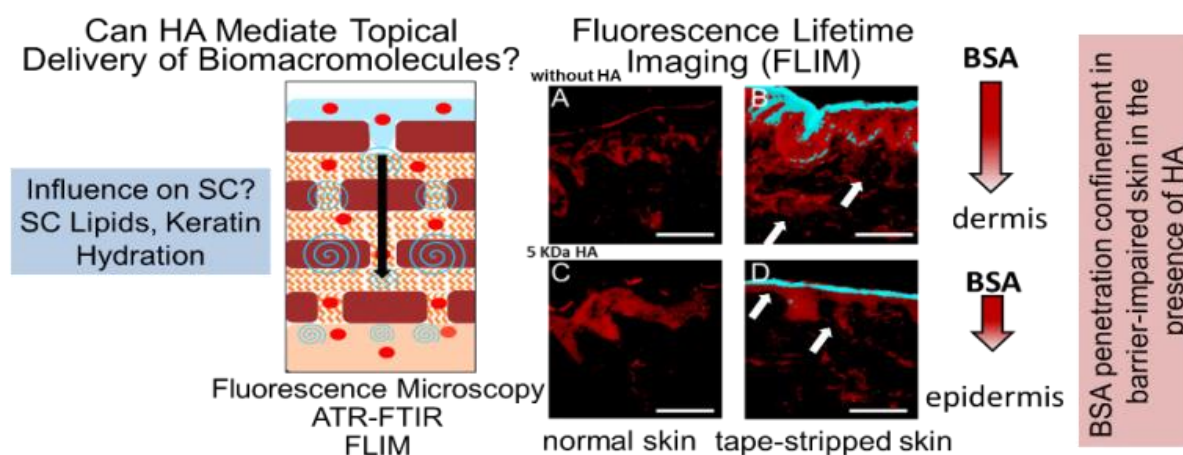
*Interactions of Hyaluronic Acid with the Skin and Implications for the Dermal Delivery of Biomacromolecules*

Mol Pharmaceutics 12, 5, (2015) 1391 - 1401

Online available: <http://pubs.acs.org/doi/abs/10.1021/mp500676e>

The personal contribution covers the written parts of the introduction, the results and discussion as well as the experimental set-up and execution with exception of the entire parts concerning the fluorescence lifetime measurements (FLIM).

### Graphical Abstract



## Abstract

Hyaluronic acid (HA) hydrogels are interesting delivery systems for topical applications. Besides moisturizing the skin and improving wound healing, HA facilitates topical drug absorption and is highly compatible with labile biomacromolecules. Hence, in this study we investigated the influence of HA hydrogels with different molecular weights (5 kDa, 100 kDa, 1 MDa) on the skin absorption of the model protein bovine serum albumin (BSA) using fluorescence lifetime imaging microscopy (FLIM). To elucidate the interactions of HA with the stratum corneum and the skin absorption of HA itself, we combined FLIM and Fourier-transform infrared (FTIR) spectroscopy. Our results revealed distinct formulation and skin-dependent effects. In barrier deficient (tape-stripped) skin, BSA alone penetrated into dermal layers. When BSA and HA were applied together, however, penetration was restricted to the epidermis. In normal skin, penetration enhancement of BSA into the epidermis was observed when applying low molecular weight HA (5 kDa). Fluorescence resonance energy transfer analysis indicated close interactions between HA and BSA under these conditions. FTIR spectroscopic analysis of HA interactions with stratum corneum constituents showed an  $\alpha$ -helix to  $\beta$ -sheet interconversion of keratin in the stratum corneum, increased skin hydration, and intense interactions between 100 kDa HA and the skin lipids resulting in a more disordered arrangement of the latter. In conclusion, HA hydrogels restricted the delivery of biomacromolecules to the stratum corneum and viable epidermis in barrier deficient skin, and therefore seem to be potential topical drug vehicles. In contrast, HA acted as an enhancer for delivery in normal skin, probably mediated by a combination of cotransport, increased skin hydration, and modifications of the stratum corneum properties

Key words: hyaluronic acid, proteins, skin penetration, skin hydration, epidermal drug delivery, FLIM, FTIR

## 1. Introduction

Over the last decades, biopharmaceuticals such as proteins, peptides, and nucleic acids have become increasingly important as therapeutic options for the treatment of diverse diseases such as cancer, infections, and autoimmune diseases. The conventional administration form of biopharmaceuticals is a directed injection or infusion. Due to limited patient compliance and associated side effects, alternative application methods are under investigation including pulmonary, nasal, topical, and buccal delivery [1, 2].

For the treatment of severe skin diseases including psoriasis and atopic dermatitis, efficient protein formulations such as Enbrel<sup>®</sup> (etanercept) or Remicade<sup>®</sup> (infliximab) are on the market, but they can solely be administered by injection [3]. To reduce systemic side effects and to increase both patient compliance and local bioavailability, a topical application seems beneficial [4]. However, the excellent barrier properties of the skin almost completely restrict the absorption of biomacromolecules due to their high molecular weight and hydrophilicity [4, 5]. To overcome this obstacle, and to allow for efficient protein delivery into the skin, tailored drug delivery systems are necessary. This is of particular interest for a topical substitution therapy of proteins that are deficient in the skin due to genetic mutations and, hence, are the underlying cause of severe skin diseases such as ichthyosis vulgaris [6] or atopic dermatitis [7]. This approach, requiring only rather low doses, was pursued for filaggrin delivery in atopic skin [8] and for the enzyme transglutaminase I for the restoration of autosomal-recessive congenital ichthyosis [9] with very promising results. In this context, the different properties of normal and diseased skin are of importance since diseased skin is characterized by increased transepidermal water loss [10], impaired skin barrier function, and altered dermal drug absorption compared to intact skin [11]. To study barrier disrupted skin *in vitro*, tape-stripping is a common and well-established method [10, 12, 13].

Hyaluronic acid (HA) based hydrogels have been in the focus for the treatment of skin diseases for several years [14, 15] and are an attractive candidate for dermal drug delivery [14, 16, 17]. HA is a linear polysaccharide of *N*-acetyl glucosamine and glucuronic acid in alternating sequence with an average molecular weight of approximately  $2 \times 10^5$  to  $10^7$  Da. It forms highly viscoelastic gels in aqueous solution [18], and when applied to the skin it provides beneficial effects such as skin hydration, elasticity regeneration, and improved wound healing [19]. Moreover, HA may also facilitate dermal drug delivery as shown for anti-cancer drugs [20, 21] and for diclofenac. In the latter case, HA significantly enhanced the partitioning, retention, and localization of diclofenac in human epidermis compared with an aqueous solution [4, 22, 23].

The mechanisms of HA mediated skin penetration, however, are still poorly understood. Various factors are discussed involving an active transport via HA receptors [17, 24] and the specific structure of hydrated HA [25]. Alternatively, the general effect of skin hydration may

facilitate dermal drug absorption and can aid the retention of drugs within the more hydrated epidermal layers [14]. Others hypothesize that the skin penetration of HA itself can facilitate drug delivery via a co-transport [14, 26]. Moreover, HA is well suited for biomacromolecules as it provides good protein stabilizing properties [16, 17, 21]. Nevertheless, the exact mechanism for transdermal transport remains to be elucidated.

In this study, we set out to identify formulations of HA and the model protein bovine serum albumin (BSA) that exhibit improved skin penetration, either transdermal or topical, compared to the application of the protein alone. Furthermore, we aimed to understand the mechanism by which HA acts on protein penetration. Therefore, BSA skin penetration was investigated in normal and tape-stripped skin. Using fluorescence lifetime imaging microscopy (FLIM), we localized HA and BSA in the skin and analyzed the effect of different molecular weight HA (5 kDa, 100 kDa and 1 MDa) on BSA penetration. Interactions between HA, skin lipids, and proteins in terms of organization and conformation, and the impact of hydration effects were studied by Fourier-transform infrared (FTIR) spectroscopy. Co-localization of HA and the protein BSA in the skin were investigated using fluorescence resonance energy transfer (FRET)-FLIM.

## **2. Materials and Methods**

### **2.1 Materials**

Sodium hyaluronate 5 kDa was obtained from Wellcos Cosmetics (Gladbeck, Germany). 100 kDa and 1 MDa sodium hyaluronate were a gift from Shiseido Co., Ltd (Shizuoka, Japan). Hydroxyethyl cellulose (HEC) Natrosol® 250 HHX PH was purchased from Ashland Aqualon (Covington, KY, USA). BSA, dimethyl sulfoxide (DMSO), rhodamine B isothiocyanate (mixed isomers), and the buffer reagents were purchased from Sigma-Aldrich (Steinheim, Germany). *N*-methylisatoic anhydride for HA labeling was purchased from Invitrogen Molecular Probes® (Darmstadt, Germany).

For skin penetration experiments, pig skin of the flank region from “Deutsche Landrasse” (30-50 kg, 10-20 weeks old) was used (Clinic of Swine, Ludwig-Maximilians University, Munich, permission no. DE 09 162 0017 X-1).

### **2.2 HEC and HA solution Preparation**

#### **2.2.1 Fluorescence Labeling of BSA and HA**

Fluorescence labeling of BSA was performed using rhodamine B isothiocyanate (RhB ITC). The dye was dissolved in DMSO to 1 mg/mL and added to a 6 mg/mL BSA solution in a 0.1 M sodium bicarbonate buffer (pH 9.0). While stirring slowly, protein and dye solution were

mixed at a ratio of 1:170 w/w (dye : protein) under light protection. After 120 minutes, the solution was transferred to a Vivaspin 20 tube (PES membrane MWCO 30000, Sartorius AG, Göttingen, Germany) and centrifuged for 45 min at 4.000 rpm at 5 °C. Subsequently, several washing steps were performed to remove unbound dye. The absence of free dye was confirmed by high pressure size exclusion chromatography (HP-SEC) (UV (protein) = 280 nm, UV (dye) = 555 nm; fluorescence (protein) = exc. 280/em. 350 nm, fluorescence (dye) = exc. 540 nm/em. 580 nm) and UV spectroscopy of the washing phases at 555 nm. Protein concentration (between 20-25 mg/ml) and degree of labeling (between 0.95 - 1.3) were determined according to the manufacturer's protocol. Regarding the stability of the conjugate, the lysine-dye bond is stable for up to 10 days [27]. The absorption and emission spectra of BSA-RhB were recorded showing an absorption maximum at 558 nm and an emission maximum at 585 nm, respectively (Figure SI 1A).

Fluorescence labeling of HA was performed using *N*-methylisatoic anhydride (MIA) [28]. The dye was dissolved in DMSO to 200 mg/mL and added to a 4 mg/mL HA solution in 0.1 M sodium borate buffer (pH 8.0). While stirring slowly, HA and dye solution were mixed at a ratio of 1:10 w/w (dye : HA) under light protection. After 15 minutes, the labeled HA was precipitated with ethanol 70 %. The precipitate was washed twice, centrifuged at 4.000 rpm, 4°C and the HA pellet was vacuum dried. The absence of free dye was confirmed by HP-SEC (UV (HA) = 215 nm, UV (dye) = 351 nm; fluorescence (free dye) = exc. 316 nm/em. 386 nm, fluorescence (HA-dye conjugate) = exc. 366 nm/em. 440 nm) and fluorescence spectroscopy at exc. 366 nm/em. 440 nm. Additionally, the degree of HA modification was determined to be 1 molecule N-MANT per 40-50 disaccharide HA units. The labeled *N*-methylantraniloyl (MANT)-HA was reconstituted with PBS (pH 7.4) to stock concentrations of 40 mg/mL. Successful labeling was confirmed by UV-Vis absorption (Shimadzu UVPC 2450) and fluorescence spectroscopy (Cary Eclipse, Varian GmbH, Darmstadt, Germany). The absorption maximum was at 350 nm and the emission maximum at 440 nm. The absorption and emission properties of HA-MANT samples were independent of the molecular weight (Figure SI 1 B). Furthermore, the HA-MANT sample was subjected to fluorescence microscopy (instrument-specific DAPI filter setting exc. 360/40 nm, em. 460/50 nm; BZ-8000, Keyence, Neu-Isenburg). According to DeAngelis, 2000 [28], the labeling procedure yields a stable conjugate. The labeled proteins and HA were stored at -20°C until further use.

## 2.2.2 Preparation of Protein-Containing HEC and HA Hydrogels

2% and 5% w/v HEC solutions were prepared by mixing 4% and 10% w/v stock gels 1:1 with PBS or BSA-RhB ITC (20 mg/mL) to reach a final BSA concentration of 10 mg/mL. The 5 kDa and 100 kDa HA hydrogels were prepared correspondingly. For the 10% w/v HEC and HA solutions, 100 mg/mL of the dry HEC or HA material was rehydrated and mixed with either PBS or a 10 mg/mL BSA-RhB ITC solution. The gels were kept at 2-8°C for at least 12

h before use to guarantee complete rehydration. A solution of 10 mg/mL BSA in PBS pH 7.4 served for reference.

### **2.3 Attenuated Total Reflectance Fourier Transform Infrared (ATR-FTIR) Spectroscopy Measurements**

In order to evaluate the effects of HA formulations on skin hydration, keratin secondary structure, and the organization of skin lipids, FTIR measurements on isolated stratum corneum (SC) sheets were performed. For SC isolation, pig skin was covered with 0.1 % trypsin in 150 mM PBS pH 7.4. The samples were kept at 4°C for 20 h and were subsequently incubated at 37 °C until the SC could be removed. The isolated SC sheets were washed with water and dried for 3 days in a desiccator filled with silica gel (24 °C, 27 % relative humidity). Subsequently, the SC sheets were quartered, placed in petri dishes and covered with 50 µL/cm<sup>2</sup> HA formulations (without BSA), respectively. All samples were incubated for 6 h at room temperature (23 - 24 °C, 37 % relative humidity). The water content in the SC was determined using a TENSOR 27 FT-IR Spectrometer with HYPERION 3000 FT-IR Microscope connected to an ATR objective (Bruker Optik GmbH, Ettlingen, Germany). The spectra were generated from 240 scans collected at 4 cm<sup>-1</sup> resolution at 20°C and analyzed with the Bruker OPUS software. The exact peak positions were determined after vector normalization. The degree of water uptake was defined as the area under the secondary O-H stretching (water) absorbance at around 2100 cm<sup>-1</sup> in relation to the dry SC [29]. Changes in the lipid chain order were defined as redshifts to higher wavenumbers for the methylene symmetric and asymmetric stretching vibrations [30, 31]. For keratin secondary structure analysis, the second derivative was determined from the normalized spectra and evaluated regarding the amide I band [32]. ATR-FTIR control spectra were recorded for plain 1 % HEC, 5 % 5 kDa HA, 5 % 100 kDa HA, and 1 % 1 MDa HA hydrogels (Figure SI 4, SI 5).

### **2.4 Skin Penetration Experiments**

Validated test procedures using the Franz cell set up and the infinite-dose approach were performed according to previously published procedures (300 µl test sample onto 1.72 cm<sup>2</sup> skin for 6 h, removal of excess formulation after incubation) [33]. Pig skin was used as it has comparable properties like human skin and is a well-established model for skin absorption testing *in vitro* [11, 34]. To create barrier deficient skin, tape-stripping was performed 30 times by pressing adhesive tape strips (10 cm length; tesapack<sup>®</sup> 4120 PVC, Tesa SE, Hamburg) [35] and SC thickness was measured in skin sections using a Keyence BZ-8100E microscope and BZ-Analyzer software (Keyence, Neu-Isenburg, Germany). The SC thickness was reduced from 13 to 6 µm. For data analysis, skin sections (5 µm) were

prepared by cutting from the dermis to the SC to prevent dragging of HA and BSA from the skin surface into deeper dermal layers.

For initial screening, the skin sections were subjected to normal and fluorescence microscopy (100 and 200 x magnification, BZ-8100, Keyence, Neu-Isenburg) and representative images were recorded. The fluorescence was recovered in the red band exciting the samples at 560 nm for BSA-RhB (instrument-specific TexasRed filter setting exc. 560/40 nm, em. 630/60 nm). To detect MANT-HA, the fluorescence was recorded in the blue band exciting the samples at 360 nm (instrument-specific DAPI filter setting exc. 360/40 nm, em. 460/50 nm).

## **2. 5 Fluorescence Lifetime Imaging Microscopy (FLIM)**

To investigate the dermal absorption of protein (10 mg/ml BSA-RhB in aqueous solution) and HA (5 % 5 kDa, 100 kDa and 1 MDa HA-MANT), sections of normal and barrier disrupted skin were subjected to FLIM.

The time-resolved fluorescence decay curves in each image pixel were obtained by time-correlated single photon counting (TCSPC) with a confocal laser scanning FLIM setup. The setup consists of an Olympus IX71 inverted microscope equipped with a 40x objective lens, a confocal scanning unit (DCS-120, Becker & Hickl, Berlin, Germany), and a Ti:Sapphire laser system (Spectra Physics, Santa Clara, USA) in the mode-locked picosecond-pulsed regime [36–43]. The Ti:Sapphire Tsunami laser was pumped by a 5 W solid state Millennia V laser and the laser output was frequency doubled to obtain the excitation wavelength of 488 nm for the RhB dye. A pulse picker reduced the repetition rate to 4 MHz. A color glass filter OG515 and a high quality long pass filter HQ545LP were used as emission filters. To excite MANT fluorescence, a pulsed diode laser (BDL-405-SMT; Becker&Hickl) with a wavelength of 405 nm and a repetition rate of 20 MHz was used. A high quality long pass filter HQ435LP and a band-pass filter HQ480/40 were used as emission filters. The time range was set to 20 ns for 256 channels resulting in a resolution of 78 ps/ch. Single photon counting was performed using a TCSPC module (SPC-150, Becker & Hickl, Berlin, Germany).

For FRET experiments [44], samples containing both HA-MANT and BSA-RhB were excited with 405 nm and a high quality long pass filter HQ545LP and a band-pass filter HQ480/40 were used as emission filters. For reference, BSA-RhB was excited with 488 nm and emission was detected using the same emission filter set.

FLIM images were analyzed using self-written routines in C++. Fluorescence decay curves were partitioned into classes (i.e. clusters) using a multivariate pattern recognition method [44, 45]. The fluorescence decays of the individual clusters were fitted with a sum of exponentials using  $\chi^2$  minimization. False-color images were generated by assigning a distinct color to all pixels containing a fluorescence decay curve that belongs to one cluster.

Steady-state fluorescence spectra were recorded using an SPEX Fluoromax-3 from Horiba Jobin Yvon and the DataMax Software Version 2.20 [38, 42].

## **2.6 Statistical Analysis**

To semi-quantify the penetration enhancing (PEE) or penetration confinement effect (PCE), we compared the background-corrected average pixel intensities of the different samples in the skin layers of interest (SC, viable epidermis, superficial dermis). The background-corrected average pixel intensities of a sample treated with BSA-RhB solution served as reference and was set to 1. All PEE/PCE values are expressed relative to this value. The PEE/PCE results are presented as average results  $\pm$  SEM obtained from 3 independent experiments. Statistical analysis is based on the Wilcoxon-Mann-Whitney test;  $p \leq 0.05$  indicates a statistically significant difference.

## **3. Results**

### **3.1 Penetration of HA into normal and tape-stripped skin**

We investigated the skin absorption of HA in normal and tape-stripped skin to substantiate the findings in the literature that HA itself is able to penetrate into the skin [14, 26]. FLIM measurements were performed on cryosections of pig skin treated with HA-MANT and the penetration of different molecular weights of HA (5 kDa, 100 kDa, and 1 MDa) was assessed. With cluster-based FLIM image analysis, one lifetime cluster belonging to HA-MANT was identified in both normal (Figure 4-1 A-C) and tape-stripped skin (Figure 4-1 D-F). In normal skin, 5 kDa HA was localized in the stratum corneum and epidermis, albeit rather patchy (Figure 4-1 A). The higher molecular weight HAs were basically confined to the SC (Figure 4-1 B, C). In contrast, in tape-stripped skin the lifetime cluster belonging to HA-MANT was localized in both SC and epidermis, with slightly higher concentrations for 100 kDa and 1 MDa HA compared to 5 kDa HA (Figure 4-1 D-F).

### **3.2 Penetration of BSA into normal and tape-stripped skin**

Next, the skin penetration of the model protein BSA with a molecular weight of  $\sim 66$  kDa was investigated. Again, FLIM measurements were performed on cryosections of pig skin treated with BSA-RhB and subjected to cluster-based FLIM analysis. Since dermal absorption of proteins is highly limited owing to the proteins' hydrophilic nature and large size, we did not expect high amounts of BSA in normal skin. As expected, BSA skin absorption is much less in normal skin compared to barrier deficient skin (Figure 4-1 G and H). Nevertheless, residual

fluorescence intensity belonging to BSA-RhB could be identified by cluster-based FLIM analysis in normal skin (colored red in Figure 4-1 G).

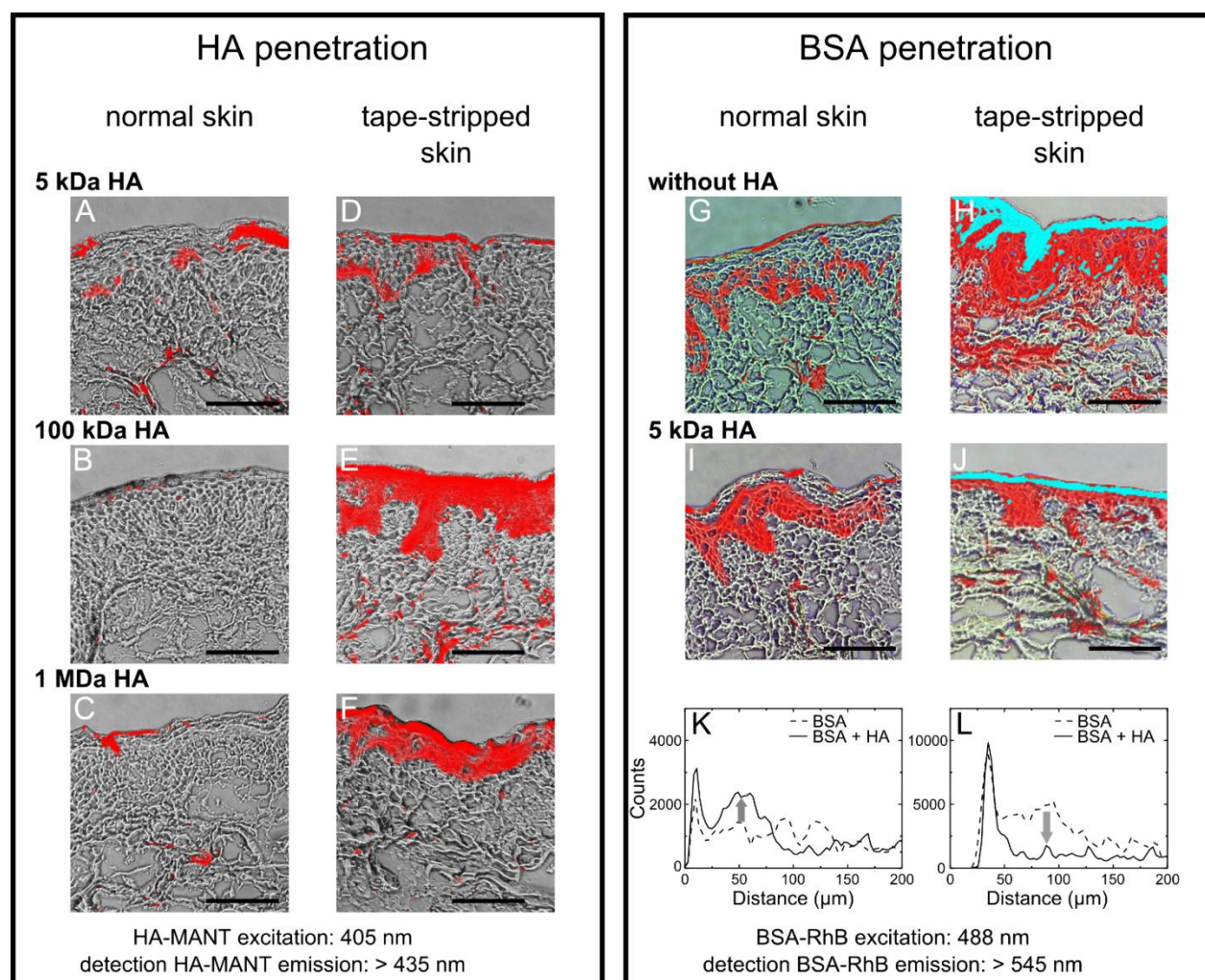


**Figure 4-1** Penetration patterns of HA-MANT and BSA-RhB in normal and tape-stripped skin. (A-F) HA-MANT penetration in normal (A,B,C) and tape-stripped skin (D,E,F) as determined by MANT fluorescence. (G-J) BSA-RhB-ITC penetration into normal (G,I) and tape-stripped (H,J) skin without HA (G,H) and with 5 % 5 kDa HA (I,J). Images are false color coded according to the measured BSA-RhB fluorescence lifetime. Scale bars represent 100 μm. Effect of HA on BSA penetration. (K,L) Average of three intensity line scans for BSA-RhB alone (dashed line) and with 5 kDa HA (solid line) in (K) normal skin and (L) tape-stripped skin. Arrow indicates increased or decreased BSA penetration in the presence of HA.

This cluster is localized in the SC and the epidermis. In tape-stripped skin, two distinct lifetime clusters belonging to BSA-RhB were identified (Figure 4-1 H). One is localized in the remainder of the SC and part of the viable epidermis (colored cyan in Figure 4-1 H). The corresponding lifetime deviates strongly from the auto fluorescent background as well as from the lifetime of the single cluster observed for normal skin (Figure SI 2). The second cluster is primarily located in the dermis, colored red in Figure 4-1H, and its fluorescence

decay is similar to the one determined for BSA-RhB in normal skin (Figure SI 2). Since the cyan colored areas correspond to areas with the highest fluorescence intensity (Figure SI 3), the different fluorescence lifetimes may reflect this concentration difference, in particular as high fluorophore concentrations may lead to quenching effects.

### 3.3. Effects of HA on BSA penetration

To investigate the effect of HA on BSA penetration, cryosections of intact and tape-stripped pig skin treated with different molecular weight HA-MANT together with BSA-RhB were analyzed.

In normal skin, a single lifetime cluster belonging to BSA-RhB was identified for all three HA molecular weights (colored in red in Figures 4-1 I and SI 3). For 5 kDa HA, localization of BSA-RhB in the SC and the viable epidermis was observed (Figure 4-1I). In the presence of 100 kDa and 1 MDa HA the localization of BSA was limited to the SC (Figure SI 3).

In tape-stripped skin, again two clusters with different lifetimes belonging to BSA were identified for all HA molecular weights (Figure 4-1I and SI 3). One cluster, colored in cyan, was localized in the SC and the other, colored in red, in the epidermis, and to a much lesser extent in the dermis. The localization of BSA was independent of the molecular weight of HA. To compare the amounts of penetrated BSA with and without HA, we used the fluorescence intensity of the identified FLIM clusters belonging to BSA. Averaged intensity line scans for BSA alone and BSA with 5 kDa HA were compared (Figure 4-1 K,L). In normal skin, the intensity for BSA-RhB with 5 kDa HA (Figure 1 K, solid line) was increased in the SC (first 15  $\mu\text{m}$ ) and epidermis (up to 50  $\mu\text{m}$ ) compared to BSA-RhB alone (Figure 4-1 K, dashed line), where the observed intensities were close to the auto fluorescent background. In tape-stripped skin, the intensities observed for BSA-RhB alone were well above the auto fluorescent background (Figure 4-1 L, dashed line), in particular close to the surface of tape-stripped skin, and up to 100  $\mu\text{m}$  into the skin. In the presence of 5 kDa HA-MANT (Figure 4-1 L, solid line), high peak values close to the skin surface were also found, but the intensity dropped to background levels at 50  $\mu\text{m}$  skin depth.

To quantify the effects of HA on BSA penetration, we evaluated the background-corrected average pixel intensities of the different samples in a semi quantitative way. Intensity changes in the different skin layers of interest were calculated with respect to the sample treated with BSA only, as outlined in Material and Methods. For normal skin, a 2.5 fold intensity increase of BSA-RhB fluorescence was observed in the stratum corneum for 5 % 5 kDa HA (Figure 4-2 A). In the viable epidermis, the penetration enhancement effect of 5 % 5 kDa HA was even higher with a 7.5-fold increase in BSA-RhB fluorescence intensity (Figure 4-2 A). Samples with 5 % 100 kDa or 1 MDa HA did not show any penetration enhancement effects for BSA (Figure SI 3). For tape-stripped skin, however, a different picture evolved.

Comparison with the BSA control (without HA) showed that protein penetration in the presence of HA is confined to the SC and the viable epidermis. The BSA-RhB fluorescence in the dermis was reduced to 20 % of the intensity found in the control BSA sample (Figure 4-2 B).

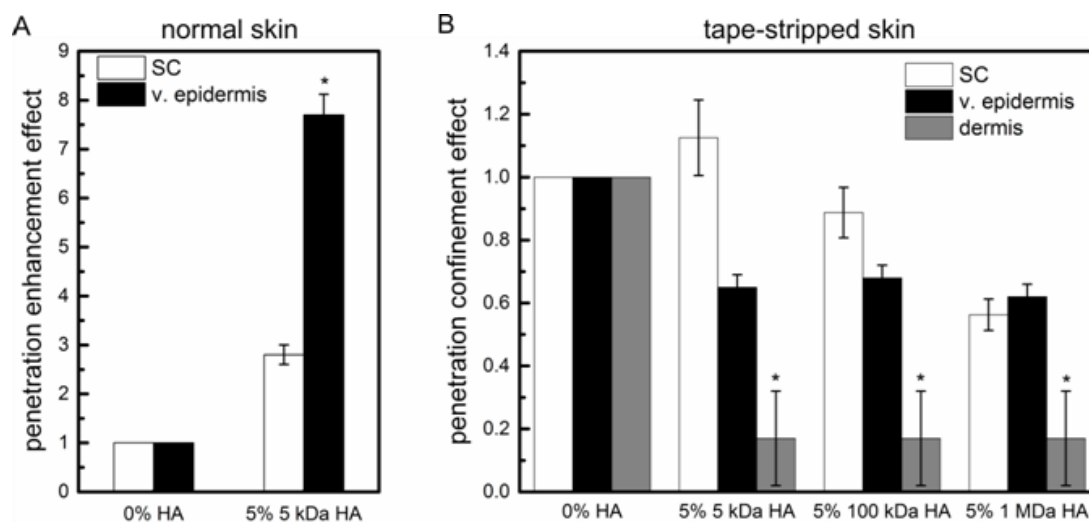


**Figure 4-2** Penetration enhancing effect (PEE) and penetration confinement effect (PCE) of HA on BSA penetration. The penetration of BSA-RhB without HA served for reference, and the respective intensity above background was set to 1. (A) PEE of 5 % 5 kDa HA on BSA-RhB penetration into normal skin measured by fluorescence microscopy. Mean values are presented for the SC (white bars) and the viable epidermis (black bars) (n=3, mean values  $\pm$  SEM \*p  $\leq$ 0.05). (B) Penetration confinement effect (PCE) of HA samples on BSA-RhB penetration in tape-stripped skin. Protein penetration into the dermis was significantly reduced with HA (n=3, mean values  $\pm$  SEM \*p  $\leq$ 0.05). Mean values are presented for SC (white bars), viable epidermis (black bars), and dermis (grey bars).

This effect was observed for all three HA molecular weights. Despite a HA independent overall localization of BSA, we detected concentration differences in the remaining SC of damaged skin. We found a molecular weight dependent effect on the accumulation of BSA with decreasing intensity for 5 kDa > 100 kDa > 1 MDa HA. This behavior, however, did not affect the penetration yield into the viable epidermis. For all HA molecular weights, we found a similar accumulation of BSA in the viable epidermis with about 65 % of the BSA control sample intensity.

### 3.4 Molecular interactions between HA and BSA in skin

Since several publications discuss that HA itself penetrates [17, 46-48] and co-transport drugs into the skin and into deeper dermal layers [26], we aimed to test this hypothesis. To determine whether co-localization of HA and BSA in terms of molecular contact between these two molecules in the skin exist, we used FRET [49]. FRET is highly sensitive for measuring distances between two fluorophores since the rate constant of energy transfer is

proportional to the inverse 6<sup>th</sup> power of the distance. Typical FRET distances are between 1 - 10 nm.

Fluorescence energy transfer from HA-MANT to BSA-RhB can occur, according to the spectral overlap between HA-MANT emission and BSA-RhB absorption (Figure 4-3 A). Hence, the occurrence of FRET emission was investigated on skin samples containing both HA-MANT and BSA-RhB by exciting the samples with 405 nm and detecting the emission between 590 nm and 650 nm, termed FRET channel in the following, specific for BSA-RhB emission. However, the spectroscopic analysis also showed that BSA-RhB exhibits absorption at 405 nm (Figure SI 1 A). Therefore, fluorescence emission detected in the FRET channel cannot be solely attributed to FRET between HA-MANT and BSA-RhB.

In order to determine if the fluorescence signal in the FRET channel contains FRET emission, non-FRET and FRET contribution to the total fluorescence signal have to be separated. The non-FRET contribution can be determined by excitation of BSA-RhB alone. To account for the different laser output powers in the FLIM setup, the RhB fluorescence intensity after excitation at 405 nm and 488 nm was measured in a pig skin sample only treated with BSA-RhB (Figure 4-3 B). Intensity line scans at identical sample positions showed a fluorescence intensity difference between excitation at 405 nm and 488 nm. The intensity ratio  $I_{405}/I_{488}$  was 2.5.

Using this ratio the non-FRET contribution (dashed line in Figure 4-3 D) can now be determined from a measurement with 488 nm excitation in BSA-RhB and HA-MANT samples. If FRET occurs, the emission detected for 405 nm excitation should be more than 2.5 times higher than the emission detected for 488 nm excitation, due to the additional RhB emission excited by FRET (Figure 4-3 D, additional intensity above the dashed curve (non-FRET intensity) indicating the FRET contribution). If the ratio of the intensities  $I_{405}/I_{488}$  is 2.5 (Figure 4-3 C), no FRET occurs as the observed RhB intensity at 405 nm excitation is due to non-FRET.

This approach was employed to analyze skin treated with BSA-RhB together with different HA-MANT molecular weights. The false color coded images from cluster-based FLIM analysis are presented alongside a comparison of line scans measured at 405 and 488 nm, allowing for the detection of FRET emission (Figure 4-3 E-J). An intensity ratio  $I_{405}/I_{488}$  larger than 2.5, indicative of FRET, was only observed in normal skin for BSA-RhB in the presence of 5 and 100 kDa HA (Figure 4-3 E,F). For all other samples no contribution from FRET emission to the total fluorescence intensity was detected (Figure 4-3 G-J). Since we have observed a clear penetration enhancement effect for BSA when normal skin was treated with 5 kDa HA, the FRET measurements indicated that this effect was accompanied by a co-localization of BSA and HA.

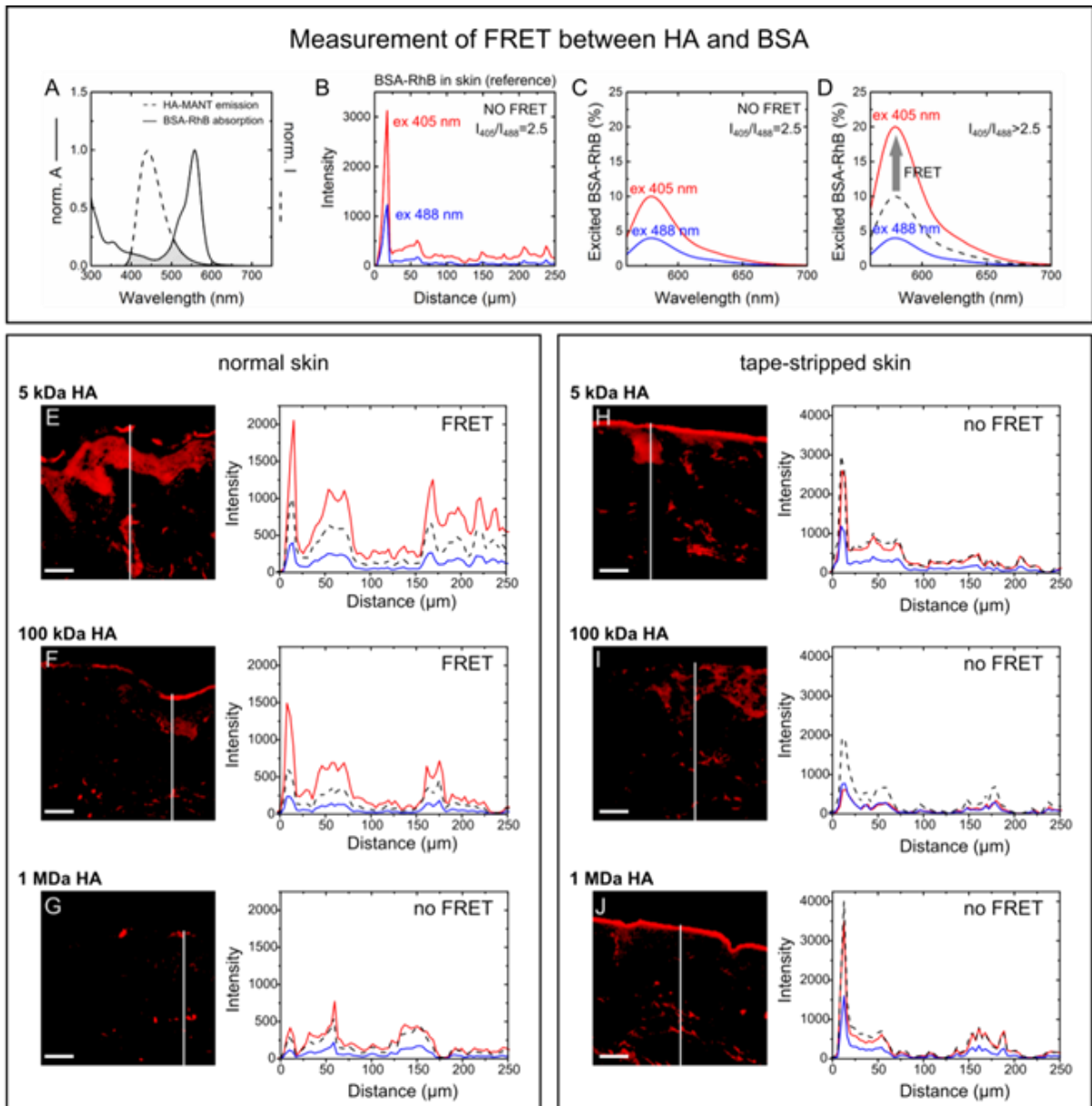


**Figure 4-3** Measurement of FRET between HA and BSA. (A) Emission spectrum of HA-MANT and BSA-RhB in solution. The shaded region indicates the overlap area. (B) Characteristic intensity line scan of a sample only treated with BSA-RhB and excited either at 405 nm (upper curve, pulsed diode laser) or 488 nm (lower curve, Ti:Sa laser). The correction factor of 2.5 was determined from the intensity ratio of the respective peak intensities. Emission filter: HQ620/60. (C) Theoretical emission spectra for the situation without FRET from HA-MANT to BSA-RhB under the given excitation conditions. (D) Theoretical emission spectra for the situation with FRET, indicated by the increase in emission by the 405 nm excitation compared to the situation without FRET as assessed from the corrected (correction factor 2.5) emission curve by the 488 nm excitation (dashed curved). (E-J) Cluster FLIM images for analysis of FRET induced BSA-RhB emission and characteristic emission intensity line scans for excitation at 405 nm (red curve) and 488 nm (blue curve) together with the theoretical curve without FRET (dashed black curve) for normal (E-G) and tape-stripped skin (H-J). Vertical white lines in the images indicate the position at which the line scan was taken. Scale bars: 50  $\mu\text{m}$ .

### 3.5 Stratum corneum hydration, keratin conformation, and interactions with the skin lipids

To further elucidate the interactions between HA and the SC, we investigated the effects of HA molecular weight and concentration on SC hydration, keratin secondary structure, and the lipid chain order using FTIR spectroscopy.

SC hydration was assessed from the area under the O-H stretching absorbance ( $\sim 2100 \text{ cm}^{-1}$ ) which increased significantly by water uptake [50]. Furthermore, the frequency shift of the amide I ( $\sim 1640 \text{ cm}^{-1}$ ) and amide II ( $\sim 1565 \text{ cm}^{-1}$ ) band absorbance maxima in the normalized FTIR spectrum indicated the level of hydrogen bonding of the protein amide linkages within the SC. The amide I band corresponded to the carbonyl-stretch of the keratin -CO-NH group. The stretching was more pronounced when the C=O band was involved in increased hydrogen bonding resulting in an absorbance at lower wavenumbers [29]. The amide II band reflected the amide N-H in-plane bending mode. Bending of the N-H bond becomes more difficult when the amide hydrogen is influenced by increased H-bonding to oxygen from water. This could be detected as a shift of the amide II band to higher wavenumbers [29]. Figure 4-4 summarizes the changes of SC hydration (calculated from increased areas under the O-H stretching absorbance), given as relative water content (%) of the SC, after incubation with different formulations (Figure SI 6). After 6 h, the SC hydration increased drastically for 2 %, 5 %, 10 % 5 kDa, and 5 % 100 kDa HA formulations to relative water contents over 200 % compared to dry skin (Figure 4-4). The evaluation of the amide I and II band peak shifts confirmed these findings (data not shown). HEC hydrogels were included for comparison but did not show significant effects.

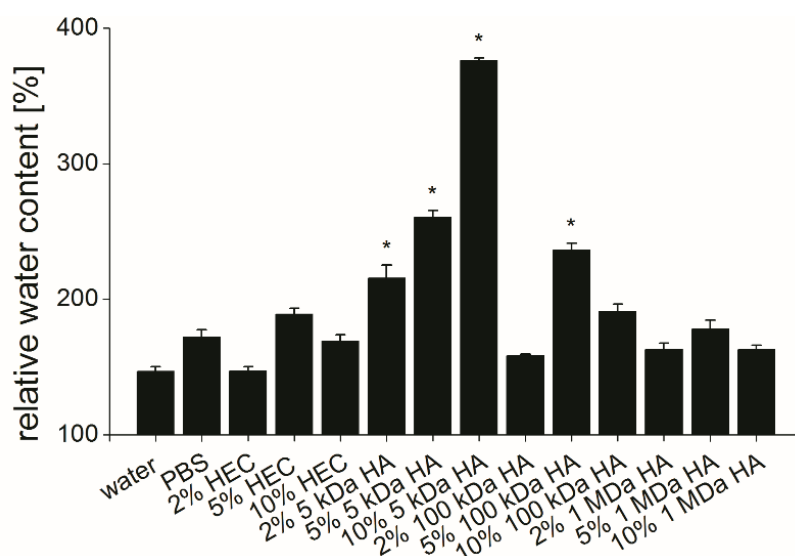


**Figure 4-4** SC hydration expressed as relative water content within the SC (% uptake compared to dry SC) after 6 h incubation with water, HEC, 5 kDa, 100 kDa, and 1 MDa HA (2 %, 5 %, and 10 %, respectively). n = 3; mean values  $\pm$  SEM, \*p  $\leq$  0.05 compared to water treated samples.

Next, changes of the keratin secondary structure as a function of different HA and HEC formulations were assessed by FTIR. The shape of the amide I band of proteins is characteristic for their secondary structure. Changes in the protein conformation are reflected by a splitting of the amide I band at  $\sim 1650\text{ cm}^{-1}$  when random coil and  $\alpha$ -helical structures convert to  $\beta$ -sheet structures. Changes in keratin structure, for example induced by the formation of  $\beta$ -sheet structures, can contribute to a decreased skin barrier function [32]. The 5 kDa HA exhibited the most prominent effects (Figure 4-5 A). With increasing concentrations, the conversion from  $\alpha$ -helical to  $\beta$ -sheet structures increased drastically from 25 % to 60 % and even to  $\sim 90\%$ . Compared to 5 kDa HA, the other formulations (100 kDa HA, 1 MDa HA, and the HEC gels) showed only minor effects on the keratin structure (Figure 4-5 B-D). Almost no changes were seen for 100 kDa HA (Figure 4-5 B). Compared to the dry and water treated SCs, only the 2 % sample showed significant shifts to 50 %  $\beta$ -sheet structures, whereas the 5 % and 10 % 100 kDa HA samples formed more random-coiled protein structures indicated by a shift of the peak from  $\sim 1648\text{ cm}^{-1}$  to  $1640\text{ cm}^{-1}$ .

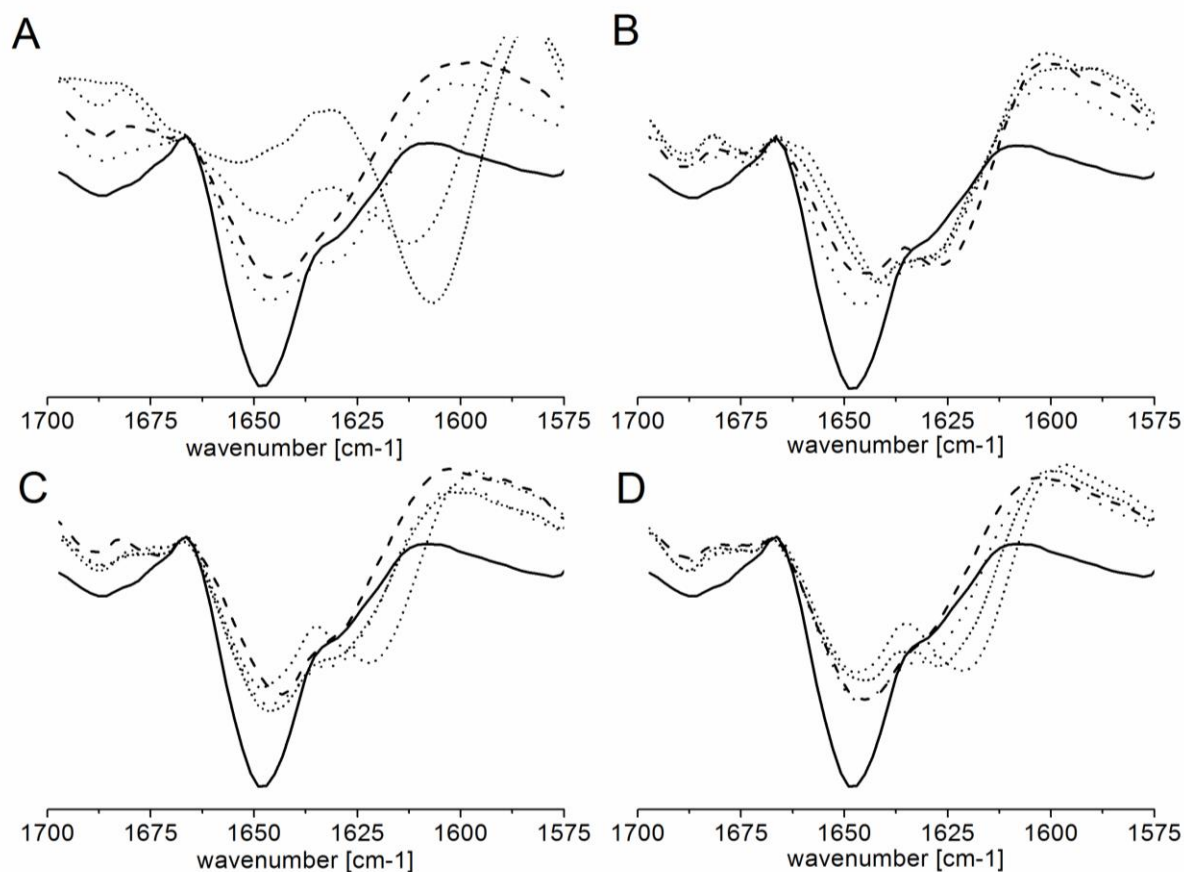


**Figure 4-5** Normalized second derivative FTIR spectra of the SC keratin (amide I region at  $\sim 1650\text{ cm}^{-1}$ ) after 6 h incubation with 5 kDa HA (A), 100 kDa HA (B), 1 MDa HA (C), and HEC (D). The formulations with concentrations of 2 % (dashed line), 5 % (medium dotted line) and 10 % (highly dotted line) were compared to dry SC (black line) and water (dotted line).

To gain more insight into the effects of HA on the skin lipids, we had a closer look at the spectral region between 3100-2700  $\text{cm}^{-1}$ . Changes in the intercellular lipid chain order are indicated by a shift of the methylene symmetric and asymmetric stretching vibrations ( $\sim 2850.5 \text{ cm}^{-1}$  and  $\sim 2920 \text{ cm}^{-1}$  in dry and hydrated SC control) toward higher wavenumbers [30]. Besides the shift of the wavenumbers, a flattening of the IR spectra indicates an increase in SC hydration [32, 51]. After 6 h, the most prominent shifts of  $9.7 \pm 2.8 \text{ cm}^{-1}$  and  $8.7 \pm 1.3 \text{ cm}^{-1}$  to higher wavenumbers for the symmetric  $\text{CH}_2$  stretching band were observed for SC samples treated with 5 % and 10 % 100 kDa HA formulations (Figure 4-6 A), indicating significantly higher shares of disordered lipids compared to all other SC samples.

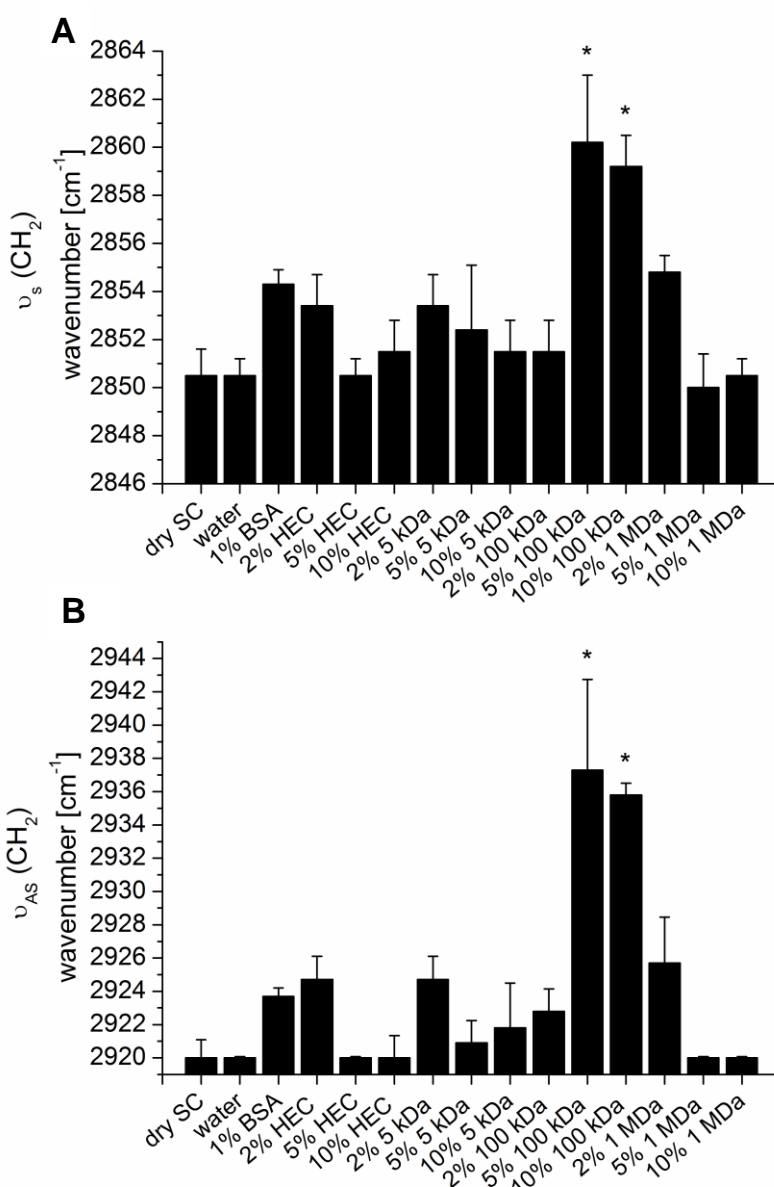


**Figure 4-6** SC lipid chain orders after incubation with water, HEC, 5 kDa, 100 kDa, and 1 MDa HA (2 %, 5 %, and 10 %, respectively). The SC lipid order is displayed as the change of the wavenumbers for the IR methylene symmetric (A) and asymmetric (B) stretching vibration compared to a dry SC control after 6 h incubation.  $n = 3$ ; mean values  $\pm$  SEM; \*  $p \leq 0.05$ .

The same holds true for the asymmetric CH<sub>2</sub> stretching band (Figure 4-6 B). Here, even more pronounced wavenumber shifts for 100 kDa HA occurred ( $2.2 \pm 1.3 \text{ cm}^{-1}$ ,  $16.7 \pm 5.4 \text{ cm}^{-1}$  and  $15.3 \pm 0.7 \text{ cm}^{-1}$  for 2 %, 5 %, and 10 % HA, respectively) further underlining a significant change in the lipid chain order. Minor effects were observed for 2 % HEC, 2 % 5 kDa HA, and 2 % 1 MDa HA (Figure 4-6 B). Measurements on tape-stripped SC gave the same results. Additionally, reference measurements showed no interactions between BSA and skin lipids or proteins.

## 4. Discussion

In this study, we compared the effect of HA on the skin penetration properties of the model biomacromolecule BSA in both intact and barrier deficient skin. In intact skin, absorption of biomacromolecules such as proteins is generally low due to their high molecular weight, distinct hydrophilicity and charged state [4, 5]. Up to now, only few studies describe effective protein delivery into the skin using nanoparticles, sonophoresis or iontophoresis [52-54].

HA has been used for topical drug delivery repeatedly, with Solaraze<sup>®</sup> (3 % diclofenac in 2.5 % HA) as a prominent example, which is an alternative to the common destructive surgery used for the treatment of actinic keratosis. Solaraze<sup>®</sup> is well-tolerated, shows good efficacy and exhibits less side effects compared to photodynamic or cryotherapy [22]. Brown et al. [14, 55] have shown that HA enhanced significantly the partitioning of diclofenac into human skin as well as its retention and localization in the epidermis. Twice as much diclofenac was delivered into the epidermis compared to an aqueous control [56]. Diclofenac, however, with a molecular weight of ~300 Da is a small drug compared to a biomacromolecule such as BSA with 66 kDa. Hence, the mechanisms by which a protein is delivered into or through the skin most likely differs considerably from the delivery of smaller molecules.

Two decades ago HA was recognized as a protective vehicle for the delivery of proteins such as growth factors and interferon [16]. Recently, human growth hormone-HA conjugates were delivered through the skin into the blood stream [17]. However, the exact mechanism for dermal transport and an explanation for the topical delivery properties of HA still need to be elucidated.

**Intact skin.** HA itself was found to penetrate into the skin in several studies [14, 17, 46]. Our imaging results showed a deeper skin penetration of the low molecular weight HA (5 kDa) compared to higher molecular weight HA (100 kDa and 1 MDa). This is in agreement with recent Franz diffusion cell data also showing a molecular weight dependency on HA penetration [46].

Regarding the skin absorption of BSA, it is known from the literature that this high molecular weight protein cannot penetrate into deeper layers of intact skin [57]. However, an enhanced

transport of BSA into the dermis was found when intact skin was hydrated for 4 - 10 h [57]. In our experiments, BSA was applied onto intact skin for 6 hours in a Franz diffusion cell. Under these conditions skin hydration to a certain extent is expected, which explains the small amounts of BSA penetration we observed in normal skin (Figure 4-1 G).

Binding of HA to BSA is known both from biochemical [58] and physicochemical studies [59, 60], with binding modes depending on a variety of conditions. Although BSA is overall negatively charged at neutral pH, it is known to bind to negative surfaces, probably due to 60 surface lysine groups [60]. Thus, it is very likely that BSA can interact with the negatively charged HA under physiological conditions. The effect of HA on BSA penetration in intact skin can be summarized as follows: while 5 kDa HA led to a penetration enhancement of BSA into the viable epidermis (Figure 4-1 I) with an enhancement factor of 7.5 (Figure 4-2 A), no effect was observed for higher molecular weight HA. There are several hypotheses how HA acts as a skin penetration enhancer. Some publications discuss that HA itself penetrates [17, 46-48] and co-transport the drug into the skin [26]. Our FRET-FLIM experiments indeed revealed a close proximity between HA and BSA (Figure 4-3) under the conditions of penetration enhancement. Since it is known that BSA can bind to HA [58, 59], the FRET-FLIM results and the observation that HA alone penetrated into the epidermis (Figure 4-1) indicated that BSA was co-transported into the epidermis by HA.

Although our results support the theory that HA penetration and co-transport are the driving force of enhanced drug delivery, this does not exclude the existence of other mechanisms such as skin hydration or the occlusive properties of HA at higher concentrations [14]. To further understand the modes of HA action when applied onto skin we performed FTIR measurements on isolated SC sheets. Besides evaluating the effect of the different molecular weights of HA, we also analyzed the dependence of skin hydration, keratin structure and lipid organization on HA concentration.

At higher HA concentrations and increasing molecular weight, the overall skin hydration capacity of the hydrogels decreased as more water was needed to equilibrate the HA gel, leaving less free water in the water phase [61, 62]. Our findings support these results. With exception of 5 kDa HA, the use of a 10 % HA gel led to lower skin hydration compared to the 5 % hydrogels (Figure 4-4). The best hydration effects, however, were observed for 5 kDa formulations. Under these conditions we found enhanced BSA skin penetration in normal skin (Figure 4-1). Thus, skin hydration seems to be another important factor for enhanced protein delivery into intact skin. Since a direct interdependence between keratin structure and hydration exist, we also had a look at the changes of keratin structure. According to [32] the formulation driven keratin conversions from  $\alpha$ -helical structure to  $\beta$ -sheet lead to impaired barrier properties and thus enhanced skin absorption of substances. Indeed, the most prominent structural changes were again observed following the application of 5 kDa HA formulations (Figure 4-5 A), in particular at the concentrations of 5 % and 10 % HA. HEC gels

that were used as control showed no or only minor effects compared to 5 kDa HA (Figure 4-4 and 4-5).

Consequently, for enhanced protein delivery into intact skin the following picture emerged: Formulations containing low molecular weight HA (here 5 kDa HA) altered the SC barrier properties through keratin structural changes and increased skin hydration, in particular at higher concentrations (5 % and 10 % HA). Under these conditions (5 % 5 kDa HA) transport of the model protein BSA into the epidermis was observed that was absent using an aqueous control. Since close contact between HA and BSA molecules both in the SC and in the epidermis was detected, co-transport is the most plausible explanation. For the case at hand, a combination of HA-based skin hydration and co-transport of biomacromolecules was observed in conjunction with enhanced protein delivery in intact skin.

**Barrier deficient skin.** In tape-stripped skin, however, a different picture evolved. We showed that proteins can penetrate into the barrier-disrupted skin (Figure 4-1 H). Similar effects were shown for highly hydrated skin [57]. HA alone did also penetrate deep into tape-stripped skin. The highest concentration of HA in the skin was found for 100 kDa HA. This is in contrast to the HA penetration properties in intact skin (Figure 4-1 A-F). If the lipid chain order in the SC or interactions between HA and the skin lipids played a role was assessed by FTIR [29, 30, 51]. These measurements indicated a more disordered lipid organization after treatment with 5 % and 10 % 100 kDa HA preparations. We assume that the reduction in SC thickness together with a loosened and more disordered state of the SC lipids was responsible for better HA penetration in tape-stripped skin compared to intact skin.

Since both HA and BSA were shown to penetrate well into the tape-stripped skin, the observed effect when a mixture of both molecules was applied to barrier disrupted skin was surprising. Here, we observed that formulations containing both HA and the protein exhibited penetration retardation in terms of a localized epidermal absorption of BSA in barrier disrupted skin. This effect was observed for all molecular weights of HA used in this study. So called epidermal retention effects were also described by Brown et al. [14, 55] and attributed to skin hydration. HA penetration into the skin and the absence of close contact between HA and BSA in our investigations of tape-stripped skin support an effect of skin hydration. However, the exact underlying mechanism leading to intraepidermal confinement and preventing protein penetration into deeper dermal layers remains to be elucidated.

## 5. Conclusion

A combination of biophysical spectroscopic and imaging methods enabled us to shed light on the penetration behavior of HA, topical delivery of a model protein BSA and underlying mechanisms. Our data substantiate the findings in the literature that low molecular weight HA

is able to overcome the disrupted SC. We demonstrated the penetration enhancing effects of 5 kDa HA for the model protein BSA in intact skin. The enhancement effect was most likely based on an interplay of skin hydration, interaction with keratin structure and protein-HA co-transport, aiding the transport across the SC as well as the skin absorption of HA itself. Moreover, we showed HA-facilitated penetration confinement resulting in a localized epidermal absorption (stratum corneum and viable epidermis) of proteins in barrier disrupted skin. Thus, HA hydrogels seem to be potential delivery systems for barrier-deficient skin.

## 6. Acknowledgments

This work was supported by a grant from the German Research Foundation (DFG; KU 2904/2-1 S.K.) and (DFG; SFB 1112 TP B03 U.A.). Support from the Leibnitz Graduate School of Molecular Biophysics and the Helmholtz Virtual Institute on “Multifunctional Polymers for Medicine” is gratefully acknowledged. We would like to thank Dr. Tai-Yang Kim for help in the initial stage of the FLIM experiments.

## 7. References

1. Grenha, A., *Systemic delivery of biopharmaceuticals: Parenteral forever? J Pharm Bioallied Sci*, 2012; 4, 95-95.
2. Mitragotri, S., Burke, P., Langer, R. *Overcoming the challenges in administering biopharmaceuticals: formulation and delivery strategies. Nat Rev Drug Discov* 2014, 13, (9), 655-672.
3. Weinberg, J. M. *An overview of infliximab, etanercept, efalizumab, and alefacept as biologic therapy for psoriasis. Clin Ther* 2003, 25, (10), 2487-2505.
4. Schoellhammer, C. M.; Blankschtein, D.; Langer, R. *Skin permeabilization for transdermal drug delivery: recent advances and future prospects. Expert Opin Drug Deliv* 2014, 11, (3), 393-407.
5. Herwadkar, A.; Banga, A. K. *Peptide and protein transdermal drug delivery. Drug Discov Today: Technologies* 2012, 9, (2), e147-e154.
6. Smith, F. J. D.; Irvine, A. D.; Terron-Kwiatkowski, A.; Sandilands, A.; Campbell, L. E.; Zhao, Y. W.; Liao, H. H.; Evans, A. T.; Goudie, D. R.; Lewis-Jones, S.; Arseculeratne, G.; Munro, C. S.; Sergeant, A.; O'Regan, G.; Bale, S. J.; Compton, J. G.; DiGiovanna, J. J.; Presland, R. B.; Fleckman, P.; McLean, W. H. I. *Loss-of-function mutations in the gene encoding filaggrin cause ichthyosis vulgaris. Nat Genet* 2006, 38, (3), 337-342.
7. Palmer, C. N. A.; Irvine, A. D.; Terron-Kwiatkowski, A.; Zhao, Y. W.; Liao, H. H.; Lee, S. P.; Goudie, D. R.; Sandilands, A.; Campbell, L. E.; Smith, F. J. D.; O'Regan, G. M.; Watson, R. M.; Cecil, J. E.; Bale, S. J.; Compton, J. G.; DiGiovanna, J. J.; Fleckman, P.; Lewis-Jones, S.; Arseculeratne, G.; Sergeant, A.; Munro, C. S.; El Houate, B.; McElreavey, K.; Halkjaer, L. B.; Bisgaard, H.; Mukhopadhyay, S.; McLean, W. H. I. *Common loss-of-function variants of the epidermal barrier protein filaggrin are a major predisposing factor for atopic dermatitis. Nat Genet* 2006, 38, (4), 441-446.
8. Stout, T. E.; McFarland, T.; Mitchell, J. C.; Appukuttan, B.; Stout, J. T. *Recombinant Filaggrin Is Internalized and Processed to Correct Filaggrin Deficiency. J Invest Dermatol* 2014, 134, (2), 423-429.
9. Aufenvenne, K.; Larcher, F.; Hausser, I.; Duarte, B.; Oji, V.; Nikolenko, H.; Del Rio, M.; Dathe, M.; Traupe, H. *Topical Enzyme-Replacement Therapy Restores Transglutaminase 1 Activity and Corrects Architecture of Transglutaminase-1-Deficient Skin Grafts. Am J Hum Genet* 2013, 93, (4), 620-630.

10. Gao, Y.; Wang, X.; Chen, S.; Li, S.; Liu, X. Acute skin barrier disruption with repeated tape stripping: an in vivo model for damage skin barrier. *Skin Res Technol* 2013, 19, (2), 162-168.
11. KÜchler, S.; Strüver, K.; Friess, W. Reconstructed skin models as emerging tools for drug absorption studies. *Expert Opin Drug Metabol Toxicol* 2013, 9, (10), 1255-1263.
12. Gerritsen, M.; Erp, P.; Vlijmen-Willems, I.; Lenders, L.; Kerkhof, P. Repeated tape stripping of normal skin: a histological assessment and comparison with events seen in psoriasis. *Arch Dermatol Res* 1994, 286, (8), 455-461.
13. Zhai, H.; Poblete, N.; Maibach, H. Stripped skin model to predict irritation potential of topical agents in vivo in humans. *Int J Dermatol* 1998, 37, (5), 386-389.
14. Brown, M.; Jones, S. Hyaluronic acid: a unique topical vehicle for the localized delivery of drugs to the skin. *J Eur Acad Dermatol Venereol* 2005, 19, (3), 308-318.
15. Jin, Y.; Ubonvan, T.; Kim, D. Hyaluronic Acid in Drug Delivery Systems. *J Pharm Invest* 2010, 40, 33-43.
16. Meyer, J.; Whitcomb, L.; Treuheit, M.; Collins, D. Sustained in vivo activity of recombinant human granulocyte colony stimulating factor (rHG-CSF) incorporated into hyaluronan. *J Control Rel* 1995, 35, (1), 67-72.
17. Yang, J.; Kim, E.; Kwon, J.; Kim, H.; Shin, J.; Yun, S.; Choi, K.; Hahn, S. Transdermal delivery of hyaluronic acid – Human growth hormone conjugate. *Biomaterials* 2012, 33, (25), 5947-5954.
18. Michel, M.; Marguerite, R., Characterization and Properties of Hyaluronic Acid (Hyaluronan). In *Polysaccharides*, CRC Press, 2004.
19. Voigt, J.; Driver, V. R. Hyaluronic acid derivatives and their healing effect on burns, epithelial surgical wounds, and chronic wounds: A systematic review and meta-analysis of randomized controlled trials. *Wound Repair Regen* 2012, 20, (3), 317-331.
20. Balazs, E. Therapeutic use of hyaluronan. *Struct Chem* 2009, 20, (2), 341-349.
21. Gaffney, J.; Matou-Nasri, S.; Grau-Olivares, M.; Slevin, M. Therapeutic applications of hyaluronan. *Mol Biosys* 2010, 6, (3), 437-443.
22. Pirard, D.; Vereecken, P.; Mélot, C.; Heenen, M. Three percent diclofenac in 2.5% hyaluronan gel in the treatment of actinic keratoses: a meta-analysis of the recent studies. *Arch Dermatol Res* 2005, 297, (5), 185-189.
23. Moore, A.; Willoughby, D. Hyaluronan as a drug delivery system for diclofenac: a hypothesis for mode of action. *Int J Tissue React* 1995, 17, (4), 153-156.
24. Gustafson, S., *Hyaluronan in drug delivery*. Portland Press: London, 1998; 291-304.
25. Scott, E., *Secondary structures in hyaluronan solution: chemical and biological implications*. John Wiley: Chichester, 1989; 6-16.
26. Brown, T.; Alcorn, D.; Fraser, J. Absorption of Hyaluronan Applied to the Surface of Intact Skin. *J Invest Dermatol* 1999, 113, (5), 740-746.
27. Banks, P. R.; Paquette, D. M. Comparison of Three Common Amine Reactive Fluorescent Probes Used for Conjugation to Biomolecules by Capillary Zone Electrophoresis. *Bioconjugate Chem* 1995, 6, (4), 447-458.
28. DeAngelis, P. L. Polysaccharide Labeling with N-Methylisatoic Anhydride: Generation of Ultraviolet Chromophores and Blue Fluorophores. *Anal Biochem* 2000, 284, (1), 167-169.
29. Bommannan, D.; Potts, R. O.; Guy, R. H. Examination of Stratum Corneum Barrier Function In Vivo by Infrared Spectroscopy. *J Invest Dermatol* 1990, 95, (4), 403-408.
30. Vávrová, K.; Henkes, D.; Strüver, K.; Sochorová, M.; Školová, B.; Witting, M.; Friess, W.; Schreml, S.; Meier, R.; Schäfer-Korting, M.; Fluhr, J.; KÜchler, S. Filaggrin Deficiency Leads to Impaired Lipid Profile and Altered Acidification Pathways in a 3D Skin Construct. *J Invest Dermatol* 2014, 134, (3), 746-753.
31. Velkova, V.; Lafleur, M. Influence of the lipid composition on the organization of skin lipid model mixtures: An infrared spectroscopy investigation. *Chem Phys Lipids* 2002, 117, (1-2), 63-74.
32. Kaushik, D.; Michniak-Kohn, B. Percutaneous Penetration Modifiers and Formulation Effects: Thermal and Spectral Analyses. *AAPS PharmSciTech* 2010, 11, (3), 1068-1083.
33. Schäfer-Korting, M.; Bock, U.; Diembeck, W.; Düsing, H.; Gamer, A.; Haltner-Ukomadu, E.; Hoffmann, C.; Kaca, M.; Kamp, H.; Kersen, S.; Kietzmann, M.; Korting, H.; Krächter, H.; Lehr, C.; Liebsch, M.; Mehling, A.; Müller-Goymann, C.; Netzlaff, F.; Niedorf, F.; Rübbecke, M.; Schäfer, U.; Schmidt, E.; Schreiber, S.; Spielmann, H.; Vuia, A.; Weimer, M. The Use of Reconstructed Human Epidermis for Skin Absorption Testing: Results of the Validation Study. *ATLA* 2008, 36, 161-187.
34. Diembeck, W.; Beck, H.; Benech-Kieffer, F.; Courtellemont, P.; Dupuis, J.; Lovell, W.; Paye, M.; Spengler, J.; Steiling, W. Test Guidelines for In Vitro Assessment of Dermal Absorption

- and Percutaneous Penetration of Cosmetic Ingredients. *Food Chem Toxicol* 1999, 37, (2–3), 191-205.
35. Gattu, S.; Maibach, H. I. Enhanced Absorption through Damaged Skin: An Overview of the *in vitro* Human Model. *Skin Pharmacology and Physiology* 2010, 23, (4), 171-176.
  36. Alexiev, U.; Rimke, I.; Pöhlmann, T. Elucidation of the Nature of the Conformational Changes of the EF-interhelical Loop in Bacteriorhodopsin and of the Helix VIII on the Cytoplasmic Surface of Bovine Rhodopsin: A Time-resolved Fluorescence Depolarization Study. *J Mol Biol* 2003, 328, (3), 705-719.
  37. Boreham, A.; Kim, T. Y.; Spahn, V.; Stein, C.; Mundhenk, L.; Gruber, A. D.; Haag, R.; Welker, P.; Licha, K.; Alexiev, U. Exploiting Fluorescence Lifetime Plasticity in FLIM: Target Molecule Localization in Cells and Tissues. *ACS Med Chem Lett* 2011, 2, (10), 724-8.
  38. Kim, T. Y.; Winkler, K.; Alexiev, U. Picosecond multidimensional fluorescence spectroscopy: A tool to measure real-time protein dynamics during function. *Photochem Photobiol* 2007, 83, (2), 378-384.
  39. Kim, T. Y.; Moeller, M.; Winkler, K.; Kirchberg, K.; Alexiev, U. Dissection of Environmental Changes at the Cytoplasmic Surface of Light-activated Bacteriorhodopsin and Visual Rhodopsin: Sequence of Spectrally Silent Steps. *Photochem Photobiol* 2009, 85, (2), 570-577.
  40. Dutta, A.; Kim, T. Y.; Moeller, M.; Wu, J. N.; Alexiev, U.; Klein-Seetharaman, J. Characterization of Membrane Protein Non-native States. 2. The SDS-Unfolded States of Rhodopsin. *Biochemistry-Us* 2010, 49, (30), 6329-6340.
  41. Kirchberg, K.; Kim, T. Y.; Moller, M.; Skegro, D.; Raju, G. D.; Granzin, J.; Buldt, G.; Schlesinger, R.; Alexiev, U. Conformational dynamics of helix 8 in the GPCR rhodopsin controls arrestin activation in the desensitization process. *P Natl Acad Sci USA* 2011, 108, (46), 18690-18695.
  42. Boreham, A.; Pfaff, M.; Fleige, E.; Haag, R.; Alexiev, U. Nanodynamics of Dendritic Core-Multishell Nanocarriers. *Langmuir* 2014, 30, (6), 1686-1695.
  43. Boreham, A.; Brodewolf, R.; Pfaff, M.; Kim, T.-Y.; Schlieter, T.; Mundhenk, L.; Gruber, A. D.; Gröger, D.; Licha, K.; Haag, R.; Alexiev, U. Temperature and environment dependent dynamic properties of a dendritic polyglycerol sulfate. *Polym Adv Technol* 2014, DOI: 10.1002/pat.3355.
  44. Alnasif, N.; Zoschke, C.; Fleige, E.; Brodewolf, R.; Boreham, A.; Ruhl, E.; Eckl, K. M.; Merk, H. F.; Hennies, H. C.; Alexiev, U.; Haag, R.; Küchler, S.; Schäfer-Korting, M. Penetration of normal, damaged and diseased skin - An *in vitro* study on dendritic core-multishell nanotransporters. *J Control Release* 2014, 185, 45-50.
  45. Ostrowski, A.; Nordmeyer, D.; Boreham, A.; Brodewolf, R.; Mundhenk, L.; Fluhr, J. W.; Lademann, J.; Graf, C.; Rühl, E.; Alexiev, U.; Gruber, A. D. Skin barrier disruptions in tape stripped and allergic dermatitis models have no effect on dermal penetration and systemic distribution of AHAPS-functionalized silica nanoparticles. *Nanomedicine: Nanotechnology, Biology and Medicine*, (0).
  46. Farwick, M.; Gauglitz, G.; Pavicic, T.; Köhler, T.; Wegmann, M.; Schwach-Abdellaoui, K.; Malle, B.; Tarabin, V.; Schmitz, G.; Korting, H. C. Fifty-kDa Hyaluronic Acid Upregulates Some Epidermal Genes without Changing TNF- $\alpha$  Expression in Reconstituted Epidermis. *Skin Pharmacol Physiol* 2011, 24, (4), 210-217.
  47. Farwick, M.; Lersch, P.; Strutz, G. Low Molecular Weight Hyaluronic Acid: Its Effects on Epidermal Gene Expression and Skin Ageing. *SOFW Journal* 2008, 11, (134), 1-6.
  48. Birkenfeld, B.; Parafiniuk, M.; Bielecka-Grzela, S.; Klimowicz, A.; Piwowarska-Bilska, H.; Mikołajczak, R.; Listewnik, M.; Kurzejamska-Parafiniuk, M.; Osowski, A.; Byszewska-Szpocińska, E., The penetration of topically applied ointment containing hyaluronic acid in rabbit tissues. In *Pol J Vet Sci*, 2011; 14, 621.
  49. Alexiev, U.; Farrens, D. L. Fluorescence spectroscopy of rhodopsins: Insights and approaches. *Biochimica et Biophysica Acta (BBA) - Bioenergetics* 2014, 1837, (5), 694-709.
  50. Potts, R. O.; Guzek, D. B.; Harris, R. R.; McKie, J. E. A noninvasive, *in vivo* technique to quantitatively measure water concentration of the stratum corneum using attenuated total-reflectance infrared spectroscopy. *Arch Dermatol Res* 1985, 277, (6), 489-495.
  51. Lucassen, G. W.; van Veen, G. N. A.; Jansen, J. A. J. Band Analysis of Hydrated Human Skin Stratum Corneum Attenuated Total Reflectance Fourier Transform Infrared Spectra *In Vivo*. *BIOMEDO* 1998, 3, (3), 267-280.
  52. Antosova, Z.; Mackova, M.; Kral, V.; Macek, T. Therapeutic application of peptides and proteins: parenteral forever? *Trends Biotechnol* 2009, 27, (11), 628-635.
  53. Jain, A.; Jain, A.; Gulbake, A.; Shilpi, S.; Hurkat, P.; Jain, S. K. Peptide and Protein Delivery Using New Drug Delivery Systems. 2013, 30, (4), 293-329.

54. Degim, T.; Celebi, N. *Controlled Delivery of Peptides and Proteins. Curr Pharm Design* 2007, 13, (1), 99-117.
55. Brown, M.; Marriott, C.; Martin, G. *The effect of hyaluronan on the in vitro deposition of diclofenac within the skin. Int J Tissue React* 1995, 17, (4), 133 - 40.
56. Lin, W.; Maibach, H. I., *Percutaneous absorption of diclofenac in hyaluronic acid gel: in vitro study in human skin. In Hyaluronan in Drug Delivery, Willoughby, D., R.S.M. Press: London, 1996; 167-174.*
57. Tan, G.; Xu, P.; Lawson, L. B.; He, J.; Freytag, L. C.; Clements, J. D.; John, V. T. *Hydration effects on skin microstructure as probed by high-resolution cryo-scanning electron microscopy and mechanistic implications to enhanced transcutaneous delivery of biomacromolecules. J Pharm Sci* 2010, 99, (2), 730-740.
58. Lenormand, H.; Deschrevel, B.; Tranchepain, F.; Vincent, J. C. *Electrostatic Interactions Between Hyaluronan and Proteins at pH 4: How Do They Modulate Hyaluronidase Activity. Biopolymers* 2008, 89, (12), 1088-1103.
59. Cooper, C. L.; Goulding, A.; Kayitmazer, A. B.; Ulrich, S.; Stoll, S.; Turksen, S.; Yusa, S.; Kumar, A.; Dubin, P. L. *Effects of polyelectrolyte chain stiffness, charge mobility, and charge sequences on binding to proteins and micelles. Biomacromolecules* 2006, 7, (4), 1025-1035.
60. Brewer, S. H.; Glomm, W. R.; Johnson, M. C.; Knag, M. K.; Franzen, S. *Probing BSA binding to citrate-coated gold nanoparticles and surfaces. Langmuir* 2005, 21, (20), 9303-7.
61. Liao, Y.; Jones, S.; Forbes, B.; Martin, G.; Brown, M. *Hyaluronan: Pharmaceutical Characterization and Drug Delivery. Drug Deliv* 2005, 12, (6), 327-342.
62. Hoffman, A. S. *Hydrogels for biomedical applications. Adv Drug Deliv Rev* 2002, 54, (1), 3-12.

# Chapter 5

## Feasibility Study for Intra-Epidermal Delivery of Proteins Using A Solid Microneedle Array

The following chapter has been published as peer-reviewed article in the International Journal of Pharmaceutics in this thesis with the journal's permission:

Madeleine Witting , Katja Obst, Markus Pietzsch, Wolfgang Friess, Sarah Hedtrich

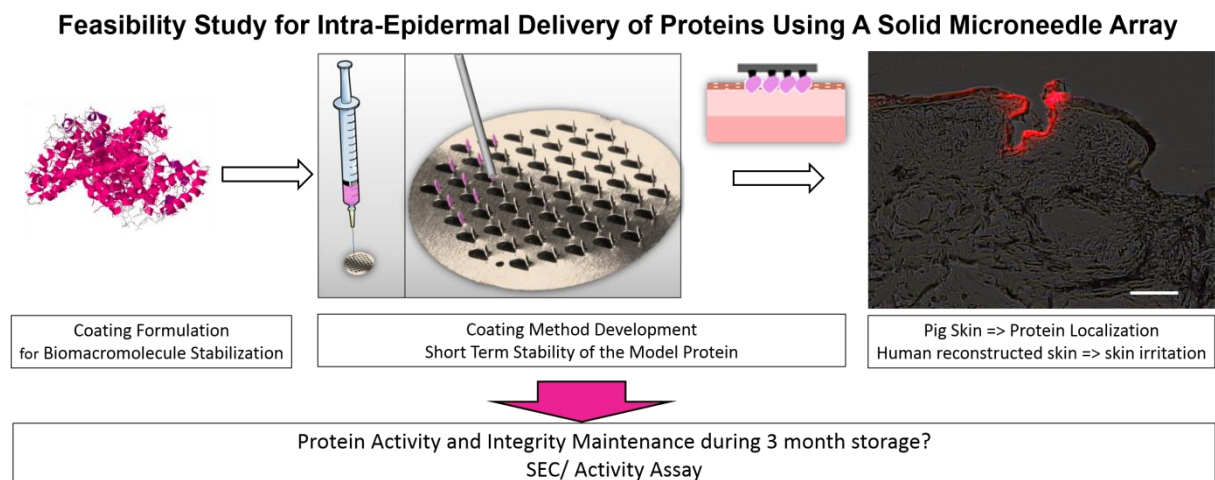
*Feasibility Study for Intra-Epidermal Delivery of Proteins Using A Solid Microneedle Array*

Int. J. Pharm. 486, 1-2, (2015) 52-58

Online available: <http://www.sciencedirect.com/science/article/pii/S0378517315002628>

The personal contribution covers the written parts of the introduction, the results and discussion as well as the experimental set-up and execution with exception of the following chapters: **2.1 / 2.2 / 2.7.2 / 2.7.3 / 2.8 / 3.1 / 3.3** (personal contribution only covers the pig skin experiments)

### Graphical Abstract



## Abstract

Solid microneedles (MN) are a promising tool for dermal drug delivery. Particular focus lies on the field of vaccination due to pain-free, safe, hygienic and patient compliant antigen deposition. Diverse coating techniques and formulations have been developed to preserve vaccine activity and to enable targeted drug deposition in the skin. Process and long-term storage stability of coated MN, however, have not yet been studied in detail. Hence, a feasibility study was conducted determining the appropriate needle length (300  $\mu\text{m}$ ) for local intraepidermal protein delivery. Moreover, a protein-stabilizing coating formulation was developed. Coating of the MN resulted in protein concentrations between 10 to 23  $\mu\text{g}$ , 90% of the bioactivity of the model protein asparaginase was maintained for 3 months. Skin experiments verified the intraepidermal deposition of  $68.0 \pm 11.7\%$  of the coated model protein after single application. Slightly increased interleukin 8 levels right after MN insertion indicated minor skin irritation due to the mechanical piercing stress. Thus, specifically highlighting protein stabilization during storage, we demonstrated that selective intraepidermal deposition of proteins or peptides' using solid MN is a feasible approach.

Key Words: solid microneedle array, proteins, coating formulation, protein stability, human reconstructed skin, skin irritation

## 1. Introduction

The application of microneedles (MN) into human skin emerged as a popular tool in both the cosmetic and pharmaceutical area. Used in the cosmetic sector, microneedling is effective in ameliorating conditions such as scars, striae, wrinkles, or dyspigmentation [1–3] since MN stimulate the differentiation of fibroblasts resulting in enhanced production of collagen and elastin fibers [2]. Besides cosmetic treatments, MN are considered useful for dermal drug delivery, which is particularly appealing for drugs suffering from low skin absorption due to hampering physicochemical properties, such as proteins, or for compounds intended for local intradermal action [4,5]. Due to needle lengths in the lower micrometer range, topical insertion of MN do not activate the nociceptors in the skin allowing a pain free drug application or vaccination [5]. Consequentially, MN are widely tested for transdermal delivery of proteins like insulin [6,7], desmopressin [8], or the human growth hormone [9] and for intradermal vaccination against e.g. measles [10] or influenza [11,12]. The latter is a particularly attractive approach since the vaccines can be directly administered into the viable epidermis or dermis resulting in a strong immune response [13,14].

The major barrier for topically applied compounds is the stratum corneum (SC), the skin's outermost layer. The application of MN enables to overcome the SC easily since the needles pierce the SC and generate microchannels [6,15] through which topically applied substances can then readily diffuse. Alternatively, the compounds can be coated onto the MN tips and directly introduced into the skin [5,16]. As for today, different coating techniques, formulations and applications are described in the literature [13,16–18]. Limited data, however, are available on the protein stability of coated MN and on potential skin irritation following MN application. The stability of coated proteins was either investigated over relatively short periods like days up to one month, or the potential induction of immune responses or skin irritation was not evaluated [8,19–22].

Hence, the aim of this work was a comprehensive feasibility study on intradermal protein delivery investigating systematically the coating efficiency of stainless-steel MN, MN insertion and required forces, a suitable coating formulation for the model proteins bovine serum albumin (BSA) and the more labile L-asparaginase II (AsnB) and the establishment of an adequate coating method. Subsequently, the protein integrity and bioactivity directly after coating and after storage at 2 - 8°C, 25°C and 40°C for up to 3 month was monitored using specific activity assays and size exclusion chromatography (SEC). Intradermal protein delivery was initially investigated in excised pig skin. Moreover, total protein amounts delivered into the skin were determined in reconstructed human skin. Skin models are suitable *in vitro* test systems to study skin absorption of substances and skin irritation potential following MN insertion [23]. Hence, to assess the skin irritation potential of MN

insertion, the amounts of the pro-inflammatory cytokines interleukin (IL) 6 and IL-8 were quantified.

## **2. Materials and Methods**

### **2.1 Materials**

Hyaluronic acid (HA; molecular weight: 1 MDa) was kindly provided by Shiseido Co., Ltd (Shizuoka, Japan). AsnB from *E. coli* was produced by Prof. Dr. Markus Pietzsch. The enzyme was isolated from frozen recombinant *E. coli* cells. 100 g bio wet mass were suspended in 1 L of buffer A (50 mM Tris-acetate buffer, pH 5.1) using an ultraturrax homogenizer. The cells were disintegrated by high pressure homogenization (APV 2000, APV Systems, Albertslund, Denmark) using four passages at a pressure of 1000 bar. The suspension was cooled to 4°C before and between the passages and subsequently centrifuged (30 min, 5000 g, Avanti J-30i, Beckman Coulter, USA) at 4°C. The pellet was discarded. To the supernatant (850 mL), 850 mL ethanol was added and incubated at room temperature for 30 min. The precipitate containing AsnB was centrifuged off and dissolved again in 550 mL buffer A. Afterwards, the same volume of ethanol was added to the supernatant to obtain a 50% (v/v) mixture. After 30 min, the precipitated AsnB was again collected by centrifugation and lyophilized. From 100 g bio wet mass, 2.7 g AsnB was obtained. The lyophilized enzyme was stored at minus 25°C.

BSA, dimethyl sulfoxide (DMSO), rhodamine B isothiocyanate (RhB ITC), methylene blue, polysorbate 80, L-asparagine monohydrate, trichloroacetic acid, and the buffer reagents were purchased from Sigma-Aldrich (Steinheim, Germany). Nessler's reagent was obtained from Merck (Darmstadt, Germany). The MN arrays (56 needles, 300 µm needle length) were purchased from Microneedle Systems (Georgia, USA).

For skin penetration experiments, pig skin of the flank region from "Deutsche Landrasse", 30-50 kg, 10-20 weeks old was used (Clinic of Swine, Ludwig-Maximilians University, Munich, permission no. DE 09 162 0017 X-1). Immediately after surgical removal, the excised skin was transferred to the laboratory. Any contact between the skin surface and the lipids of the subcutis was avoided. The skin was stored at -20°C for up to 6 month. Prior to use, the skin was thawed, gently cleaned with PBS buffer (pH 7.4) and excessive hair was removed with clippers.

### **2.2 Assessment of Optimal Insertion Depth, Fracture and Insertion Force**

The optimal insertion force for microchannel formation and the maximum force before fracture of the MN array were assessed using a texture analyzer TA.XTplus (Winopal, Elze,

Germany). The MN arrays were mounted onto the processing arm of the TA.XTplus using double-sided tape and subsequently inserted into excised pig skin. To determine the minimum insertion force that is required to pierce the SC, the MN arrays were injected with a constant speed of 0.05 mm/sec. In case of skin contact, the pressure from the MN array onto the skin surface increases. When the MN needles finally pierce the SC, a sharp drop in the otherwise gradually increasing force graph can be observed [24]. To visualize the formation of microchannels and the insertion depth after MN insertion with varying forces (1, 3, 4, 5 N, and manually (~ 3 N)), skin slices (10 µm) were stained with methylene-blue (2% w/v, 15 min incubation time) and investigated under the light microscope (VHX-2000, Keyence, Neu-Isenburg, Germany). To assess the MN fracture force, the MN arrays were moved against a flat aluminum block at a rate of 0.05 mm/sec. The data of the insertion and fracture force were collected and processed using TestXpert II software.

### **2.3 Fluorescence Labeling of Bovine Serum Albumin (BSA)**

Fluorescence labeling of BSA was performed using RhB ITC. 1 mg/mL RhB ITC in DMSO was added to 6 mg/mL BSA in 0.1 M sodium bicarbonate buffer (pH 9.0) resulting in a ratio of 1:170 (dye:protein). After 2 h stirring under light protection, the labeled protein was purified and concentrated using Vivaspin 20 tubes (PES membrane MWCO 30,000, Sartorius AG, Göttingen, Germany) and subsequently centrifuged for 45 min at 4,000 rpm at 5°C. Subsequently, several washing steps were performed by adding fresh PBS buffer pH 7.4 to remove unbound dye. The absence of free dye was confirmed by UV measurements at 541 nm. Protein concentration (between 20-25 mg/ml) and the degree of labeling (between 0.95-1.3) were determined according to the manufacturer protocols. The labeled proteins (BSA-RhB ITC) were stored at -20°C until further use.

### **2.4 Formulation of the Coating Solution**

An aqueous coating solution consisting of 5% (w/v) sucrose, 2% (w/v) L-phenylalanine, 1% (w/v) hyaluronic acid (molecular weight: 1 MDa) and 1% (w/v) model protein was prepared. BSA-RhB ITC and AsnB served as model proteins. The formulations were prepared 1 day before use and stored at 4 - 8°C.

### **2.5 Dip-Coating of the MN**

First, the MN arrays were cleaned with acetone, then rinsed with water, subsequently immersed in 0.1% w/v polysorbate 80 in PBS pH 7.4, and air-dried at room temperature. Subsequently, the MN tips were coated by dipping a 26Gx ½" syringe needle (Terumo Europe N.V., Leuven, Belgium) connected to a 1 ml syringe filled with the coating formulation onto the MN, respectively (Fig. 5-1). After coating, the MN were air-dried at room

temperature for at least 15 minutes. For multiple coatings, the procedure was repeated twice or three times.

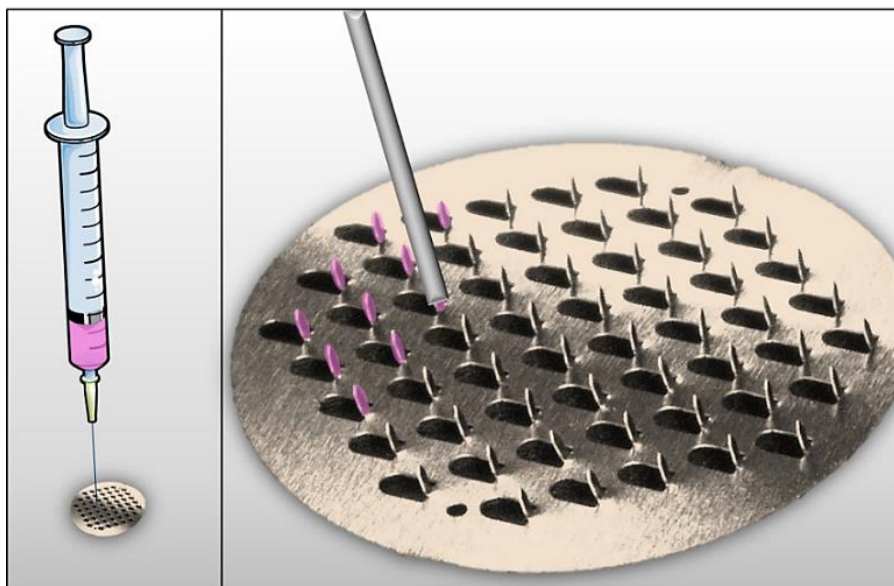


**Figure 5-1** Scheme of the syringe and needle based dip-coating method. The coating solution was directly applied onto the MN tips using a 26Gx ½” needle.

To assess the coated protein amount, the MN were immersed in 210  $\mu$ l water. Subsequently, the concentrations of BSA and AsnB were determined by a bicinchoninic acid (BCA) assay (Micro BCA™ Protein Assay Kit, Pierce Biotechnology, Illinois, USA). Therefore, 150  $\mu$ l of the coating solution were added to 150  $\mu$ l of the reaction mixture. After 2 h incubation at 37°C, the optical density was measured at 562 nm, blank corrected and compared with the BSA or AsnB standard curve.

## 2.6 Determination of Protein Activity

The bioactivity of AsnB following MN coating and drying after one, two, or three coatings was assessed as the specific enzyme activity [U/mg] according to published procedures [25]. Briefly, a mixture of 50  $\mu$ l coating solution, 100  $\mu$ l 50 mM Tris-HCl buffer pH 8.6 and 850  $\mu$ l 10 mM L-asparagine monohydrate in 50 mM Tris-HCl buffer pH 8.6 was incubated at 37°C for 10 min. After adding 50  $\mu$ l 1.5 M trichloroacetic acid solution, 100  $\mu$ l of the supernatant was added to 200  $\mu$ l Nessler’s solution. After 10 min at 22°C, the optical density was measured at UV = 436 nm, compared with the standard curve and corrected for the total enzyme amount as determined by Micro BCA™ Protein Assay Kit. The units of activity were defined as micromoles of ammonia released per minute. Freshly prepared AsnB solution served for reference.

## 2.7 Storage Stability of the MN Coatings and Proteins

AsnB coated MN were stored at 2-8°C, 25°C, and 40°C for 1 week, 1 month, and 3 months, respectively. Subsequently, AsnB activity was determined as described above (see 2.6). The amount of AsnB tetramer, the biologically active form, and the formation of protein aggregates and fragments was assessed with SEC (TSKgel® SWXL guard column (dimensions: 6.0 mm x 4.0 cm), TSKgel® G4000 PWXL column (dimensions: 300 x 7.8 mm, 10 µm particle size; TOSOH Bioscience, Stuttgart), isocratic elution at 0.4 ml/min, 100 mM Na<sub>2</sub>HPO<sub>4</sub>, 150mM NaCl, pH 7.4) with UV and fluorescence detection (UV = 280 nm, fluorescence = exc. 280/ em. 350 nm)).

## 2.9 MN Insertion in Pig Skin and Reconstructed Human Skin

**Pig Skin:** To investigate protein delivery into excised pig skin, the coated MNs were manually inserted and remained in the skin for 5 minutes. After withdrawal, the skin was punched into discs of 25 mm diameter (centering the insertion site) and frozen at - 80°C using Jung® tissue freezing medium (Leica Microsystems GmbH, Nussloch, Germany). Subsequently, cryosections (5 - 10 µm) were prepared using a Leica Cryotome CM 3050S (Leica Microsystems, Nussloch, Germany). For data analysis, the slices were subjected to normal and fluorescence microscopy (20 x magnification, BZ-8000, Keyence, Neu-Isenburg). The fluorescence was recovered in the red band exciting the samples at 560 nm for RhB ITC.

**Reconstructed Human Skin:** Reconstructed human skin was generated according to previously published procedures [26]. On day 13 of tissue cultivation, BSA-RhB ITC coated MN were inserted into the skin models. After 5 minutes, the MN arrays were carefully removed. Afterwards, the skin models were snap-frozen in liquid nitrogen and cryosections (thickness: 10 µm) were prepared (see 2.9.1).

To quantify the delivered protein amount, AsnB coated MN were inserted into the skin models on day 13 (single application), or on day 12 and day 13 (double application) of tissue cultivation. At day 14, the epidermis of the skin models was gently peeled off and AsnB was extracted using a TissueLyser II (Quiagen, Venlo, Netherlands). The AsnB amount was subsequently determined as described above (see. 2.7).

## 2.10 Cytokine Release Following MN Insertion

The secretion of the pro-inflammatory cytokines IL-6 and IL-8 was determined by an enzyme-linked immunosorbent assay (ELISA). Therefore, 100 µl cell culture medium was sampled and analyzed according to standard protocols (Human IL-6 DuoSet, DY206, R&D Systems, Minneapolis, MN, USA; Human IL-8 ELISA Ready-Set-Go, eBioscience, Frankfurt am Main, Germany).

## 2.11 Statistical Analysis

The results are presented as average values  $\pm$  SD obtained from at least 3 independent experiments. Statistical analysis is based on a Wilcoxon-Mann-Whitney-Test; \* $p \leq 0.05$  indicates a statistically significant difference.

## 3. Results and Discussion

### 3.1 Optimal Insertion Depth, Fracture and Insertion Force

The needle geometry and material of MN arrays are important factors influencing the characteristics of MN insertion. To overcome the SC and penetrate the skin layers, MN need to be sharp, robust and need to withstand the penetration pressure subjected by the skin tissue. Nevertheless, the needles also should be flexible enough to compensate the skin elasticity and have an appropriate length to avoid pain sensation. Additionally, MN arrays should be applicable manually with reasonable forces without fracturing [27]. The MN arrays used in this feasibility study were made of stainless steel consisting of 56 needles/cm<sup>2</sup>. The needle heads were triangularly shaped and arranged in a tip angle of 70° (Fig. 5-1). Since we aimed for a delivery into the epidermal skin layer, we determined the appropriate needle length by comparing 300  $\mu$ m and 800  $\mu$ m MN arrays. Controlled insertion with a speed of 0.05 mm/sec showed that the MN are able to penetrate the SC at insertion forces of  $0.88 \pm 0.01$  N and  $0.21 \pm 0.01$  N for 300  $\mu$ m and 800  $\mu$ m long needles, respectively (Table 5-1), which is in agreement with published data. Here, a general insertion force range of 0.1 to 3 N was found, which is low enough to enable manual application [24].

**Table 5-1** Insertion force required for SC penetration at an insertion speed of 0.05 mm/sec evaluated for MN arrays with 300 or 800  $\mu$ m needle length compared to a 26Gx 1/2" needle. mean values  $\pm$  SD

Needle type	Insertion force (N) $\pm$ SD*	Fracture force (N)**
MN array (300 $\mu$ m)	$0.88 \pm 0.01$	$3.8 \pm 0.01$
MN array (800 $\mu$ m)	$0.21 \pm 0.01$	-
26Gx 1/2" needle	$0.69 \pm 0.04$	-

\* in pig skin

\*\* against aluminum block

**Table 5-2:** Insertion depth and channel count dependent on insertion force and needle length.

MN length ( $\mu$ m)	Force (N)	Channel count	Insertion depth ( $\mu$ m)
300	1	$20 \pm 1$	$88 \pm 5$
	3	$16 \pm 3$	$77 \pm 4$
	4	$10 \pm 1$	$86 \pm 1$
	5	$20 \pm 2$	$80 \pm 3$
	manual (~ 3)	$20 \pm 3$	$86 \pm 2$
800	5	$30 \pm 2$	$200 \pm 4$
	manual (~ 3)	$30 \pm 1$	$280 \pm 5$

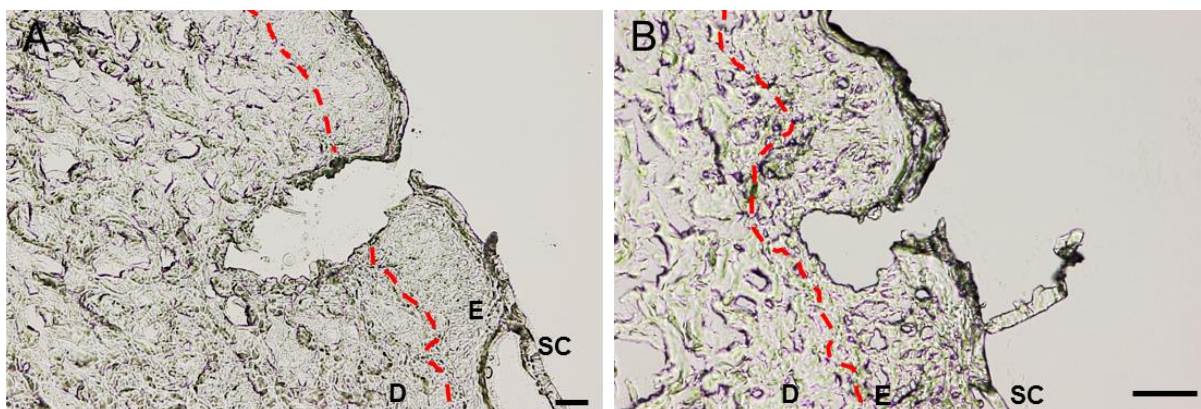


**Figure 5-2** Microscopic evaluation of the MN channel depth after manual insertion (insertion force ~ 3 N) for MN arrays with a needle length of 800 µm (A) and 300 µm (B). SC= stratum corneum, E = Viable Epidermis, D = Dermis. bar = 50 µm

Manual and automated insertion of the MN arrays resulted in insertion depths ranging from 80 to 90 µm for the 300 µm MN array and 200 to 280 µm for the 800 µm MN arrays (Fig. 5-2, Table 5-2). Consequentially, the 300 µm long MN were most suitable for intraepidermal drug delivery given that the human epidermis has a thickness of 130 - 180 µm [28, 29].

Since the stability of the MN arrays is important for an injury free application, the fracture force was determined. In an experimental setting, where the MN arrays were subjected to collision with an aluminum block, the MN tips experienced deformation at a force of  $3.8 \pm 0.01$  N. Nevertheless, in ex-vivo experiments with pig skin, where insertion forces up to 5 N were applied, and no damage of the skin tissue and no differences in microchannel count or depth (Table 5-2) were observed. Hence, the MN arrays used in this study proved to be safe, which was likewise found for a similar stainless steel MN patch [30]. In addition, successful MN insertion also depends on individual skin thickness and elasticity [31]. Regarding the applied insertion force, no correlation between force and channel count was observed (Table 5-2) and the insertion depth was hardly influenced.

### 3.2 Dip-Coating, Coating Efficiency and Protein Stability

In addition to mechanical piercing of the SC, solid MN also enable the deposition of coated drugs in the skin [5,16]. Here, specific formulations can be necessary to stabilize labile molecules such as proteins or peptides during coating procedure and storage [16,18,29]. Furthermore, the protein structure integrity can be challenged during storage since proteins are very sensitive and susceptible to degradation, unfolding, or aggregation.

Successful MN coating also depends on drug concentration, viscosity and surface activity of the solution [18]. Since the MN surface often is hydrophobic and, hence, difficult to wet, it requires a pre-treatment with surface-active detergents [18]. Here, we immersed the MN arrays in a polysorbate 80 solution. To further enhance the coating yield, hyaluronic acid (1

MDa) was added as a viscosity enhancer. The arrangement of the needles on the MN array inhibited simple dip-coating since the narrow space between the needles caused capillary effects or micro-flows resulting in a non-localized coating of the needles. Therefore, we employed a modified coating technique using a 26Gx ½” syringe (Figure 5-1). By dipping the solution filled syringe onto each single MN tip, a uniform and localized coating was achieved (Figure 5-3), that could be repeated until the desired amount of protein loading was achieved.

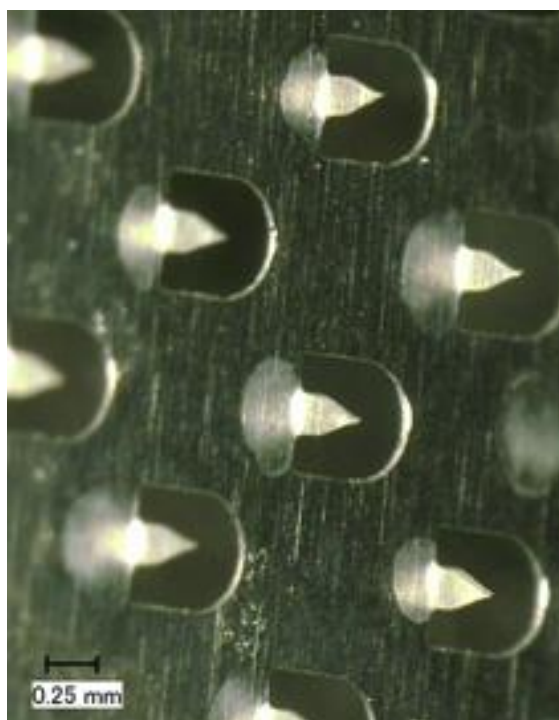


**Figure 5-3** Coated MN tips after 1 dip coating cycle; bar = 0.25 mm

As expected, the amount of protein coated on the MN steadily increased with the number of coatings. One dip-coating procedure resulted in  $11.7 \pm 1.1 \mu\text{g}$  AsnB per MN array, two coatings resulted in  $18 \pm 6.4 \mu\text{g}$  per MN array and three coatings procedure yielded  $22.7 \pm 1.0 \mu\text{g}$  per MN array, respectively (Fig. 5-4).

Protein integrity was maintained during coating: AsnB activity was  $94.6 \pm 2.2\%$  after one coating cycle (Fig. 5-4). After the second and third coating cycle, however, the AsnB activity diminished to  $78.7 \pm 2.0$  and  $80.5 \pm 11.0\%$ , respectively. The maintenance of the AsnB activity after the coating procedure can be explained by the addition of the excipients. To successfully stabilize a protein that is embedded in a dry product, the product matrix needs to be amorphous or semi-amorphous, since a crystalline matrix state is known to de-stabilize proteins [21]. In this context, sucrose is a commonly used excipient [9,18]. Since the residual moisture also affects the product stability during storage, phenylalanine was added. Phenylalanine is a poorly water soluble amino acid that proved to be effective in reducing

the residual moisture content of air-dried protein-containing matrices by crystallizing and allowing the water to be removed from the amorphous mass [32].

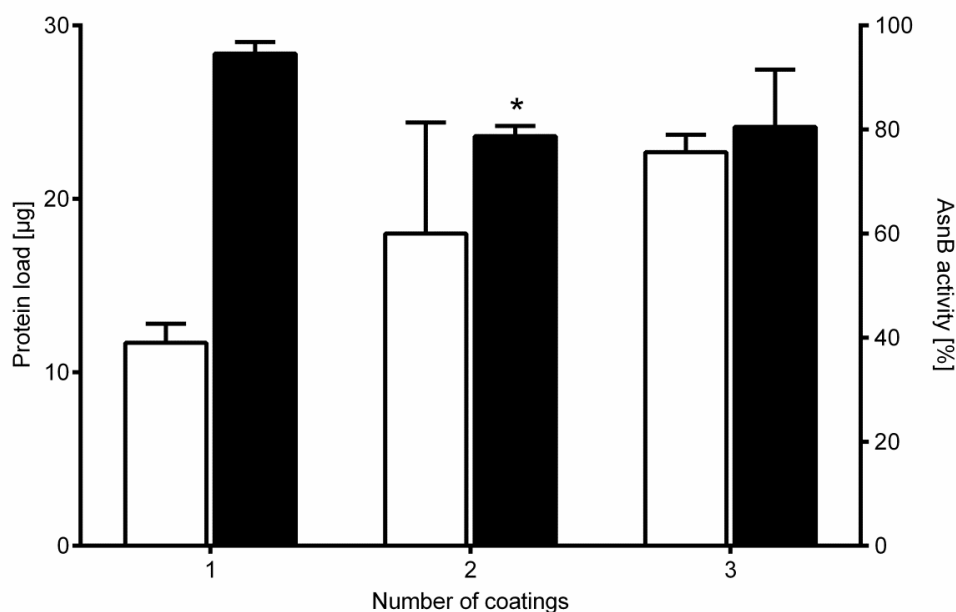


**Figure 5-4** Amount of AsnB on the MN array determined by BCA assay (white bars) and AsnB activity after 1 - 3 coating procedures determined by AsnB activity assay (black bars); mean  $\pm$  SD. \*  $p \leq 0.05$

### 3.3 Storage Stability of Protein-Coated MN Arrays

Coated MN arrays intended for pharmaceutical applications require sufficient storage stability. To assess the storage stability of the coating formulation, AsnB was chosen as model protein. In the case of physical stress, the tertiary structure of the AsnB can be compromised by either clustering of several AsnB tetramers (the biologically active form) to bigger aggregates or by separation of the tetramer into its homo-dimers, monomers or even smaller fragments. In both cases, the secondary products are biologically inactive [33]. Hence, we monitored AsnB activity and integrity over 3 months at 2-8°C, 25°C and 40°C, respectively.

The AsnB tetramer amount of a freshly prepared solution was  $88.6 \pm 6.4\%$  and did not change during 1 day storage at 25°C (Fig. 5-5A). After one week, the tetramer amount was reduced to  $80.3 \pm 6.2\%$  (4°C),  $73.2 \pm 6.2\%$  (25°C) and  $76.1 \pm 4.5\%$  (40°C), respectively. Interestingly, no further reduction of the tetramer content was observed after 1 and 3 months storage (Fig. 5-5A). Independent of the storage conditions, the tetramer amount remained stable at approximately 75% (1 month:  $74.8 \pm 2.8\%$  (4°C),  $74.9 \pm 7.4\%$  (25°C) and  $76.3 \pm 5.7\%$  (40°C); 3 month:  $78.0 \pm 7.6\%$  (4°C),  $69.6 \pm 5.3\%$  (25°C) and  $71.5 \pm 1.0\%$  (40°C)).

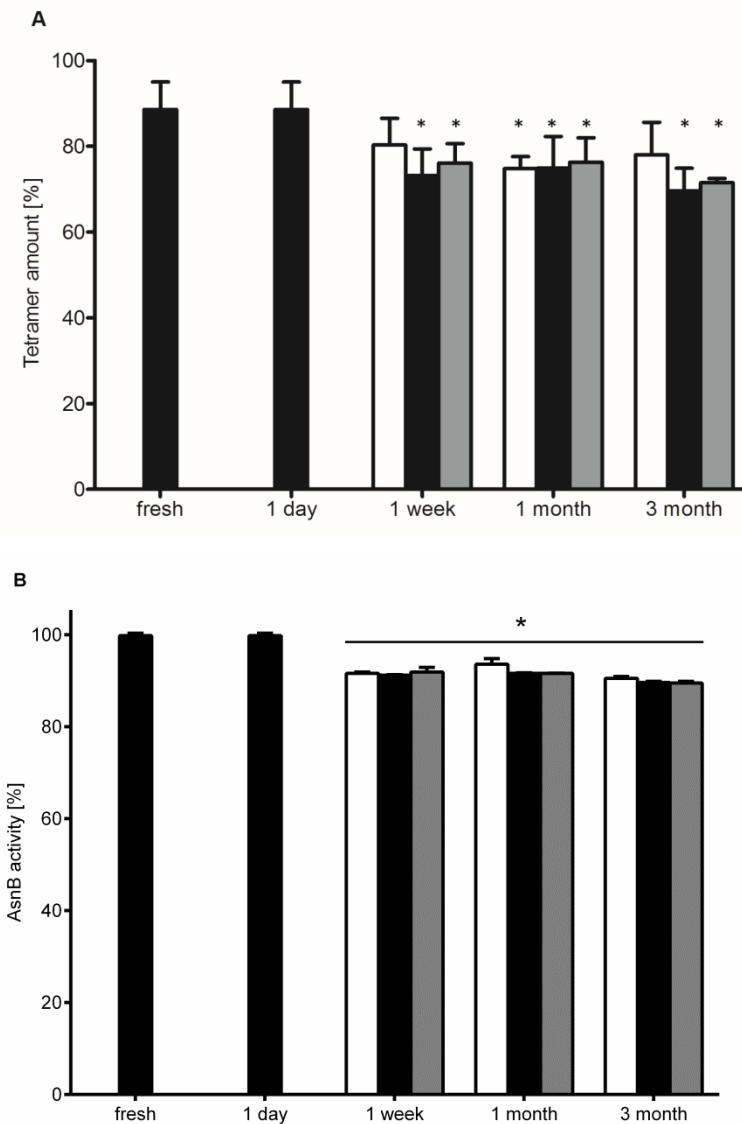


**Figure 5-5:** Storage stability of AsnB coated MN arrays determined as AsnB tetramer amount (A) and AsnB activity (B). The MN arrays were stored for 1 day, 1 week, 1 month or 3 months at 4°C (white bars), 25°C (black bars) and 40°C (grey bars), respectively. Mean values  $\pm$  SD. \*  $p \leq 0.05$

A similar trend was observed for AsnB activity which was well in line with the loss of AsnB tetramers. For all three storage conditions, no significant differences in AsnB activity were observed. After one day, the AsnB bioactivity dropped from  $99.8 \pm 0.5\%$  (fresh formulation) to  $94.6 \pm 2.2\%$  (MN coating). After 1 week, the activity reduced to  $91.6 \pm 0.3\%$  (4 °C),  $91.2 \pm 0.1\%$  (25°C) and  $91.9 \pm 1.0\%$  (40°C), respectively. Likewise the tetramer amount, the activity did not further decrease over storage time: 1 month:  $93.6 \pm 1.2\%$  (4°C),  $91.6 \pm 0.1\%$  (25°C) and  $91.6 \pm 0.0\%$  (40°C) and 3 months:  $90.5 \pm 0.4\%$  (4°C),  $89.6 \pm 0.3\%$  (25°C) and  $89.5 \pm 0.3\%$  (40°C) (Fig. 5-5B).

Our data demonstrate that the development of coating formulations, which are able to stabilize labile compounds, is generally feasible. We stabilized the model protein AsnB and maintained its structural integrity and biological activity for up to 3 months. Similar findings

were described by Ameri et al. who described the successful stabilization of human growth hormone (22 kDa) coated onto solid MN using 20% w/w sucrose and 0.2% polysorbate 20. After 6 months, SEC analysis revealed the maintenance of the monomer (approximately 96%) during storage at 40°C / 75% humidity [9]. We were able to achieve similar results even with the larger biomacromolecule AsnB (138 kDa). Another example is the study of Choi et al. observing a significantly higher residual hemagglutinin activity of 40 – 50% in trehalose-containing formulations compared to simple phosphate buffer (residual activity: 12.5%). Here, the addition of the viscosity enhancer carboxymethyl cellulose exhibited further stabilizing effects [21]. Hence, an increased viscosity seems to be beneficial for stabilization.

### 3.4 Application of Protein Coated MN into Pig Skin and Reconstructed Skin Models

To proof the applicability of the coated MN in terms of coating dissolution and protein disposition in epidermal skin layers, insertion experiments in pig skin were performed. Following the manual insertion of the coated MN, the MN coating dissolved within few minutes in the epidermal skin layers and the protein diffused homogeneously in the tissue around the insertion channel (Fig. 5-6). Only minor amounts of the fluorescently-labeled protein remained on the SC surface indicating that the coating was stable enough to withstand the insertion process. After MN withdrawal, only minor amounts of the coating remained on the MN base, whereas all the coating dissolved from the needle tip since no residual fluorescence was detectable.

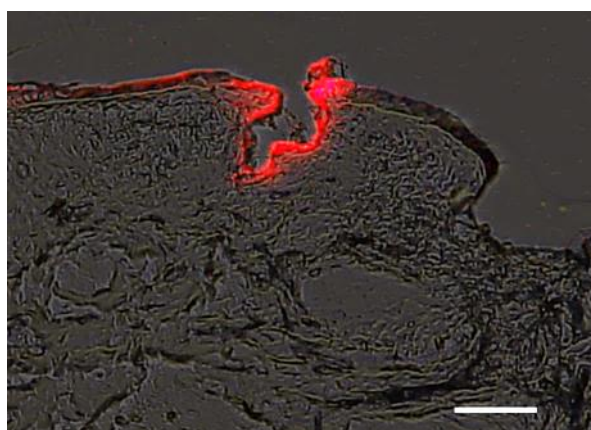


**Figure 5-6:** Fluorescence and light microscopy overlays of the BSA-RhB ITC deposition in pig skin after MN insertion. BSA-RhB ITC (white color) was coated onto the MN with an effective concentration of ~ 10 µg/ MN array. Scale bar = 50 µm

To quantify protein deposition in the skin, MN were also applied into reconstructed human skin. Following one application of a single coated MN array (AsnB concentration ~11.7 µg), we recovered  $8.0 \pm 1.4$  µg ( $68.0 \pm 11.7\%$ ) AsnB intraepidermally (Table 5-3). Repeated application of coated MN did not result in significantly higher AsnB amounts in the skin:

following two insertions of AsnB coated MN, only  $10.3 \pm 3.8 \mu\text{g}$  ( $44.0 \pm 16.1\%$ ) were recovered.

Although MN are designed for a pain-free drug delivery, the mechanical disruption of the skin barrier can cause skin irritation [34]. Here, reconstructed human skin could be a useful tool since skin models are viable and respond to irritating stimuli [26,35]. Thus, to investigate whether MN insertion triggers inflammatory responses after intradermal application, the secreted of the pro-inflammatory cytokines IL-6 and IL-8 were quantified. After one MN insertion, IL-6 levels only marginally increased from  $102.1 \pm 11.8 \text{ ng/ml}$  to  $114.4 \pm 20.7 \text{ ng/ml}$ . A second MN insertion did not result in further IL-6 secretion ( $94.1 \pm 18.2 \text{ ng/mL}$ ) (Fig. 5-7A). For IL-8, significantly higher values were measured (Fig. 5-7B). Again, the second MN insertion did not further stimulate IL-8 release. These data indicate that MN insertion causes a slight skin irritation.

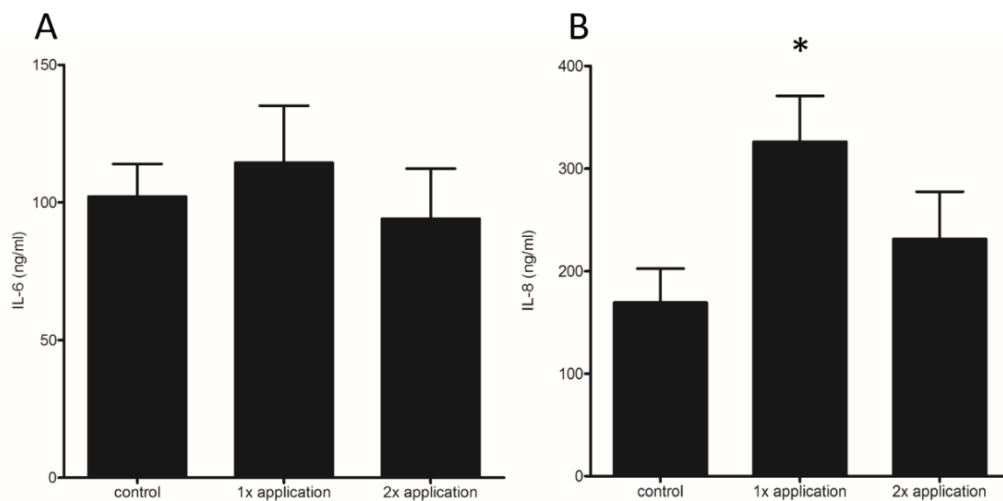


**Figure 5-7:** IL-6 and IL-8 release following the application of AsnB coated MN. Mean values  $\pm$  SEM; \*  $p \leq 0.05$

Currently, little is known about potential side effects of repeated MN insertion especially when aiming for long-term use, which might be necessary for specific applications. Although MN application is considered a non-invasive method, repeated MN microporation may have an influence on the patient's skin barrier. In few studies, the short-term effects of microneedling have been assessed describing local irritation and erythema minutes after the treatment. Nevertheless, a complete recovery of the skin barrier function and vanishing of the erythema after MN removal was observed, too [27,30,34].

## 4. Conclusion

In this feasibility study, we demonstrated that solid MN arrays are an efficient tool for intraepidermal delivery of proteins. By choosing the coating formulation carefully and by

application of a localized and product sparing coating method, reproducible MN tip coatings with protein concentrations between 10 to 23 µg were generated. Moreover, the protein activity was maintained for up to 3 months. Aiming for an intraepidermal delivery of the protein, MN with a needle length of 300 µm proved suitable and yielded an effective delivery of  $68.0 \pm 11.7\%$  of the coated model protein. Following intradermal application, the coating formulation dissolved rapidly resulting in homogeneously distributed protein in the epidermal layers. Only minor skin irritation occurred.

## 5. Acknowledgements

This work was supported by a grant from the German Research Foundation (DFG; KU 2904/2-1 S.H.).

## 6. References

1. Dogra S, Yadav S, Sarangal R. Microneedling for acne scars in Asian skin type: an effective low cost treatment modality. *J. Cosmet. Dermatol.* 13(3), 180–187 (2014).
2. Liebl H, Kloth LC. Skin Cell Proliferation Stimulated by Microneedles. *J. Am. Coll. Clin. Wound Spec.* 4(1), 2–6 (2012).
3. Schwarz M, Laaff H. A Prospective Controlled Assessment of Microneedling with the Dermaroller Device. *Plast. Reconstr. Surg.* 127(6) (2011).
4. Bariya SH, Gohel MC, Mehta TA, Sharma OP. Microneedles: an emerging transdermal drug delivery system. *J. Pharm. Pharmacol.* 64(1), 11–29 (2012).
5. Indermun S, Luttge R, Choonara YE, et al. Current advances in the fabrication of microneedles for transdermal delivery. *J. Control. Release.* 185, 130–138 (2014).
6. Cheung K, Han T, Das DB. Effect of Force of Microneedle Insertion on the Permeability of Insulin in Skin. *J. Diabetes Sci. Technol.* 8, 444–452 (2014).
7. Martanto W, Davis SP, Holiday NR, Wang J, Gill HS, Prausnitz MR. Transdermal delivery of insulin using microneedles in vivo. *Pharm. Res.* 21, 947–952 (2004).
8. Cormier M, Johnson B, Ameri M, et al. Transdermal delivery of desmopressin using a coated microneedle array patch system. *J. Control. Release.* 97, 503–511 (2004).
9. Ameri M, Kadkhodayan M, Nguyen J, et al. Human growth hormone delivery with a microneedle transdermal system: Preclinical formulation, stability, delivery and PK of therapeutically relevant doses. *Pharmaceutics.* 6, 220–234 (2014).
10. Edens C, Collins ML, Ayers J, Rota PA, Prausnitz MR. Measles vaccination using a microneedle patch. *Vaccine.* 31, 3403–3409 (2013).
11. Quan FS, Kim YC, Song JM, et al. Long-term protective immunity from an influenza virus-like particle vaccine administered with a microneedle patch. *Clin. Vaccine Immunol.* 20, 1433–1439 (2013).
12. Kang S-M, Song J-M, Kim Y-C. Microneedle and mucosal delivery of influenza vaccines. *Expert Rev. Vaccines.* 11, 547–560 (2012).
13. Prausnitz M, Mikszta J, Cormier M, Andrianov A. Microneedle-Based Vaccines. In: *Vaccines for Pandemic Influenza SE - 18.* Compans RW, Orenstein WA (Eds.). Springer Berlin Heidelberg, 369–393 (2009).
14. Van Damme P, Oosterhuis-Kafeja F, Van der Wielen M, Almagor Y, Sharon O, Levin Y. Safety and efficacy of a novel microneedle device for dose sparing intradermal influenza vaccination in healthy adults. *Vaccine.* 27(3), 454–459 (2009).
15. Mohammed YH, Yamada M, Lin LL, et al. Microneedle enhanced delivery of cosmeceutically relevant peptides in human skin. *PLoS One.* 9(7), 1–9 (2014).
16. Kim YC, Park JH, Prausnitz MR. Microneedles for drug and vaccine delivery. *Adv. Drug Deliv. Rev.* 64, 1547–1568 (2012).
17. Vrdoljak A, McGrath MG, Carey JB, et al. Coated microneedle arrays for transcutaneous delivery of live virus vaccines. *J. Control. Release.* 159(1), 34–42 (2012).

18. Gill HS, Prausnitz MR. Coating formulations for microneedles. *Pharm. Res.* 24(7), 1369–1380 (2007).
19. Peters EE, Ameri M, Wang X, Maa YF, Daddona PE. Erythropoietin-coated ZP-microneedle transdermal system: Preclinical formulation, stability, and delivery. *Pharm. Res.* 29, 1618–1626 (2012).
20. Kim Y-C, Quan F-S, Compans RW, Kang S-M, Prausnitz MR. Formulation and coating of microneedles with inactivated influenza virus to improve vaccine stability and immunogenicity. *J. Control. Release.* 142(2), 187–195 (2010).
21. Choi H-JJ, Bondy BJ, Yoo D-GG, Compans RW, Kang S-MM, Prausnitz MR. Stability of whole inactivated influenza virus vaccine during coating onto metal microneedles. *J. Control. Release.* 166(2), 159–171 (2013).
22. Quan F-S, Kim Y-C, Yoo D-G, Compans RW, Prausnitz MR, Kang S-M. Stabilization of Influenza Vaccine Enhances Protection by Microneedle Delivery in the Mouse Skin. *PLoS One.* 4(9), e7152 (2009).
23. KÜchler S, Strüver K, Friess W. Reconstructed skin models as emerging tools for drug absorption studies. *Expert Opin. Drug Metab. Toxicol.* 9(10), 1255–1263 (2013).
24. Davis SP, Landis BJ, Adams ZH, Allen MG, Prausnitz MR. Insertion of microneedles into skin: measurement and prediction of insertion force and needle fracture force. *J. Biomech.* 37(8), 1155–1163 (2015).
25. Mashburn LT, Wriston JC. Tumor inhibitory effect of L-asparaginase from *Escherichia Coli*. *Arch. Biochem. Biophys.* 105, 450–452 (1964).
26. KÜchler S, Henkes D, Eckl KM, et al. Hallmarks of atopic skin mimicked in vitro by means of a skin disease model based on FLG knock-down. *ATLA Altern. to Lab. Anim.* 39, 471–480 (2011).
27. Donnelly RF, Singh, Thakur Raghu Raj Morrow DIJ, Woolfson AD. *Microneedle-Mediated Transdermal and Intradermal Drug Delivery.* Wiley-Blackwell.
28. van der Maaden K, Varypataki EM, Yu H, Romeijn S, Jiskoot W, Bouwstra J. Parameter optimization toward optimal microneedle-based dermal vaccination. *Eur. J. Pharm. Sci.* 64, 18–25 (2014).
29. Van Der Maaden K, Jiskoot W, Bouwstra J. Microneedle technologies for (trans)dermal drug and vaccine delivery. *J. Control. Release.* 161(2), 645–655 (2012).
30. Wermeling DP, Banks SL, Hudson D a, et al. Microneedles permit transdermal delivery of a skin-impermeant medication to humans. *Proc. Natl. Acad. Sci. U. S. A.* 105(6), 2058–2063 (2008).
31. Kalluri H, Kolli CS, Banga AK. Characterization of microchannels created by metal microneedles: formation and closure. *AAPS J.* 13(3), 473–481 (2011).
32. Stabenau A, Winter G. Application and Drying of Protein Drug Microdroplets on Solid Surfaces. *Pharm. Dev. Technol.* 12(1), 61–70 (2007).
33. Jameel F, Bogner R, Mauri F, Kalonia D. Investigation of physicochemical changes to L-asparaginase during freeze-thaw cycling. *J. Pharm. Pharmacol.* 49, 472–477 (1997).
34. Bal SM, Caussin J, Pavel S, Bouwstra JA. In vivo assessment of safety of microneedle arrays in human skin. *Eur. J. Pharm. Sci.* 35(3), 193–202 (2008).
35. Danso MO, van Drongelen V, Mulder A, et al. TNF- $\alpha$  and Th2 Cytokines Induce Atopic Dermatitis-Like Features on Epidermal Differentiation Proteins and Stratum Corneum Lipids in Human Skin Equivalents. *J. Invest. Dermatol.* 134, 1941–50 (2014).

# Chapter 6

## Final Conclusion

### 1. Dendritic PG-based nanogels with trigger-mediated protein release

Concerning the dPG-based nanogels, the objective of the thesis was the implementation and modification of the nanogels to suit the requirements for topical and dermal drug delivery of sensitive biomacromolecules such as proteins, peptides and enzymes. Therefore, two different kinds of drug release modified dPG-based nanogels were characterized and investigated. In the end, their suitability as possible drug delivery vehicle for localized intra-epidermal protein substitution of a therapeutic relevant protein (TGase 1) was to be evaluated.

#### 1.1 Acid-cleavable dPG-based nanogels for targeted protein delivery

The focus was firstly set on the development of a protein-gentle technique for the manufacturing of acid-cleavable PG-based nanogels, which was done by the project partners from the FU Berlin (Dirk Steinhilber, Prof.Dr. Rainer Haag), and secondly the characterization of encapsulated and released asparaginase in terms of stability and bioactivity, which was part of the PhD thesis. As a surfactant free method, nanoprecipitation was for the first time applied to form hydrophilic dPG-based nanogel particles. The hydrated polyglycerol network creates a hydrophilic environment which is thought to stabilize labile enzymes and proteins [1–3]. With the developed preparation method, size-tunable (100 – 1000 nm) nanogels with high yields were obtained. The nanogels were freely dispersible in aqueous solution without signs of clustering or aggregation. In the past, a major concern for protein integrity during encapsulation was the harsh organic environment as organic solvents like acetone are inevitable to dissolve the polymers. In this study, inverse nanoprecipitation polymerization was applied to avoid damage of the labile asparaginase during encapsulation. Thus, we were able to obtain enzyme loaded dPG nanogels with an encapsulation yield of almost 100 %. By introducing a pH sensitive benzacetal group into the dPG nanogel network, the nanogels responded with rapid degradation to a low pH environment. This feature makes these nanogels highly interesting as delivery vehicles for the application in tissues, where a medical condition induces an acidic environment, such as inflammation and tumor tissues (pH ~ 6.0 - 6.5), or physiological compartments where a low pH is present, like intracellular endosomes (pH ~5), lysosomes (pH ~4) and the SC/ skin barrier (pH ~5 - 5.5).

Upon the pH trigger, we confirmed immediate release of the protein payload. At pH 4 and 5, drug release coincided with nanogel degradation. No significant changes in protein secondary structure and activity were observed upon encapsulation and release at pH 5.

## **1.2 Thermoresponsive dPG-based nanogels for targeted protein delivery**

In a second approach, dPG based nanogels with a different trigger mechanism were investigated. Working with thermoresponsive PNIPAM-dPG nanogels, we succeeded in incorporating bovine serum albumin and asparaginase. Loading efficiencies between 30 % and 70 % were achieved, depending on the molecular weight size of the used proteins. Unloaded nanogels underwent a decrease in size at the thermal trigger point of 33 °C, which is at a slightly higher temperature than for pure PNIPAM due to the hydrophilic input by the dPG moieties [4–6]. The shrinkage of protein loaded nanogels was less pronounced with protein load which presumably counteracts the shrinkage. In addition, the transition temperature was increased to ~35 °C as the protein further increased the hydrophilicity. As a temperature of ~ 33 to 35 °C is expected in the upper skin layers, the nanogels should thus selectively release their payload after skin application in the lower SC / upper epidermis, but stay stable at room temperature.

The proteins maintained their biological activity and structure during nanogel manufacturing as well during freeze-thaw and storage stress of the loaded nanogels, which highlights the excellent stabilizing properties of the nanogel for sensitive proteins. The dermal protein delivery efficiency was analyzed in ex-vivo pig skin and in viable reconstructed human skin. The latter offered the opportunity to analyze the drug release and delivery in TGase-1-deficient skin models that were obtained by gene knock-down in keratinocytes [7–9]. Our study showed that the two selected model proteins as well as the therapeutically interesting candidate TGase-1 were significantly enhanced in their skin deposition using the nanogels. Reviewing our data and considering that the nanogels themselves did not travel beyond the SC, we were not able to elucidate the mode of action of protein skin penetration. As our nanogels had a neutral surface charge, improved skin adhesion as a result of surface charges is unlikely [10]. In all probability, the investigated nanogels improve the skin penetration by interacting through their amphiphilic polymer groups with lipophilic SC parts [11,12]. Furthermore, the nanogels may act as penetration enhancers in terms of modulating and untightening the stiff SC protein and lipid organization [13].

Replacement therapy of underdeveloped or missing proteins and enzymes in the skin has emerged as a promising tool for treatment of some skin diseases like congenital ichthyoses, where the overall therapy options are rather poor [14]. Aiming for a restored TGase1 activity and a remodeling in the skin structure, especially focusing on the SC, we applied TGase1-loaded PNIPAM-dPG nanogels on TGase-1-deficient skin models. The protein was efficiently

delivered locally into the epidermis. Additionally, the skin barrier function was restored as assessed by a skin permeability test. To conclude, we could demonstrate that the preparation of thermoresponsive PNIPAM-dPG nanogels is a suitable tool to incorporate and to deliver labile biomacromolecules locally into the viable epidermis. As the protein's biological activity was maintained and the delivery of the therapeutic relevant TGase1 verified the feasibility of a protein substitution approach in TGase1-deficient skin conditions, these nanogels have great potential as dermal drug delivery vehicles.

## **2. HA hydrogels as dermal drug delivery vehicles for proteins**

Ever since the versatile polysaccharide HA has been used in the cosmetics sector for skin hydration and rejuvenation, it also become important in the treatment of skin diseases like actinic keratosis and related secondary symptoms such as skin dryness or irritation and inflammation [15–18]. As HA can enhance the dermal uptake of diclofenac in actinic keratosis treatment, a potential beneficial effect of HA for dermal delivery of biomacromolecules was a further objective [15–18]. We explored the delivery capacity to intact and barrier-deficient skin for BSA using HA of different size and at different concentration. Besides the delivery yield of both HA and BSA, the focus was set on unraveling the mode of action of HA-facilitated delivery, as up to now no clear and satisfactory explanation can be found in literature.

Low molecular weight HA (5kDa) penetrated into deeper dermal layers of intact skin as compared to high molecular HA species, a finding that is supported by lately published data [15,19,20]. In contrast, barrier impairment by tape-stripping facilitated the absorption of the 100 kDa HA to a greater extend. Without HA, BSA only accumulated in minor fractions in intact skin when it was applied and incubated over a longer time range on well-hydrated skin samples, whereas tape-stripping enabled an easy protein penetration regardless of the hydration state. Combining HA and BSA, the penetration of the protein into the viable epidermis of intact skin could only be provided by the 5kDa HA. FRET-FLIM analysis revealed that the HA and BSA molecules had a close proximity, which hints to interactions between both molecules at physiological conditions despite their mostly negative surface charges [21–23]. As a result, a HA-mediated co-transport of the scarcely penetrating BSA is highly likely in intact skin. To our surprise, HA-BSA hydrogels tended more to a penetration confinement effect in barrier impaired skin localizing the BSA mainly into the viable epidermis. Here, no interaction between HA and BSA was observed by FRET-FLIM. Given that HA shows good penetration yields and other publications observed similar retention effects and hypothesized underlying hydration-related contributions [15,17], it is possible that skin hydration may be the driving factor.

Concluding, FRET-FLIM results suggest an HA accompanied co-transport of the model protein into intact skin and revealed the easy accessibility of barrier disrupted skin for both HA and protein. Nevertheless, we saw that further driving forces contribute to skin penetration. Diverse previous studies demonstrated enhanced delivery of actives in the presence of HA, the delivery of HA-active conjugates or even the penetration of HA itself based on concepts like penetration enhancer properties or co-transportation, yet a distinct mode-of-action therefor could not be identified [19,20,24,25]. Hence, we included a closer look on the HA-skin interactions using isolated SC sheets and FTIR analysis.

As most proteins are hydrophilic and encounter penetration problems in intact skin due to the high extend of lipophilic moieties, increasing the water content in the SC might serve as an option for improved penetration results. After application, HA hydrogels create an occlusive film on the skin surface, which contributes to an increase in skin hydration. Depending on the HA molecular size and concentration, the hydration capacity of the SC sheet competed with the HA gel equilibration, as was seen by a decrease in skin hydration with HA concentrations exceeding 5%. Hydration of the SC was pronounced for gels with low molecular weight HA (5 kDa). With these formulations we observed the anticipated enhanced BSA penetration into intact skin. Skin hydration is accompanied by structural changes in the skin's keratins [26]. This could be demonstrated for SC sheets, especially when incubated with low molecular weight HA and at higher HA concentrations (5-10 %). Those also showed the best skin penetration properties. This change in keratin structure may contribute to a weakened skin barrier and as a result may facilitate a better skin penetration. Another way to impair the barrier and enhance penetration is the alteration of the skin lipid organization. Regardless of being intact or tape-stripped, we observed significantly less lipid rigidity after application of 100 kDa HA at higher concentrations.

Thus, HA, especially the low to medium molecular weight forms formulated at more than 5 % has a beneficial effect on the skin partitioning of topically applied proteins in both intact and barrier deficient skin. Although the exact mechanism could not be clarified, the data obtained with FRET-FLIM and FT-IR strongly suggest the theory of a HA-mediated co-transport of the protein. In addition, the protein penetration is further facilitated by more hydrophilic environment due to SC hydration and by an interference with the skin lipid organization and keratin structure. The observed penetration confinement in barrier impaired skin, however, could not be explained.

### **3. Solid MN arrays for the intra-epidermal delivery of proteins**

Over the last decades, solid stainless steel MN arrays became interesting devices for topical delivery systems for vaccines, pain medication and hormones. We aimed for a feasibility test

of the use of solid MN arrays for dermal protein delivery. As literature scarcely describes coating formulation development with regard to process and storage stability we had a closer look at this aspect. Not only should MNs be of a robust, inert and sharp construction to smoothly insert into skin, but they also need to come with an easy handling and minimal pain. Comparing needles of 300  $\mu\text{m}$  and 800  $\mu\text{m}$  length, MN arrays with 300  $\mu\text{m}$  needles were most suitable to locally target the epidermis resulting in punctures of 80 to 90  $\mu\text{m}$  depth (epidermis thickness 130 - 180  $\mu\text{m}$ ) [27,28]. The manual insertion with reasonable force resulted in reproducible channel depth and count which is prerequisite for a reproducible drug delivery.

A biocompatible coating which stabilizes the protein drug is inevitable for a successful drug delivery as proteins are generally very sensitive towards external stress factors like heat, moisture or oxygen leading to unfolding, aggregation and degradations. Hence, the stabilizer sucrose was added that provides an amorphous matrix for the proteins [29–31]. By adding phenylalanine, the residual moisture content in the final dry coatings can be kept low which is beneficial for protein stability [30]. Polysorbate 80 was added to prevent the protein drug from surface induced aggregation and to reduce the surface tension for improved wetting of the MN during the coating process [32]. In addition, 1 MDa HA served as viscosity enhancer to increase the coating efficiency on the MN tips. With an in-house developed manual coating technique, we were able to yield ~ 12  $\mu\text{g}$  for single coated arrays, ~18  $\mu\text{g}$  for twice and ~ 23 $\mu\text{g}$  for three-times coated MN arrays without loss of protein bioactivity. Despite the protein stabilizing excipients in the coating formulation, the coated MNs are presumably still susceptible to environmental stress factors like humidity and oxygen. As the coating needs to ensure the maintenance of the protein activity over a longer storage time, a 3 month stability study at 2-8°C, 25°C and 40°C was executed and the biological activity of asparaginase as well as the tetramer amount, the biologically active species, was monitored. The tetramer content stayed stable at ~ 75 % for all storage conditions (naive state: 89 % tetramer content). Likewise, the biological activity remained high during the 3 month of storage independent of the storage temperature with an overall activity of ~92 % (naive state: 99.8 % activity). Hence, it is possible to prepare a MN array with coating which provides adequate protein dosing and stability for medical treatment.

The coated MN arrays were furthermore manually assessed for application to pig and reconstructed skin. Shortly after the insertion, the coatings evenly dissolved and distributed the model proteins in the tissue around the insertion sites in both skin models. Only minor residues were left on the MN arrays, mainly on areas where the coating was not precisely placed on the needles themselves but spread to the MN base as well. This phenomenon might be prevented by coating the MN with an automated process which was beyond the scope of the thesis. Protein quantification in reconstructed skin yielded delivery  $68.0 \pm 11.7\%$

( $8.0 \pm 1.4 \mu\text{g} / 4.7 \mu\text{g per cm}^2$ ) of the loaded model protein asparaginase for single coated MN arrays which is similar to other published data [33–35].

In contrast to vaccination, where immunization can be obtained after one MN application, the use of MN in skin disease treatment will most likely comprise repeated applications to the same skin area. Consequently, irritation effects, as described in literature [36–38], due to application of our MN arrays were examined in this study via the secretion of the pro-inflammatory cytokines IL-6 and IL-8 from the viable epidermis into the culture medium. The data indicated that a first MN application led to slight skin irritation, but a second insertion did not result in a further increase of the IL levels. Thus, close follow-ups by trained physicians and disinfection may be crucial to avoid infections and the development of scarified skin tissue in a possible treatment of skin diseases with MN arrays [39].

## 4. Prospects

Although the dPG-based nanogels turned out to be promising vehicles for dermal drug delivery of labile biomacromolecules, especially in barrier impaired skin, further studies are necessary. Starting with the acid-cleavable nanogels, we succeeded in generating nanogels that offer a quick protein release at a physiologically useful pH. Bioactivity and structural integrity of the protein payload were maintained. Skin penetration experiments need to follow, as these nanogels are not yet characterized for in-vitro or ex-vivo skin delivery. Adequate skin models need to be chosen, as for example ex vivo pig skin may no longer exhibit the physiologically occurring skin pH of 5.5 due to cleaning or freezing steps. The use of reconstructed skin may be preferred. Overall, future work needs to focus on the long-term stability of the nanogels. It is necessary to evaluate the benefits of adding stabilizers to facilitate longer shelf-lives. In aqueous solution, the probability of deterioration and nanogel clustering is high. Therefore, freeze-drying could be a valuable option. To unravel the mode of action of the dPG nanogels, FRET-FLIM as well as FT-IR measurements could be valuable tools.

Although HA hydrogels successfully delivered loaded model proteins into barrier-disrupted skin, further studies need to be performed to close the gap in understanding the mode of action of HA in the SC and the upper skin, focusing especially on the penetration retardation in barrier-impaired skin. As an addition, mixtures of 5kDa and 100 kDa could be investigated to combine all skin barrier altering effects for a potential increase in delivery efficiency. Finally, the effectiveness of HA hydrogels as dermal protein delivery vehicles in skin disease adapted skin models with therapeutically relevant proteins should be tested.

MN arrays are very versatile devices for localized and systemically delivery of low and high molecular weight drugs. The coating formulations developed in this thesis provided promising

storage stability and quick release of the loaded proteins after insertion in the skin. However, the coating technique and the resulting applied protein concentration should be further improved to yield even and more reproducible delivery of higher protein payloads. Subsequently, as proof of concept these proteins coated MN arrays need to be applied to diseased skin models to study whether the skin barrier at the insertion site or in the whole model is restored. When the distribution of the dissolved coating and thus the proteins is insufficient, a switch to dermal rollers for narrow and repeated skin piercing might be an option.

## 5. References

1. Siegers C, Biesalski M, Haag R. Self-assembled monolayers of dendritic polyglycerol derivatives on gold that resist the adsorption of proteins. *Chem. - A Eur. J.* 10(11), 2831–2838 (2004).
2. Weinhart M, Grunwald I, Wyszogrodzka M, Gaetjen L, Hartwig A, Haag R. Linear poly(methyl glycerol) and linear polyglycerol as potent protein and cell resistant alternatives to poly(ethylene glycol). *Chem. - An Asian J.* 5(9), 1992–2000 (2010).
3. Ekinci D, Sisson AL, Lendlein A. Polyglycerol-based polymer network films for potential biomedical applications. *J. Mater. Chem.* 22(39), 21100 (2012).
4. Cuggino JC, Alvarez I. CI, Strumia MC, et al. Thermosensitive nanogels based on dendritic polyglycerol and N-isopropylacrylamide for biomedical applications. *Soft Matter.* 7(23), 11259 (2011).
5. Bhuchar N, Sunasee R, Ishihara K, Thundat T, Narain R. Degradable thermoresponsive nanogels for protein encapsulation and controlled release. *Bioconjug. Chem.* 23, 75–83 (2012).
6. Pelton R. Poly(N-isopropylacrylamide) (PNIPAM) is never hydrophobic. *J. Colloid Interface Sci.* 348(2), 673–674 (2010).
7. K uchler S, Henkes D, Eckl KM, et al. Hallmarks of atopic skin mimicked in vitro by means of a skin disease model based on FLG knock-down. *ATLA Altern. to Lab. Anim.* 39, 471–480 (2011).
8. Mildner M, Jin J, Eckhart L, et al. Knockdown of filaggrin impairs diffusion barrier function and increases UV sensitivity in a human skin model. *J. Invest. Dermatol.* 130(9), 2286–2294 (2010).
9. Oji V, Eckl KM, Aufenvenne K, et al. Loss of corneodesmosin leads to severe skin barrier defect, pruritus, and atopy: Unraveling the peeling skin disease. *Am. J. Hum. Genet.* 87(2), 274–281 (2010).
10. Abdel-Mottaleb MMA, Moulari B, Beduneau A, Pellequer Y, Lamprecht A. Surface-charge-dependent nanoparticles accumulation in inflamed skin. *J. Pharm. Sci.* 101(11), 4231–4239 (2012).
11. K uchler S, Radowski MR, Blaschke T, et al. Nanoparticles for skin penetration enhancement - A comparison of a dendritic core-multishell-nanotransporter and solid lipid nanoparticles. *Eur. J. Pharm. Biopharm.* 71(2), 243–250 (2009).
12. Alnasif N, Zoschke C, Fleige E, et al. Penetration of normal, damaged and diseased skin - An in vitro study on dendritic core-multishell nanotransporters. *J. Control. Release.* 185(1), 45–50 (2014).
13. Venuganti VVK, Perumal OP. Poly(amidoamine) dendrimers as skin penetration enhancers: Influence of charge, generation, and concentration. *J. Pharm. Sci.* 98(7), 2345–2356 (2009).
14. Hern andez-Mart ın A, Gonz alez-Sarmiento R. Recent advances in congenital ichthyoses. *Curr. Opin. Pediatr.* 26(4), 473–479 (2015).
15. Brown MB, Jones SA. Hyaluronic acid: A unique topical vehicle for the localized delivery of drugs to the skin. *J. Eur. Acad. Dermatology Venereol.* 19(3), 308–318 (2005).
16. Pirard D, Vereecken P, M elot C, Heenen M. Three percent diclofenac in 2.5% hyaluronan gel in the treatment of actinic keratoses: A meta-analysis of the recent studies. *Arch. Dermatol. Res.* 297, 185–189 (2005).

17. Brown MB, Marriott C, Martin GP. The effect of hyaluronan on the *in vitro* deposition of diclofenac within the skin. *Int. J. Tissue React.* 17(4), 133–140 (1995).
18. Mohammed YH, Yamada M, Lin LL, et al. Microneedle enhanced delivery of cosmeceutically relevant peptides in human skin. *PLoS One.* 9(7), 1–9 (2014).
19. Yang J-A, Kim E-S, Kwon JH, et al. Transdermal delivery of hyaluronic acid – Human growth hormone conjugate. *Biomaterials.* 33(25), 5947–5954 (2012).
20. Farwick M, Lersch P, Strutz G. Low Molecular Weight Hyaluronic Acid: Its Effects on Epidermal Gene Low Molecular Weight Hyaluronic Acid: (2008).
21. Lenormand H, Deschrevel B, Tranchepain F, Vincent JC. Electrostatic interactions between hyaluronan and proteins at pH 4: How do they modulate hyaluronidase activity. *Biopolymers.* 89(12), 1088–1103 (2008).
22. Cooper CL, Goulding A, Kayitmazer AB, et al. Effects of polyelectrolyte chain stiffness, charge mobility, and charge sequences on binding to proteins and micelles. *Biomacromolecules.* 7(4), 1025–1035 (2006).
23. Brewer SH, Glomm WR, Johnson MC, Knag MK, Franzen S. Probing BSA binding to citrate-coated gold nanoparticles and surfaces. *Langmuir.* 21(20), 9303–9307 (2005).
24. Brown TJ, Alcorn D, Fraser JRE. Absorption of hyaluronan applied to the surface of intact skin. *J. Invest. Dermatol.* 113(5), 740–746 (1999).
25. Birkenfeld B, Parafiniuk M, Bielecka-Grzela S, et al. The penetration of topically applied ointment containing hyaluronic acid in rabbit tissues. *Pol. J. Vet. Sci.* 14(4), 621–627 (2012).
26. Kaushik D, Michniak-Kohn B. Percutaneous penetration modifiers and formulation effects: thermal and spectral analyses. *AAPS PharmSciTech.* 11(3), 1068–1083 (2010).
27. van der Maaden K, Varypataki EM, Yu H, Romeijn S, Jiskoot W, Bouwstra J. Parameter optimization toward optimal microneedle-based dermal vaccination. *Eur. J. Pharm. Sci.* (2014).
28. Van Der Maaden K, Jiskoot W, Bouwstra J. Microneedle technologies for (trans)dermal drug and vaccine delivery. *J. Control. Release.* 161(2), 645–655 (2012).
29. Edens C, Collins ML, Ayers J, Rota PA, Prausnitz MR. Measles vaccination using a microneedle patch. *Vaccine.* 31, 3403–3409 (2013).
30. Quan FS, Kim YC, Song JM, et al. Long-term protective immunity from an influenza virus-like particle vaccine administered with a microneedle patch. *Clin. Vaccine Immunol.* 20, 1433–1439 (2013).
31. Kang S-M, Song J-M, Kim Y-C. Microneedle and mucosal delivery of influenza vaccines. *Expert Rev. Vaccines.* 11, 547–560 (2012).
32. Ameri M, Kadkhodayan M, Nguyen J, et al. Human growth hormone delivery with a microneedle transdermal system: Preclinical formulation, stability, delivery and PK of therapeutically relevant doses. *Pharmaceutics.* 6, 220–234 (2014).
33. Gill HS, Prausnitz MR. Coating formulations for microneedles. *Pharm. Res.* 24(7), 1369–1380 (2007).
34. Zhang Y, Brown K, Siebenaler K, Determan A, Dohmeier D, Hansen K. Development of lidocaine-coated microneedle product for rapid, safe, and prolonged local analgesic action. *Pharm. Res.* 29, 170–177 (2012).
35. Kim Y-C, Quan F-S, Compans RW, Kang S-M, Prausnitz MR. Formulation and coating of microneedles with inactivated influenza virus to improve vaccine stability and immunogenicity. *J. Control. Release.* 142(2), 187–195 (2010).
36. Donnelly RF, Singh, Thakur Raghu Raj Morrow DIJ, Woolfson AD. *Microneedle-Mediated Transdermal and Intradermal Drug Delivery.* Wiley-Blackwell.
37. Wermeling DP, Banks SL, Hudson D a, et al. Microneedles permit transdermal delivery of a skin-impermeant medication to humans. *Proc. Natl. Acad. Sci. U. S. A.* 105(6), 2058–2063 (2008).
38. Bal SM, Caussin J, Pavel S, Bouwstra JA. *In vivo* assessment of safety of microneedle arrays in human skin. *Eur. J. Pharm. Sci.* 35(3), 193–202 (2008).
39. Sachdeva V, Banga AK. Microneedles and their applications. *Recent Pat. Drug Deliv. Formul.* 5, 95–132 (2011).

# Chapter 7

## Summary

Local and targeted delivery of labile biomacromolecules, such as proteins, peptides, and enzymes, is of high interest and needs to take the well-known instability and delivery problems of these APIs into account. To offer new options for local and targeted intraepidermal and dermal drug delivery, the goal of the thesis was the development, investigation and characterization of promising delivery devices and vehicles. Efficient protein delivery into the skin may enable a substitution therapy approach of skin diseases like atopic dermatitis which come along with a lack of certain structural proteins.

For the first time, dPG-based nanogels were investigated for their suitability to encapsulate and release proteins. Using two different types of release trigger mechanisms, we succeeded in developing biocompatible dPG nanogels with high protein load. Acidic-cleavable and thermoresponsive nanogels offered mild encapsulation conditions, where proteins were kept intact without activity loss during manufacturing and after the triggered release. Furthermore, the thermoresponsive PNIPAM-dPG nanogels were able to deliver TGase1 locally to the epidermis of TGase-1-deficient skin models. Here, the restoration of a normal skin barrier function was observed, which verifies their feasibility in delivering therapeutically relevant concentrations into diseased skin.

The very versatile polysaccharide HA was investigated for its beneficial effects on the enhanced dermal delivery of low molecular weight drugs in the past. Successful topical delivery of biomacromolecules using HA gels was demonstrated using FRET-FLIM and FT-IR analysis. Substantiating literature findings on HA skin penetration, we observed enhanced BSA delivery to intact skin with 5 kDa HA, presumably as a result of protein-HA co-transport supported by SC hydration as well as keratin and lipid structure interactions. In barrier-disrupted skin, we observed a localized penetration confinement of the protein to the epidermis, which could not be unraveled so far, but demonstrates the supposedly great potential of HA in dermal drug delivery.

Finally, solid stainless steel MN arrays were characterized and analyzed for their feasibility to locally deliver proteins. 300  $\mu\text{m}$  long MN arrays were coated with an optimized aqueous protein formulation and technique to yield up to 68 % of the protein payload ( $8.0 \pm 1.4$  mg per skin model /  $4.7 \pm 0.8$  mg/cm<sup>2</sup>) in the skin tissue after dissolution. The coated protein was stable up to 3 month storage without loss of activity and integrity. Following MN repeated insertions, reconstructed skin showed minor increases in interleukin levels, which indicates a slight but not critical skin irritation.

# Annex

## 1. Biodegradable dendritic polyglycerol nanogels for encapsulation and release of pharmaceutical biomacromolecules

### 1.1 Experimental section – general considerations

All moisture sensitive reactions were carried out in flame-dried glass-ware under a positive argon pressure. Organic solvents were removed using a rotary evaporator and is referred as concentrated in vacuo. <sup>1</sup>H NMR and <sup>13</sup>C NMR spectra were recorded on a Bruker ECX 400 spectrometer (400 and 100 MHz for <sup>1</sup>H and <sup>13</sup>C respectively), at 25 °C using deuterated water, acetone, and chloroform as solvent. UV/Vis spectra were recorded on a Scinco S-3100 UV/Vis spectrometer. Fluorescence spectra were recorded on a Jasco FP-6500 fluorometer. Optical microscopy measurements were performed and micrographs were recorded on a Zeiss Axioskop microscope. Melting points were determined using a Büchi 510 melting point apparatus. Transmission electron microscopy samples were prepared on carbon coated copper grids by blotting samples in 1% aqueous phosphotungstic acid and visualizing them with a Philips CM12 electron microscope.

### 1.2 Materials

Anhydrous solvents were purchased as “extra dry” from either Acros or Aldrich and used as received, or taken from MBraun MB SPS-800 solvent purification system. Trizma hydrochloride (Tris-HCl pH 8.6), trichloroacetic acid and L-asparagine monohydrate CuOAc, trimethylorthoformate, NaHCO<sub>3</sub>, anhydrous N-Methyl-Pyrrolidone (NMP), sodium ascorbate (NaAsc), CuSO<sub>4</sub>, dialysis tubes (2 kDa cut-off), and p-toluenesulfonic acid (PTSA) were purchased from Sigma-Aldrich (Steinheim, Germany). Dry PTSA was obtained by Dean Stark distillation from toluene. The anhydrous PTSA was stored in a NMP stock solution. Aqueous ammonia (25 wt%) was obtained from ROTH. Ammonium sulfate and Nessler's Reagent were purchased from Merck (Darmstadt, Germany). Recombinant L-asparaginase II derived from *E. coli* (95% pure) was a gift from Prof. Dr. Markus Pietzsch, Martin-Luther University Halle-Wittenberg. dPG with a number average molecular weight (M<sub>n</sub>) of 5 kDa and a weight average molecular weight (M<sub>w</sub>) of 7.7 kDa (dPG7.7) was prepared as reported previously [1]. THPTA [2], and dPG7.7 Heptaazide (dPG7.7[N<sub>3</sub>]<sub>7</sub>) [3] and alkyne modified rhodamin B [4] have been prepared according to literature procedures.

## 1.3 Synthetic procedures

### 1.3.1 Preparation of p-propargyloxy-benzaldehyde (pPBA)

In a 100 ml two-necked flask with drop funnel and magnetic stirrer 4-hydroxybenzaldehyde (pHBA) (2.00 g, 16.38 mmol) was dissolved in acetone (50 ml). K<sub>2</sub>CO<sub>3</sub> (15.15 g, 109.62 mmol) was added and the suspension was stirred for 30 min under reflux. After the solution cooled down to RT propargylbromide (2.12 ml, 19.10 mmol) was added over 2.5 h. Then the suspension was heated to reflux for 1.5 h. The suspension was filtrated and the solvent of the filtrate was evaporated in vacuo. DCM (50 ml) was added and the organic phase was washed twice with 1 M NaOH (20 ml) and once with water (20 ml). The organic phase was dried over MgSO<sub>4</sub>. The crude product was recrystallized from toluene three times to obtain a white crystalline solid. (Full conversion, yield: 91 %).

<sup>1</sup>H NMR (400 MHz, CDCl<sub>3</sub>, 25 °C): <sup>1</sup>H NMR (CDCl<sub>3</sub>, 400 MHz): δ (ppm) = 9.90 (s, 1H, aldehyde-H), 7.93-7.68 (m, 2H, aromatic), 7.14-6.91 (m, 2H, aromatic), 4.77 (d, 2H, benzaldehyd-O-CH<sub>2</sub>), 2.57 (t, 1H, CCH). <sup>13</sup>C NMR (125 MHz, CDCl<sub>3</sub>, 25 °C): δ=190.7, 162.2, 131.8, 130.4, 115.0, 77.4, 76.3, 55.8. ppm; IR: 3206, 2749, 2360, 2121, 1677, 1600, 1573, 1505, 1454, 1426, 1395, 1378, 1314, 1300, 1247, 1237, 1213, 1166, 1107, 1006, 968, 860, 808, 792, 762, 658, 651 = cm<sup>-1</sup>; EIMS (40 °C) found for C<sub>16</sub>H<sub>28</sub>O<sub>6</sub> (calcd. 160.05): m/z experimentally found: 160.7. Melting point: 81 °C.

### 1.3.2 Preparation of p-propargyloxy-benzdimethylacetale (pPBDMA)

pPBA (1g, 6.29 mmol) was dissolved in trimethyl orthoformate (10 mL) and dry LiBF<sub>4</sub> (108 mg, 1.16 mmol) was added. The reaction was heated at 65 °C for 1h and quenched by addition of saturated NaHCO<sub>3</sub> solution (25 mL). The mixture was extracted 3 times by ethylacetate (25 mL) and the fractions were combined and dried over Na<sub>2</sub>SO<sub>4</sub>. Ethylacetate was evaporated and pPBDMA was obtained as yellow oil (full conversion, yield 90 %). <sup>1</sup>H NMR (400 MHz, CDCl<sub>3</sub>, 25 °C): δ (ppm) = 7.35-7.33 (m, 2H, aromatic), 6.98-6.95 (m, 2H, aromatic), 5.33 (s, 1H, benzacetal) 4.72-4.71 (d, 2H, benz-O-CH<sub>2</sub>), 3.29 (s, 6H, O-CH<sub>3</sub>), 2.94 (t, 1H, CCH). <sup>13</sup>C NMR (125 MHz, CDCl<sub>3</sub>, 25 °C): δ=159.1, 133.9, 129.7, 116.1, 104.5, 80.7, 78.0, 58.2, 53.6 ppm; IR: 3288, 2936, 2829, 1611, 1588, 1509, 1446, 1351, 1302, 1216, 1171, 1098, 1048, 980, 823 = cm<sup>-1</sup>; EIMS (40 °C) found for C<sub>16</sub>H<sub>28</sub>O<sub>6</sub> (calc 206.1): Experimental value m/z: 206.35.

### 1.3.3 Preparation of fluorescent nanogels

dPG7.7[N3]7 (7mg, 0.79 μmol) and alkyne modified rhodamine B (0.03 mg, 0.06 μmol) was dissolved separately in Milli-Q-water (0.05 mL). THPTA (500 μg, 1.15 μmol), CuSO<sub>4</sub> (72 μg, 0.3 μmol), and NaAsc (228 μg, 1.15 μmol) were added exactly in this sequence to the solution. After 12 h (complete conversion was confirmed by IR) additional Milli-Q-Water was

added (0.45 mL). dPG7.7-10-p-PBDMA (5 mg, 0.6  $\mu\text{mol}$ ) was also dissolved in Milli-Q-Water. The solutions were cooled down to 4  $^{\circ}\text{C}$ , mixed, and added quickly to magnetically stirred acetone (20 mL). Precipitated polyglycerol nanoparticles were obtained as blue shining dispersions and the particle size was determined by DLS (table 1). After 3 h the reaction was quenched by the addition of excess propargylalcohol (50 mg, 893  $\mu\text{mol}$ ). After 12 h Milli-Q-water (20 mL) was added and acetone was evaporated to obtain blue shining nanogel dispersions in water. The nanogels were collected by centrifugation (4000 rpm) and washed 5 times with Milli-Q-water. The nanogels were characterized by DLS (table 1) optical and fluorescence microscopy.

### **1.3.4 GPC characterization of dPG7.7-10- p-PBDMA**

Molecular weight distributions were determined by size exclusion chromatography coupled to a refraction index detector to obtain the complete distribution ( $M_n$ ,  $M_p$ ,  $M_w$ , DI). Measurements were performed under highly diluted conditions (10 mg / mL, injected volume 20  $\mu\text{L}$ ) from a SEC consisting of an Agilent 1100 solvent delivery system with dosing pump, manual injector, and an Agilent 1100 differential refractometer. Three 30 cm columns (PSS SUPREMA, 5  $\mu\text{m}$  particle size) were used to separate polymer samples using water at a flow rate of 1.0 mL/min. The columns were operated at room temperature and the differential refractometer at 50  $^{\circ}\text{C}$ . WinGPC Unity from PSS was used for data acquirement and interpretation.

### **1.3.5 Dynamic light scattering measurements**

Dynamic light scattering measurements were performed on a Malvern Zeta-sizer Nano-ZS ZEN 3600 instrument equipped with a He-Ne laser (633 nm) and a fixed detector oriented at 173 $^{\circ}$ . Nanogel dispersions (0.5 mL, 0.5 mg/mL) were analyzed in quartz fluorescence cuvettes with a round aperture. The autocorrelation functions of backscattered light were analyzed using the Zetasizer DTS software from Malvern to determine the size distribution by intensity and the polydispersity index. The measurements were performed at 25  $^{\circ}\text{C}$  in acetone or water, equilibrating the system at this temperature for 120 s. Measurements were performed in triplicate with the error given as standard deviation from the mean value.

### **1.3.6 Circular dichroism (CD) measurements**

All CD measurements were performed on a Jasco-J810 spectropolarimeter by the use of 1 mm path-length cuvette at 20  $^{\circ}\text{C}$  (Jasco PTC-348 WI peltier thermostat). CD spectra were the average of 4 scans obtained by the collection of data from 190 to 240 nm with a 1 nm interval on 50 nm per minute.

## 1.4 Figures

### 1.4.1 NMR spectra

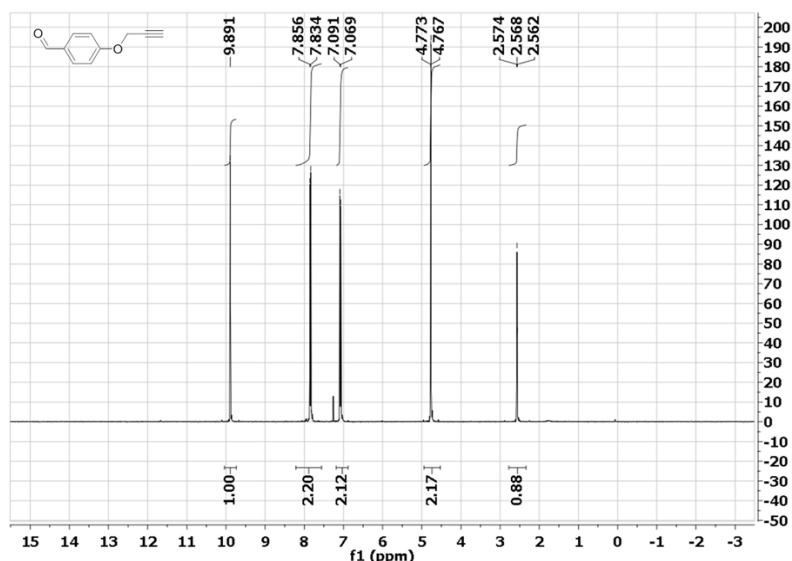


Figure S1 <sup>1</sup>H NMR (CDCl<sub>3</sub>, 400 MHz) p-propargyloxy-benzaldehyde (pPBA).

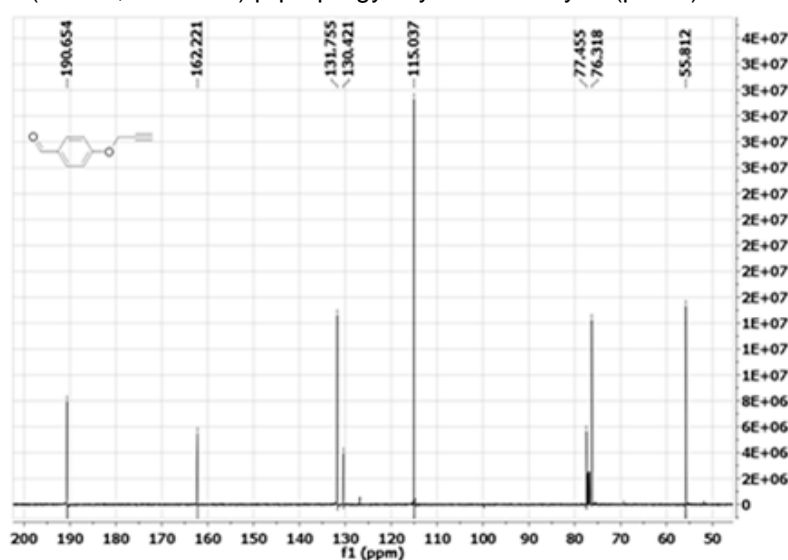


Figure S2 <sup>13</sup>C NMR (CDCl<sub>3</sub>, 400 MHz) p-propargyloxy-benzaldehyde (pPBA).

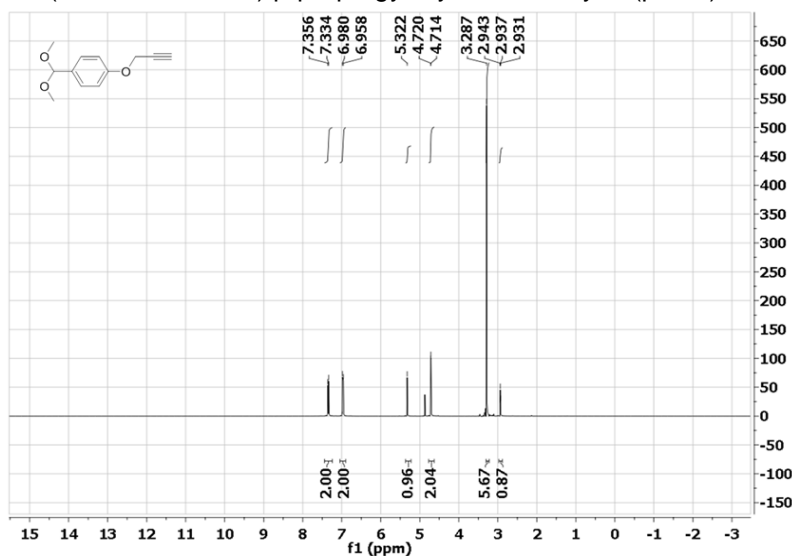
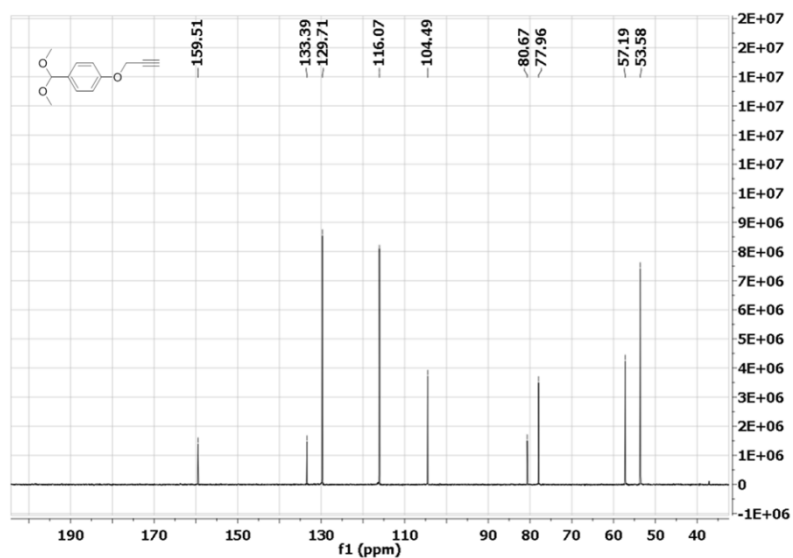
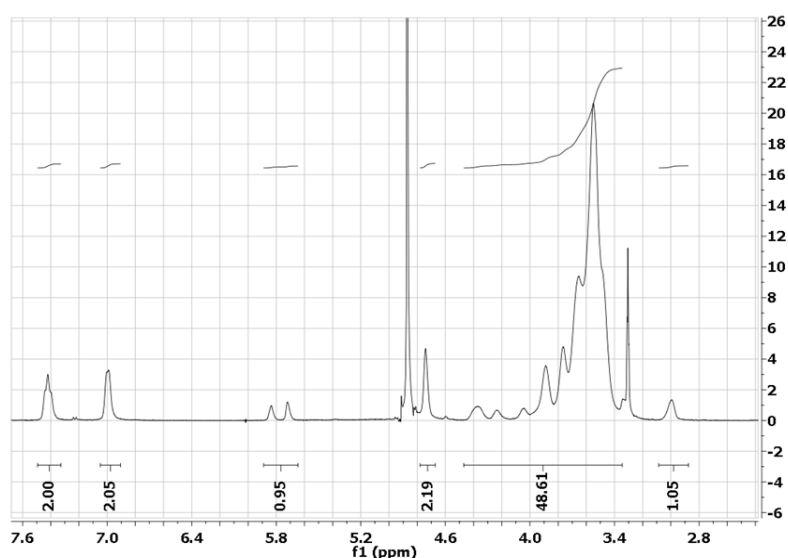


Figure S3 <sup>1</sup>H NMR (CD<sub>3</sub>OD, 400 MHz) p-propargyloxy-benzdimethylacetale (pPBDMA).



**Figure S4**  $^{13}\text{C}$  NMR ( $\text{CD}_3\text{OD}$ , 400 MHz) p-propargyloxy-benzdimethylacetale (pPBDMA).



**Figure S5**  $^1\text{H}$  NMR ( $\text{CD}_3\text{OD}$ , 400 MHz) dPG7.7-10-p-propargyloxy-benzacetale.

### 1.4.2 Asparaginase release measured by HPLC

L-asparaginase can be determined quantitatively and qualitatively via HPLC analysis without interference with polyglycerol fragments. Chromatograms of the intact, asparaginase-loaded nanogel showed that the encapsulation efficiency is 100%, as no free L-asparaginase II was detected. The asparaginase activity assay of the intact and loaded PG nanogel gave an enzyme activity of 44.5%. The activity is related to asparaginase molecules located at the surface of PG nanogel particles, as no free L-asparaginase II was detectable. The release study verified the pH dependent degradation / release of the PG nanogels. 100% drug release was obtained at pH 4 after 3 days. At pH 5, particle degradation and drug release was slower.

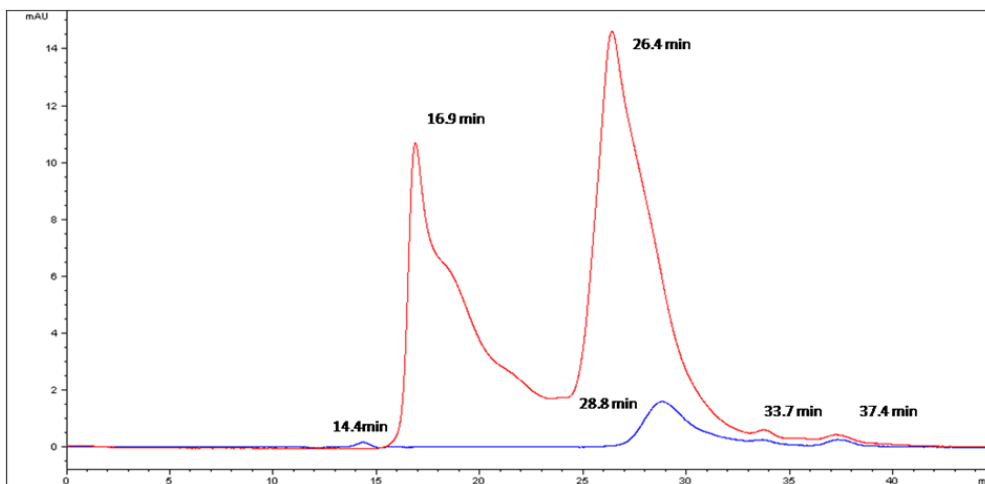


**Figure S6** HPLC chromatogram – UV detection at 280 nm; blue line: PG Nanogel; red line: PGNanogel intact spiked with L-asparaginase 1 mg/mL

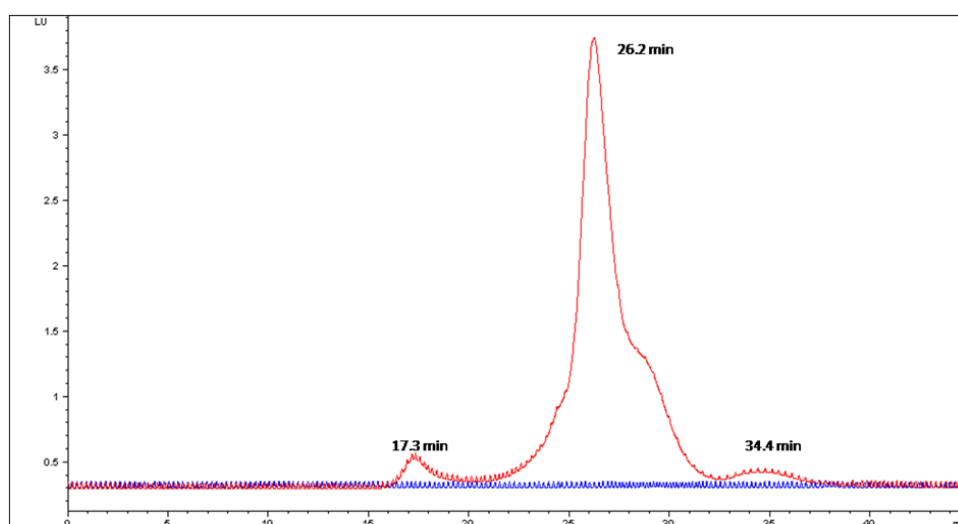


**Figure S7** HPLC chromatogram – fluorescence detection at 348 nm; blue line: asparaginase-loaded nanogel intact; red line: nanogel intact spiked with L-asparaginase 1 mg/mL.

### 1.4.3 Circular dichroism spectra of proteins

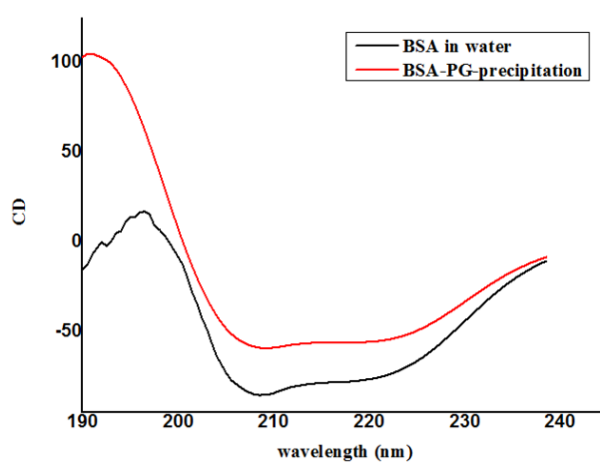


**Figure S8** CD spectra of fresh BSA in water (lower line) and released BSA (upper line)

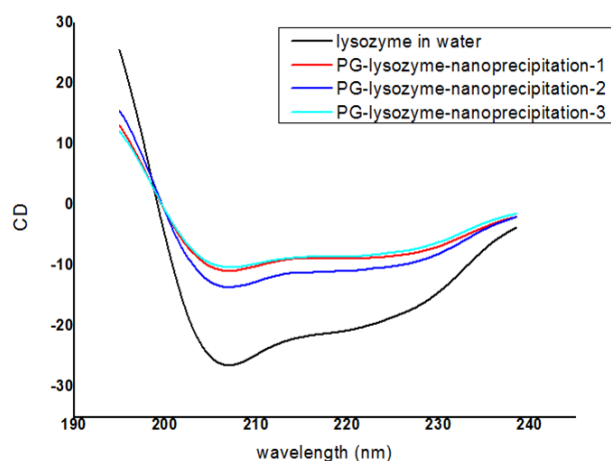


**Figure S9** CD spectra of fresh lysozyme in water (lower line) and released lysozyme.

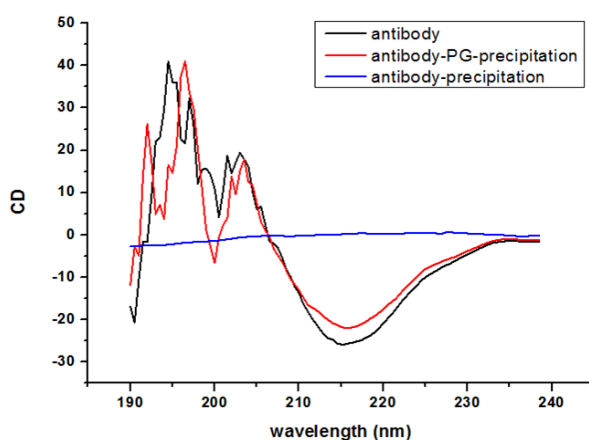


**Figure S10** CD spectra of fresh IgG (c), released IgG (b), and antibody precipitated without stabilizing dPG (a).

## 2. Thermosensitive dendritic polyglycerol-based nanogels for cutaneous delivery of biomacromolecules

### 2.1 Materials

The chemicals were used as purchased: N-isopropylacrylamide (NIPAM), acryloyl chloride (Ac, 96 %), ammonium persulphate (APS, 98 %), N,N,N',N'-tetramethylethylenediamine (TEMED, 99 %), bovine serum albumin (BSA), sodium chloride (NaCl), L-asparagin monohydrate, trichloroacetic acid, Nessler's solution, Igepal® CA-630, the buffer substances, and rhodamine B isothiocyanate (RhB-ITC) were purchased from Sigma-Aldrich Corporation, Taufkirchen, Germany. Extra dry dimethylformamide (DMF, 99.8 %), dimethyl sulfoxide (DMSO), triethylamine (TEA), and sodium dodecyl sulphate (SDS, 98 %) and the Micro BCA™ Protein Assay Kit were obtained from Fisher Scientific GmbH, Schwerte, Germany. N-methylisatoic anhydride was purchased from Molecular Probes®, Invitrogen, Darmstadt,

Germany. Human TGase-1 was purchased from Zedira, Darmstadt, Germany, 1,2,6,7- <sup>3</sup>H-testosterone was obtained from Amersham, Glattbrugg, Switzerland.

## 2.2 Synthesis and fluorescence labeling of acrylated dPG (dPG-Ac 5 %)

dPG with an average Mw of 10 kDa (PDI 1.3) was synthesized according to previously reported methodologies 32. The dPG was dried overnight under vacuum prior to the acrylation reaction. A solution of acryloyl chloride (0.65 mmol, 52  $\mu$ L) in dry DMF (1 mL) was added drop wise to a stirred solution of dPG (1 g, 10 kDa, 13.51 mmol OH equivalent) and TEA (1.08 mmol, 150  $\mu$ L) in DMF (7 mL) at 0 °C. The reaction mixture was stirred at room temperature for at least 4 h and subsequently purified by dialysis (MWCO 2000) in water for at least 48 h. The dPG-Ac with a yield of 90 % was preferably used directly after purification. Otherwise the product was stored in dark at room temperature in the presence of p-methoxyphenol, which was dialyzed out before usage. 1H-NMR spectra were recorded with a Bruker DRX 500 MHz instrument. D2O was used as the deuterated solvent. Chemical shifts  $\delta$  are given in ppm relative to TMS as an internal standard or relative to the resonance of the solvent (1H-NMR: D2O:  $\delta$  = 4.79 ppm). 1H-NMR (500 MHz, D2O),  $\delta$ : 3.20 – 4.30 (m, 5 H, dPG scaffold protons), 5.88 – 6.00 (m, 1H, vinyl), 6.08 – 6.28 (m, 1H, vinyl), 6.32 – 6.44 (m, 1H, vinyl).

Alternatively, dPG was labeled with N-methylanthraniloyl group (MANT) before the acrylation reaction. This method is a modification of a previously described synthesis of fluorescent polysaccharide 33. 50 mg of dPG (20 mg mL<sup>-1</sup>) in milliQ water was adjusted to 50 % dimethyl sulfoxide (DMSO) (v/v). A stock solution of 10–20 mg mL<sup>-1</sup> high-purity N-methylisatoic anhydride (MIA) (w/v) in neat DMSO was prepared by vortexing. This stock solution was used immediately. The MIA stock solution is added to the polymer solution, mixed thoroughly, and incubated at room temperature overnight. The successful labeling reaction was probed by thin layer chromatography, 2-propanol/ammonium hydroxide/water, (6:3:1) was used to separate free hydrolyzed reagent from the MANT-labeled polymer. The fluorescent compounds were detected on the plate by excitation with long-wave ultraviolet (366 nm) light. The label dPG was further purified by dialysis against water for 48 h.

## 2.3 Skin penetration tests

The pig skin was punched to 1.5 cm discs, and mounted onto static-type Franz cells (diameter 15 mm, volume 12 ml, 1.72 cm<sup>2</sup> application area, PermeGear Inc., Bethlehem, PA, USA) filled with phosphate buffered saline pH 7.4 (PBS). After 30 min equilibration, 200  $\mu$ L of the test formulations (350  $\mu$ g cm<sup>-2</sup>) were applied onto the skin surface. A temperature ramp of 32 °C - 37 °C was applied during incubation to mimic the temperature gradient in native skin. After 6 h, the skin was dismantled and excessive formulation was gently removed. For

data analysis, 5  $\mu\text{m}$  skin sections were prepared by cutting from the dermis to the stratum corneum (SC). The cross-sections were subjected to normal light and fluorescence microscopy (100 and 200x magnification, BZ-8100, Keyence, Neu-Isenburg) and the fluorescence of RhB ITC (filter setting: exc. 560/40 nm, em. 630/60 nm) and MANT-labeled nanogels (filter setting: exc. 360/40 nm, em. 460/50 nm) were detected. The exposure time was set to values, where no auto-fluorescence of the skin was detectable. The pixel brightness was assessed as arbitrary brightness units (ABU) using the image analysis software BZ Analyzer 3 .

## 2.4 Figures

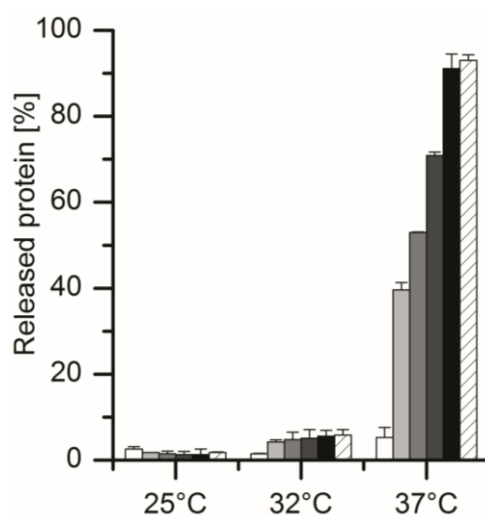


**Figure S1** The amount of free BSA-RhB ITC was determined after 0 min (white bars), 5 min (light grey bars), 15 min (grey bars), 30 min (dark grey bars), 1 h (black bars), and 4 h (shaded bars) following incubations at 25 °C, 32 °C, and 37 °C, respectively.  $n=3$ , mean  $\pm$  SD.

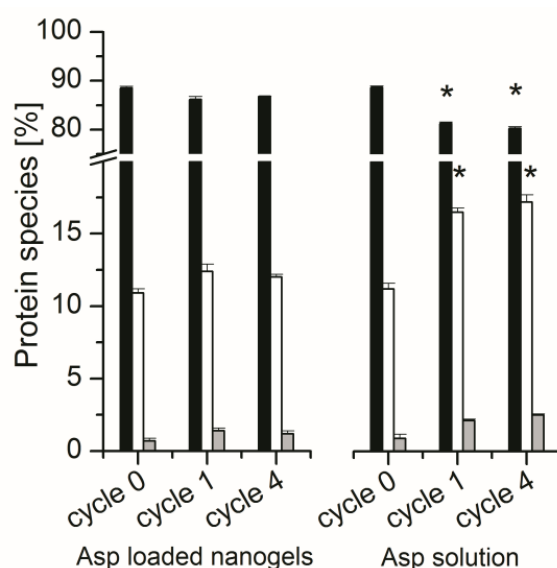


**Figure S2** Protein species distribution of Asp loaded onto nanogels and free Asp in an aqueous following 4 freeze-thaw cycles: tetramer (black bars), aggregates (white bars), and fragments (grey bars).  $n = 3$ , mean  $\pm$  SD. \* $p < 0.05$ .

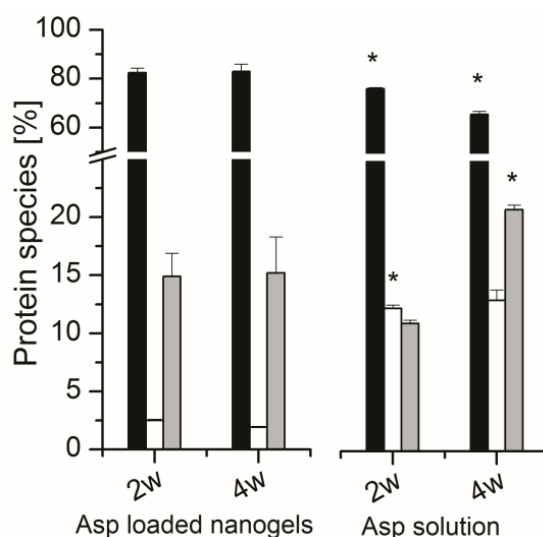


**Figure S3** Protein species distribution of asparaginase (Asp) loaded onto nanogels and free Asp in an aqueous solution after 2 weeks and 4 weeks of storage at 25 °C: tetramers (black bars), aggregates (white bars), and fragments (grey bars).  $n = 3$ , mean  $\pm$  SD, \*  $p < 0.05$ .

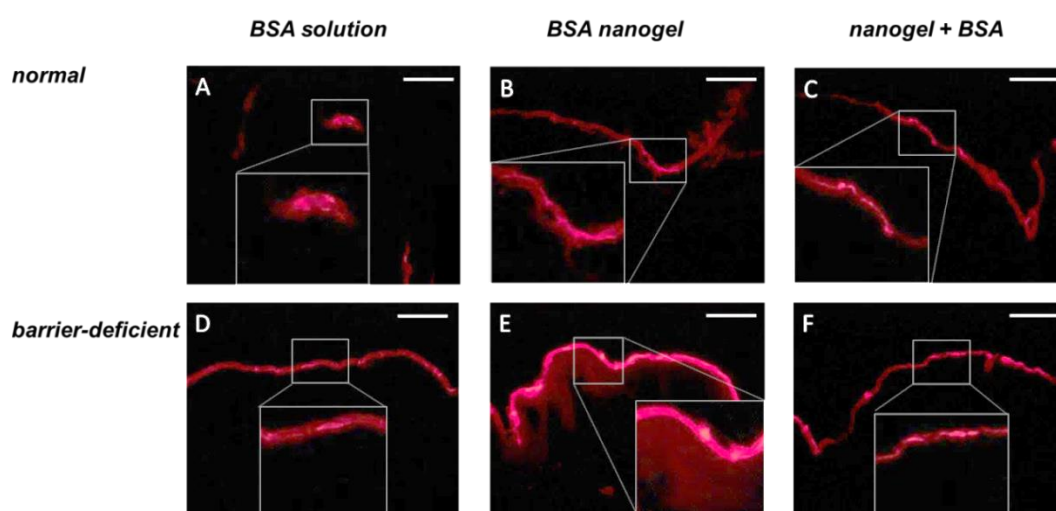


**Figure S4** Skin absorption of BSA-RhB ITC in normal (A-C) and tape-stripped (D-F) pig skin following the application of BSA-RhB ITC solution (A, D), BSA-RhB ITC loaded PNIPAM-dPG nanogels (B, E), and PNIPAM-dPG nanogel spiked with free BSA-RhB ITC (C, F). Scale bar = 50  $\mu\text{m}$ .

**Table S1:** BSA-RhB-ITC content in the SC and viable epidermis following the application of BSA-RhB ITC solution, PNIPAM-dPG nanogels spiked with free BSA-RhB ITC, and BSA-RhB ITC loaded PNIPAM-dPG nanogels depicted as arbitrary pixel brightness units (ABU).  $n=3$  donor

		SC $\pm$ SD [ABU]	Viable Epidermis $\pm$ SD [ABU]
Normal skin	BSA-RhB ITC solution	154.1 $\pm$ 6.8	0
	BSA-RhB ITC loaded nanogel	125.0 $\pm$ 13.5	0
	nanogel spiked with 3 mg mL <sup>-1</sup> free BSA-RhB ITC	118.8 $\pm$ 9.5	0
Tape-stripped skin	BSA-RhB ITC solution	151.5 $\pm$ 11.9	5.8 $\pm$ 0.7
	BSA-RhB ITC loaded nanogel	202.1 $\pm$ 7.6	23.6 $\pm$ 2.3
	nanogel spiked with 3 mg mL <sup>-1</sup> free BSA-RhB ITC	140.5 $\pm$ 11.9	4.6 $\pm$ 2.3

### 3. Interactions of Hyaluronic Acid with the Skin and Implications for the Dermal Delivery of Biomacromolecules

#### 3.1 Figures

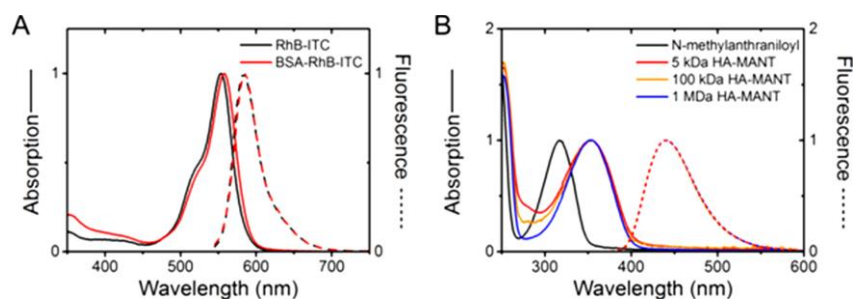


**Figure SI 1** Spectral characteristic of HA-MANT and BSA-RhB samples. (A) Absorption spectra, shown as solid line, and emission spectra, depicted as dashed lines, of HA-MANT samples (5 kDa, 100 kDa, 1 MDa). For comparison the absorption spectrum of MIA is also shown. (B) Absorption spectra, shown as solid line, and emission spectra, depicted as dashed lines, for BSA-RhB and RhB.

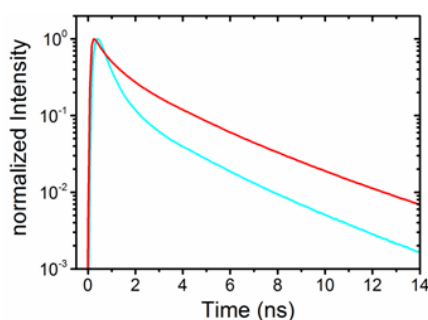


**Figure SI 2** Fluorescence lifetime decay curves of BSA-RhB in the respective skin regions as shown in Figure 1. The BSA-RhB fluorescence lifetime decay curve (upper line) was observed in both normal and tape-stripped skin, while the decay curve (lower line) was only observed in tape-stripped skin

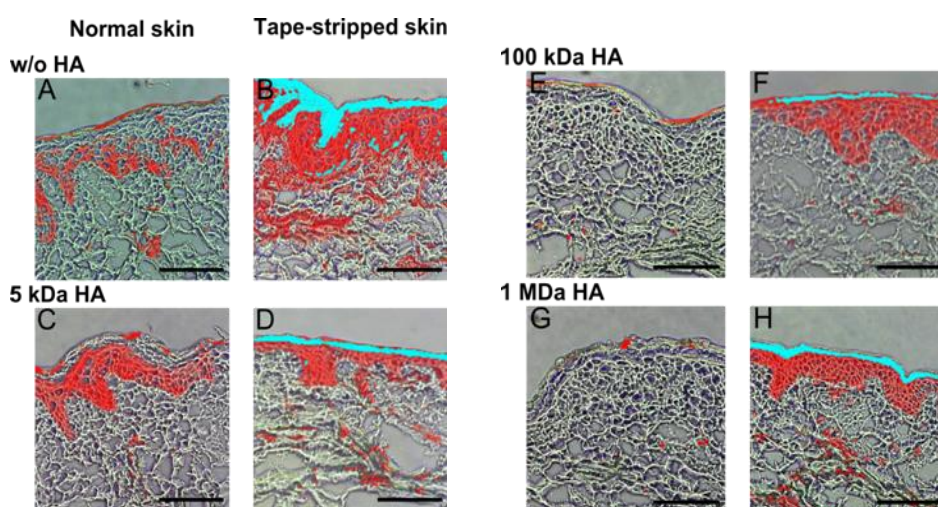


**Figure SI 3** Overlays of false color coded FLIM images and bright field images for BSA-RhB penetration into normal skin (A,C,E,G) and tape-stripped skin (B,D,F,H). Scale bars represent 100  $\mu\text{m}$ .

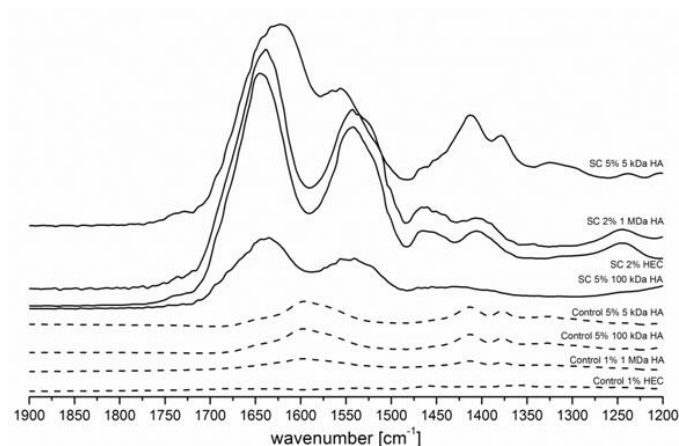


**Figure SI 4** Normalized FT-IR spectra of incubated SC samples (6h incubation; 5% 5 kDa HA, 2% 1 MDa HA, 2% HEC, 5% 100 kDa HA) versus the corresponding plain hydrogel controls (5% 5 kDa HA, 5% 100 kDa HA, 1% 1 MDa HA and 1% HEC,) recorded in the amide I and II region between 1700-1500  $\text{cm}^{-1}$ . mean values of  $n=3$

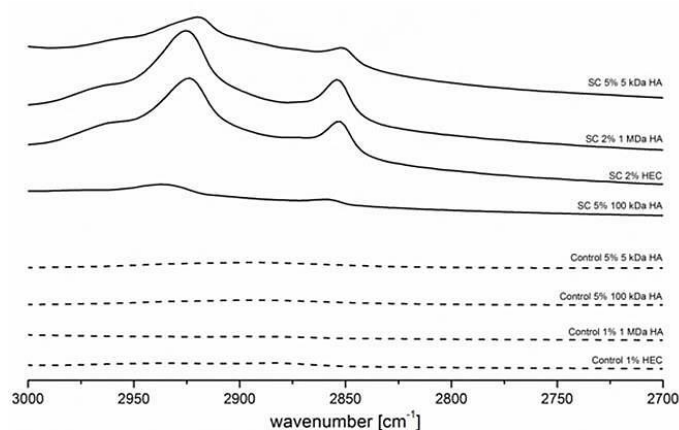


**Figure SI 5** Normalized FT-IR spectra of incubated SC samples (6h incubation; 5% 5 kDa HA, 2% 1 MDa HA, 2% HEC, 5% 100 kDa HA) versus the corresponding plain hydrogel controls (5% 5 kDa HA, 5% 100 kDa HA, 1% 1 MDa HA and 1% HEC) recorded in the CH stretching region between 3000-2800  $\text{cm}^{-1}$ . mean values of  $n=3$

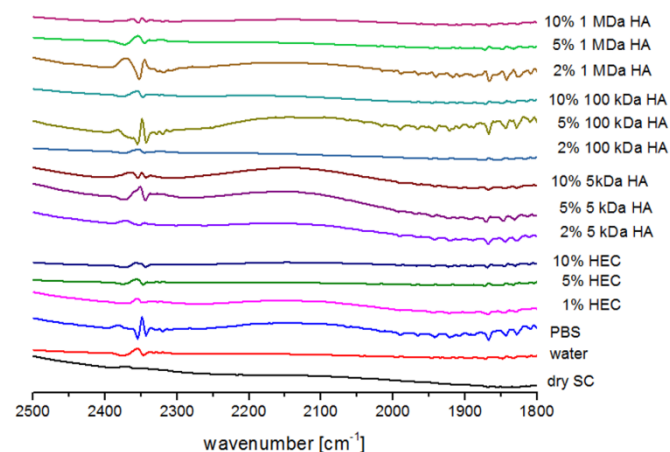


**Figure SI 6** Normalized FT-IR spectra of incubated SC samples (6h incubation) recorded in the OH stretching region between 2500-1800  $\text{cm}^{-1}$ . mean values of  $n=3$

## 4. References

1. Rainer Haag, Holger Tuerk SM. *Preparation of highly branched polyols based on glycosides useful as an additive in paints and adhesives, additive and crosslinker in polymers, in cosmetics, preparation of nano particles and active substance carrier.* (2002).
2. Hong V, Presolski SI, Ma C, Finn MG. *Analysis and optimization of copper-catalyzed azide-alkyne cycloaddition for bioconjugation.* *Angew. Chemie - Int. Ed.* 48(52) (2009).
3. Sisson AL, Papp I, Landfester K, Haag R. *Functional Nanoparticles from Dendritic Precursors: Hierarchical Assembly in Miniemulsion.* *Macromolecules.* 42(2), 556–559 (2009).
4. He H, Zhang Y, Gao C, Wu J. *“Clicked” magnetic nanohybrids with a soft polymer interlayer.* *Chem. Commun. (Camb).* (13), 1655–1657 (2009).

## **Publications and presentations associated with the thesis**

### Review articles

**M. Witting**, K. Obst, W. Frieß, S. Hedtrich; Recent advances in topical delivery of proteins and peptides mediated by soft matter nanocarriers, *Biotechnol Adv.* (2015) 33 (6 Pt 3):1355-69

### Research articles

**M. Witting**, A. Boreham, R. BrodWolf, K. Vávrová, U. Alexiev, W. Frieß, S. Hedtrich; Interactions of hyaluronic acid with the skin and implications for the dermal delivery of biomacromolecules, *Mol Pharm* (2015) 12(5):1391-401

**M. Witting**, K. Obst, M. Pietzsch, W. Frieß, S. Hedtrich; Feasibility study for intraepidermal delivery of proteins using a solid microneedle array, *Int J Pharm* (2015) 486(1-2):52-8

**M. Witting**, M. Molina, K. Obst, R. Plank, K.M. Eckl, H.C. Hennies, M. Calderón, W. Friess, S. Hedtrich; Thermosensitive dendritic polyglycerol-based nanogels for cutaneous delivery of biomacromolecules, *Nanomedicine* (2015) 11(5):1179-87

D. Steinhilber, **M. Witting**, X. Zhang, M. Staegemann, F. Paulus, W. Friess, S. Küchler, R. Haag; Surfactant free preparation of biodegradable dendritic polyglycerol nanogels by inverse nanoprecipitation for encapsulation and release of pharmaceutical biomacromolecules, *J Controll Release* (2013) 169:289-295 .

### Patents

„Verfahren zur Herstellung eines Polyglycerin Nanogels zur Verkapslung und Freisetzung biologisch aktiver Substanzen“ Patent Application 09/2012, WO 2014/037429 A2

### Poster Presentations

**M. Witting**, A. Boreham, R. BrodWolf, K. Vávrová, U. Alexiev, W. Frieß, S. Küchler; Influence of hyaluronic acid on dermal drug delivery of biomacromolecules and the underlying mechanism, 14th International Conference Perspectives in Percutaneous Penetration, La Grande Motte, France, April 23-25, 2014

**M. Witting**, D. Steinhilber, M. Molina Soler, M. Calderon, R. Haag, W. Frieß, S. Kuchler; Hyperbranched polyglycerol nanogels – a new tool for dermal drug delivery?, 9th World Meeting on Pharmaceutics, Biopharmaceutics and Pharmaceutical Technology, Lisbon, Portugal, March 31 - April 3, 2014

**M. Witting**, K. Vávrová, W. Frieß, S. Kuchler; Influence of hyaluronic acid type and concentration on dermal drug delivery and stratum corneum properties, Barrier Function of Mammalian Skin, Gordon Research Conference, Waterville Valley, NH, August 18-23, 2013

**M. Witting**, W. Friess, S. Kuchler; Characterization of microneedles and hyaluronic acid as intraepidermal drug delivery systems for proteins aiming for new therapeutic approaches for the treatment of skin diseases, 8th World Meeting on Pharmaceutics